MSc. Thesis

Technische Universiteit Delft

MSc. Thesis

Estimating impact of Vehicle-to-Grid operation on automotive fuel cell performance

Samrudh Alva

TU Delft Delft University of Technology

Challenge the future

Estimating impact of Vehicle-to-Grid operation on Automotive Fuel Cell Performance

by

Samrudh Alva

to obtain the degree of Master of Science
at the Delft University of Technology,
to be defended publicly on Friday September 29, 2017.

Student number:	4510364	
Project duration:	December 1, 2016 – September 29, 2017	
Report number:	2845	
Thesis committee:	Associate Professor Dr. P. V. Aravind	TU Delft
	Professor dr. A. J. M. van Wijk	TU Delft
	Assistant Professor Dr. R. Lindeboom	TU Delft
	Ir. V. D. W. M. Oldenbroek	TU Delft

An electronic version of this thesis is available at `http://repository.tudelft.nl/`.

TU Delft

Abstract

In a future scenario electric vehicles (EV) could be operated in Vehicle to Grid (V2G) mode to support the national and renewable energy electricity grid by providing ancillary services such as peak shaving and frequency regulation. While developing financial models to price these services it is important to include the impact of Vehicle to Grid operation on the power-delivery components of these Electric Vehicles. Considerable amount of academic research has been focused on understanding the impact of Vehicle to Grid operation on Battery Electric Vehicles (BEVs). However, information about the impact of Vehicle to Grid operation on the fuel cells (FCs) of Fuel Cell Electric Vehicles (FCEVs) and Fuel Cell Range Extender Electric Vehicles (FCREEVs) is scarce.

Long term tests are required to asses the impact of Vehicle to Grid operation on these fuel cells. The fuel tank volume limitation of the TU Delft Hyundai FCEV does not allow for long term Vehicle to Grid experiments using the operational Vehicle to Grid set-up at the TU Delft Green Village site. Furthermore, there exist limited control over the power management strategy programmed in the Hyundai FCEV; the power management strategy defining the load cycle it's Fuel Cell undergoes in Vehicle to Grid operation. This study therefore proposes a method to conduct simulated long term Vehicle to Grid experiments on a laboratory test bench. The method has also been applied, and the impact of simulated Vehicle to Grid operation on the Fuel Cell of the PEMFC test bench estimated. Most importantly, the experimental conditions simulated on the laboratory test-bench were derived from data recorded in the Hyundai FCEV during actual Vehicle to Grid operation. Simulated Vehicle to Grid operation under three aging cycles: high constant load (CC1), low constant load (CC2) and cyclic load (CC3), was found to cause a performance loss in the range of 31.4 μVh^{-1} to 40.9 μVh^{-1}, 62.5 μVh^{-1} to 63.9 μVh^{-1} and 36.1 μVh^{-1} to 92.4 μVh^{-1} respectively.

Contents

Abstract i

List of Figures v

List of Tables vii

Acknowledgements ix

1 Introduction 1
- 1.1 Electric Vehicles . . . 1
- 1.2 Vehicle to Grid and Grid to Vehicle operation of Electric Vehicles . . . 1
- 1.3 Significance of estimating performance degradation due to Vehicle to Grid operation . . . 3
- 1.4 Need for conducting simulated Vehicle to Grid experiments . . . 4
  - 1.4.1 Inability to perform long-term Vehicle to Grid experiments using Hyundai Fuel Cell Electric Vehicle . . . 6
  - 1.4.2 Variety of applicable power management strategies . . . 9
  - 1.4.3 Inability to change power management strategy programmed in Hyundai Fuel Cell Electric Vehicle: . . . 16
  - 1.4.4 Advantages of small-scale experiments . . . 18
- 1.5 Research Question and Outline . . . 18
- 1.6 Summary . . . 19

2 Experiment 21
- 2.1 Set-up for simulated Vehicle to Grid experiments . . . 21
  - 2.1.1 Fuel Cell . . . 22
  - 2.1.2 Supporting Equipment . . . 26
- 2.2 Determining experimental conditions for simulated Vehicle to Grid experiments . . . 29
- 2.3 Fuel Cell load cycles simulated . . . 32
  - 2.3.1 Literature Survey . . . 32
  - 2.3.2 Power management strategy selected for simulation . . . 35
  - 2.3.3 Types of Fuel Cell load cycles selected for simulation . . . 36
  - 2.3.4 Translating selected Hyundai FCEV specific Fuel Cell load cycle to equivalent current cycle specific to the laboratory PEMFC used for simulated Vehicle to Grid experiments . . . 39
- 2.4 Summary . . . 43

3 Experimental Methodology 45
- 3.1 MEA activation procedure applied before staring simulated Vehicle to Grid experiments . . . 45
- 3.2 Computing impact of simulated Vehicle to Grid operation . . . 46
  - 3.2.1 Defining measurement period . . . 46
  - 3.2.2 Computing rate of voltage decay . . . 47
- 3.3 Summary . . . 48

4 Results and Discussions 49
- 4.1 Electrochemical characterization of MEAs . . . 49
  - 4.1.1 Polarization Curve . . . 49
- 4.2 Description of the recorded voltage evolution data of simulated Vehicle to Grid experiments . . . 50
  - 4.2.1 Voltage evolution characteristics under each type of equivalent current cycle . . . 50
  - 4.2.2 Effect of laboratory temperature on the simulated Vehicle to Grid experiments . . . 52

4.3 Computed performance loss in simulated Vehicle to Grid Experiments 53
4.3.1 Performance loss computed from the voltage evolution data recorded during simulated Vehicle to Grid Experiments 53
4.3.2 Impact of simulated Vehicle to Grid operation on Polarization Curves 60
4.4 Summary 63

5 Conclusions **65**

6 Recommendations **67**

A Graph depicting experimental measurement period for computing voltage degradation **69**

B General Theory regarding degradation in PEMFCs **71**
B.1 Fuel Cell theory 71
B.2 Construction of PEM fuel cells 75
B.3 Automotive Fuel Cell Systems 77
B.4 Degradation mechanisms that occur in PEM fuel cells 78

C Piping and Instrumentation Diagram for experimental set-up **83**

D Steps followed while conducting the experiments **87**

E Relation between Hyundai's Vehicle speed and Fuel Cell power **91**

Bibliography **93**

List of Figures

1.1 Schematic of Vehicle to Grid (V2G) and Grid to Vehicle (G2V) operation of Electric Vehicles 2
1.2 V2G and G2V operation of different types of Electric Vehicles 2
1.3 Schematic describing the impact of Vehicle to Grid services on Fuel Cell and Fuel Cell Range Extender Electric Vehicles and the impact on the cost of V2G energy delivered . 4
1.4 Electrical architecture schematic of the Hyundai ix35 FCEV modified for Vehicle to Grid capabilities [34] 5
1.5 Electrical architecture schematic of the discharger unit connecting the FCEV to the National Grid [34] 5
1.6 Hyundai ix35 Fuel Cell Electric Vehicle operating in V2G mode in a actual V2G set-up at the TU Delft Green Village site 6
1.7 PEMFC processes and their time scales [51] 7
1.8 Fuel and Energy Relation during Hyundai FCEV2G operation 8
1.9 Types of drivetrain architecture in Fuel Cell Electric Vehicles and Fuel Cell Range Extender Electric Vehicles 9
1.10 Schematic describing Translation of Grid load to Fuel Cell load cycle inside the Electric Vehicle 10
1.11 Constant Load needed to be serviced by the Electric Vehicle 11
1.12 Power management strategy employed to service a given grid load, by some types of FC-HVB combinations connected in series or parallel drivetrain architecture 15
1.13 Power management strategy of the Hyundai FCEV operating in Vehicle to Grid mode at 9.5kW Vehicle to Grid load 16
1.14 Power management strategy of the Hyundai FCEV operating in Vehicle to Grid mode at 7kW Vehicle to Grid load 17
1.15 Fuel Cell load cycle of the Hyundai FCEV while servicing two different Vehicle to Grid loads 17

2.1 Schematic of the laboratory PEMFC set-up on which all simulated Vehicle to Grid experiments were conducted 21
2.2 Generic single cell PEMFC construction [30] 22
2.3 MEA and Monopolar plates of laboratory PEMFC used during this research 23
2.4 Half-cell PEMFC assembly without MEA 24
2.5 Assembled PEMFC used during this research 25
2.6 Assembled PEMFC connected in the set-up used during this research 26
2.7 Picture of the laboratory PEMFC set-up on which all simulated Vehicle to Grid experiments were conducted 28
2.8 Fuel Cell Pressure measured in the Hyundai during 1 hour of Vehicle to Grid operation . 29
2.9 Fuel Cell Coolant outlet temperature measured in the Hyundai during 1 hour of Vehicle to Grid operation 29
2.10 Cathode stoichiometry in the region of interest 30
2.11 Reported Degradation Results 34
2.12 Selected power management strategy for simulated Vehicle to Grid experiments 35
2.13 First type of Fuel Cell load cycle simulated in this study (LC1) 36
2.14 Second type of Fuel Cell load cycle simulated in this study (LC2) 37
2.15 Third type of Fuel Cell load cycle simulated in this study (LC3) 38
2.16 Load cycles selected to be simulated 39
2.17 Fuel Cell Power, Current and Voltage relation during 1000s of Vehicle to Grid operation at 9.5kW AC using the Hyundai FCEV 40
2.18 Polarization and Percentage Power curve for MEA1 in the test-bench PEMFC 41

2.19 All Translated Current Cycles unique to the laboratory PEMFC set-up which were tested during this research 43

4.1 Polarization Curve of all MEAs before start of simulated Vehicle to Grid experiments . . 49
4.2 Voltage evolution characteristic of test bench Fuel Cell in simulated Vehicle to Grid operation under equivalent constant current aging cycles CC1 in Experiment 2 51
4.3 Voltage evolution characteristic of test bench Fuel Cell in simulated Vehicle to Grid operation under equivalent cyclic current aging cycle CC3 in Experiment 6 51
4.4 Relation between voltage evolution data under simulated Vehicle to Grid operation and the laboratory temperature during Experiment 3 52
4.5 Relation between voltage evolution data under simulated Vehicle to Grid operation and the water flow rate measured in the humidification unit 53
4.6 Computed rate of voltage decay caused by simulated Vehicle to Grid operation under aging cycle CC1 54
4.7 Computed rate of voltage decay caused by simulated Vehicle to Grid operation under aging cycle CC2 55
4.8 Computed rate of voltage decay caused by simulated Vehicle to Grid operation under aging cycle CC3 56
4.9 Polarization Curves measured at the start and end of Sequence 1 of Vehicle to Grid operation under aging cycle CC1 60
4.10 Polarization Curves measured at the start and end of Sequence 1 of Vehicle to Grid operation under aging cycle CC2 61
4.11 Polarization Curves measured at the start and end of Sequence 1 of simulated Vehicle to Grid operation under aging cycle CC3 61
4.12 Side-view of the PEMFC connected in the test-bench 62

A.1 Voltage evolution curve for Experiment 3 depicting the sequences and the performance measurement periods 69

B.1 Typical polarization curve for a PEMFC [57] 73
B.2 Typical power curve for a PEMFC [57] 74
B.3 Generic construction of a single-cell PEMFC [57] 75
B.4 Control system components and electricity flow within the Hyundai FCEV [3] 78

C.1 P&ID 83
C.2 Instrument List of the setup 84
C.3 Pipeline List of the setup 85
C.4 Equipment and Valve List of the setup 86

E.1 Vehicle speed and Fuel Cell Power relation for Hyundai ix35 Fuel Cell Electric Vehicle . 91

List of Tables

2.1 Experimental conditions for simulated Vehicle to Grid experiments 31
2.2 Reactant conditions for simulated Vehicle to Grid experiments 31
2.3 Reported Degradation Results 34
2.4 Translating load cycle specific to the Hyundai FCEV's Fuel Cell stack to it's equivalent current cycle specific to the test bench PEMFC 42

4.1 Computed rate of voltage decay caused by simulated Vehicle to Grid operation under the various aging cycles 57

Acknowledgements

First I would like to thank my family for encouraging me to dream and also for constantly providing me with the strength, inspiration, support and training required to achieve them. Furthermore, I will also be indebted forever to my extended family of friends for their sustained support and understanding.

I thank Ad for your critique, encouragement and support during the course of my internship and this thesis. Most importantly I have been able to learn from you how to perceive concepts and their impact from a macro applicability scale, and I am certain that this skill will be immensely helpful to me throughout my lifetime.

I also thank Aravind for you constant support, encouragement and guidance throughout the course of this thesis. Your work ethic is very impressive and I shall constantly draw inspiration from it.

I also extend my gratitude to Vincent. Your patience, understanding and organizational skills are only some of the aspects that I have observed and consciously try to imbibe in my own life.

I also thank Alexa for proof-reading this thesis and giving me valuable inputs and suggestions.

Finally, the unsung heroes of our lives who do so much for us but get little or no credit, also deserve a shout out. So I thank Jaap, Michel, Henneke, Bas, Martijn, Daniel, Eveline and all the other individuals working tirelessly to help the Process and Energy Department operate smoothly. Your contribution to our lives is humbling!

Nomenclature

EV	Electric Vehicle
V2G	Vehicle to Grid
FC	Fuel Cell
BEV	Battery Electric Vehicle
PHEV	Plug-in Hybrid Electric Vehicle
FCEV	Fuel Cell Electric Vehicle
FCREEV	Fuel Cell Range Extender Vehicle
FCEV2G	Fuel Cell Electric Vehicle to Grid
HVB	High Voltage Battery
PEMFC	Proton Exchange Membrane Fuel Cell
RH	Relative Humidity
LC	Load Cycle specific to the Fuel Cell in the TU Delft Hyundai FCEV
CC	Equivalent Current Cycle specific to the test bench PEMFC on which V2G operation is simulated
VPP	Virtual Power Plant
DC	Direct Current
AC	Alternating Current
CEM system	Controlled Evaporation and Mixing system
$P_{FC-rating}$	Fuel Cell power rating in kW
kW	Kilowatt
kWh	Kilowatt-hour
μVh^{-1}	micro-Volts per hour
mVh^{-1}	millivolts per hour

1 Introduction

1.1. Electric Vehicles

The increase in economic and population growth has led to a rise in the transportation sector's share of world-wide energy consumption. The world delivered energy consumption in the transportation sector is projected to increase at a rate of 1.4% annually [11]. More than 95% of the fuel used for transportation purposes is produced from fossil sources of energy [9, 11]. Light duty automobiles consume 44% of this total world transportation energy [11]. There is therefore a pressing need to control the consumption and carbon dependence of automotive transportation fuels.

Switching to a low noise, electric powered automobiles will certainly help vastly alleviate the detrimental effects of the automotive sector on the environment [16]. This has led automotive manufacturers to constantly expand their low or zero-emission electric powered product ranges. These electric power train automobiles or Electric Vehicles (EVs) mainly consist of Battery Electric Vehicle (BEVs), Fuel Cell Electric Vehicles (FCEVs) and Plug-in Hybrid Electric Vehicles (PHEVs) [6]. Lately, the use of Fuel Cell Range Extender Electric Vehicles (FCREEVs) have also been proposed [42].

1.2. Vehicle to Grid and Grid to Vehicle operation of Electric Vehicles

In recent years the concept of using Electric Vehicles to serve the electric grid as independent distributed energy storage and supply units, has gained momentum. This form of Electric Vehicle operation is termed as Vehicle to Grid (V2G) operation [20]. Furthermore, the idea of converting and storing excess energy available in the national or renewable energy grid, by operating Electric Vehicles in Grid to Vehicle (G2V) mode has also been put forth. Authors of Ref. [10, 15] suggest that Electric Vehicles operating in Vehicle-to-Grid and Grid-to-Vehicle mode can support the grid by providing ancillary services such as voltage and frequency regulation, peak shaving, spinning reserves, and variable renewable energy grid integration.

Figure 1.1 represents Vehicle to Grid and Grid to Vehicle operation of Electric Vehicles. Vehicle to Grid operation is shown by the flow of power from the Electric Vehicle to the National Electricity Grid, indicating delivery of V2G services such as voltage and frequency regulation, peak shaving and spinning reserves. Delivery of Vehicle to Grid power by the EV to the Renewable Energy Grid represents Electric Vehicle supplementing other renewable sources of energy. Grid to Vehicle operation is shown by flow of power in the reverse direction. This indicates conversion for storage of excess electric energy available in the National or Renewable Energy Electric Grid.

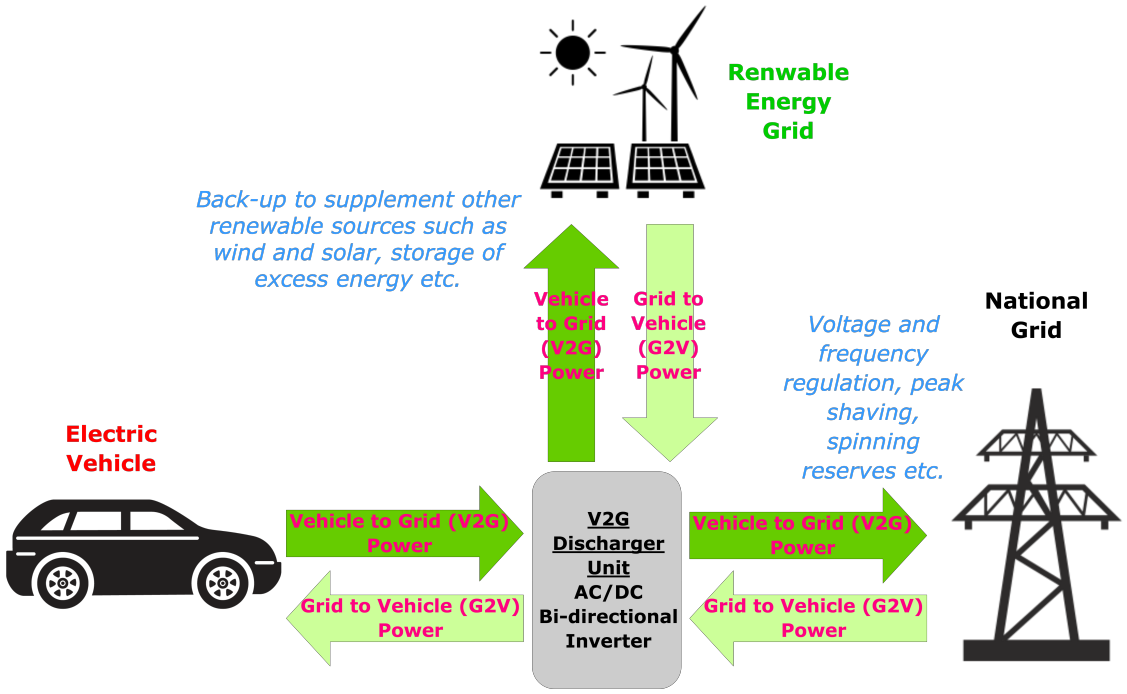

Figure 1.1: Schematic of Vehicle to Grid (V2G) and Grid to Vehicle (G2V) operation of Electric Vehicles

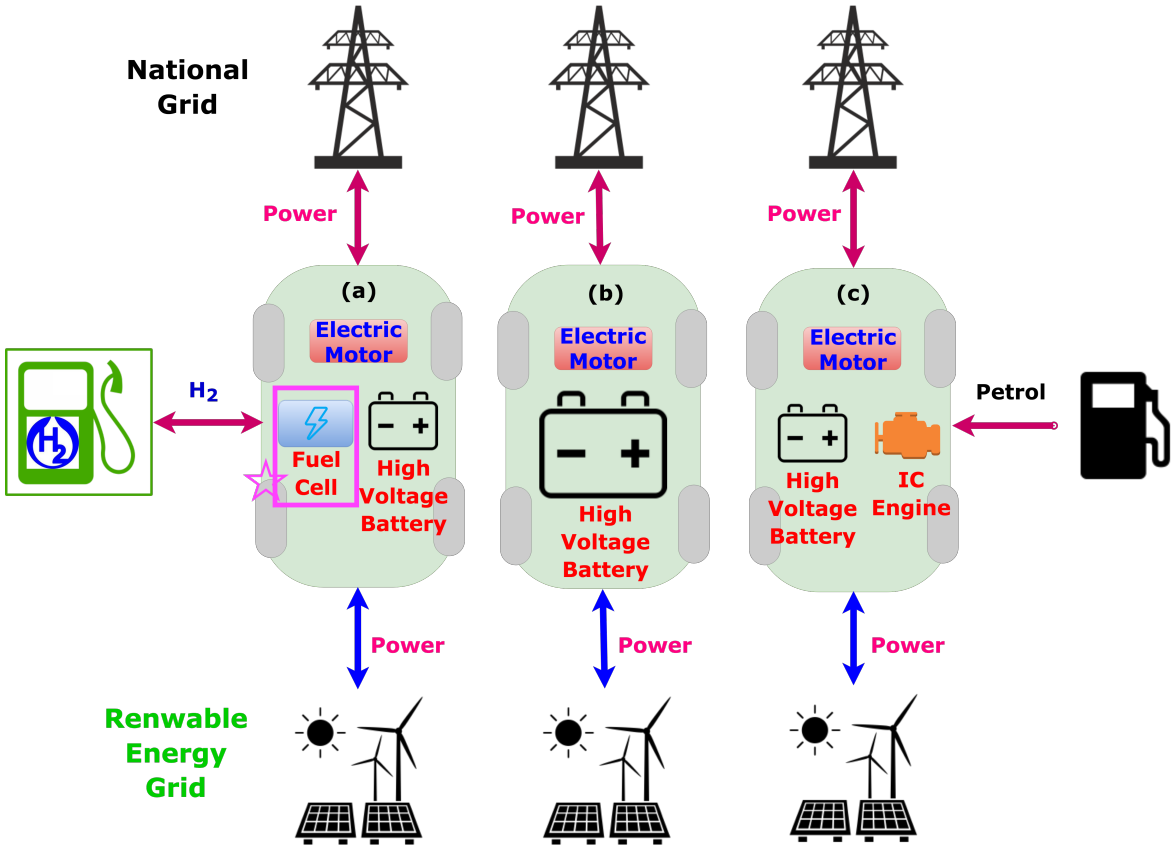

Figure 1.2: V2G and G2V operation of different types of Electric Vehicles
(a) FCEVs and FCREEVs (b) BEVs (c) PHEVs

Figure 1.2 represents the Vehicle to Grid and Grid to Vehicle operation of different types of Electric Vehicles. Figure 1.2 (a) shows the operation of Hydrogen-powered Fuel Cell Electric Vehicles (FCEVs) and Fuel Cell Range Extender Electric Vehicles (FCREEVs). Fuel Cell Electric Vehicles and Fuel Cell Range Extender Electric Vehicles are characterized by a power delivery unit that consists of a Proton Exchange Membrane Fuel Cell stack (PEMFC) coupled with a High Voltage Battery (HVB). Their power unit characteristics allow FCEVs and FCREEVs to interact with the national grid to provide ancillary electrical services. Furthermore, on availability of excess electrical energy in the Grid, the excess energy can either be stored in the High Voltage Battery of these Vehicles or can be converted to Hydrogen through water electrolysis before storage. This Hydrogen can be consumed by the fuel cell in the vehicle thereafter.

Figure 1.2 (b) shows the V2G operation of Battery Electric Vehicle (BEV). These vehicles are powered only by an on-board High Voltage Battery. Besides providing ancillary V2G services, the High Voltage Battery can also be used to store excess electrical energy at times of availability. Finally, Figure 1.2 (c) represents the V2G operation of Plug-in Hybrid Electric Vehicles (PHEVs). These types of EVs have a High Voltage Battery and a conventional petrol-powered Internal Combustion (IC) Engine on-board. The High Voltage Battery of these vehicle can also participate in V2G and G2V services by interacting with the national and renewable energy grid. The IC engine does not participate in V2G operation directly, but in certain cases it may be used to charge the High Voltage Battery.

Here it should be noted that Grid to Vehicle (G2V) operation of Electric Vehicles is out of the scope of this study and therefore all subsequent discussions consider only Vehicle to Grid (V2G) operation of Electric Vehicles.

Almost all V2G related studies focus on battery performance degradation due to operation of Battery Electric Vehicles [8, 40, 52]. But as described above, even Fuel Cell Electric Vehicles (FCEV), Fuel Cell Range Extender Electric Vehicles (FCREEVs) and Plug-in Hybrid Electric Vehicles (PHEVs) are capable of providing V2G services [26, 50]. Battery performance degradation studies may be applicable to the batteries of PHEVs as well. But FCEV and FCREEV operation in V2G mode is different because of the simultaneous presence and varied V2G abilities of both: the High Voltage Batteries and the Fuel Cell.

Although battery related studies may also be applicable to the High Voltage Batteries of Fuel Cell and Fuel Cell Range Extender Electric Vehicles, no study in literature focuses purely on the impact of V2G operation only on the Fuel Cell of these FCEVs and FCREEVs. This study therefore focuses only on the impact of Vehicle-to-Grid operation on the Fuel Cell of Fuel Cell Electric Vehicles and Fuel Cell Range Extender Electric Vehicles. Impact of Vehicle to Grid (V2G) operation on the High Voltage Battery of FCEVs and FCREEVs and on the High Voltage Battery of Battery Electric Vehicles and Plug-in Hybrid Electric Vehicles operating in V2G mode, has also been left out of the scope of this research.

1.3. Significance of estimating performance degradation due to Vehicle to Grid operation

In order to understand, optimize and price Vehicle to Grid services, it is essential to quantify the magnitude of automotive power component (Fuel Cell and/or High Voltage Battery) degradation caused due to Vehicle to Grid operation. Figure 1.3 schematically represents how Vehicle to Grid operation impacts the Electric Vehicle, specifically the Fuel Cell of Fuel Cell and Fuel Cell Range Extender Electric Vehicles; and how the caused performance degradation of the Fuel Cell in-turn impacts the cost of Vehicle to Grid energy delivered by the Electric Vehicle.

The cost of operation is composed of fuel cost and depreciation of power components. Depreciation of power components is a consequence of performance decay. This depreciation of power components also causes a depreciation of the Electric Vehicle itself. To maintain profits, this depreciation would have to be accounted for over time and usage, while computing cost of the Vehicle to Grid

energy produced by the Electric Vehicle. The depreciation would cause a rise in the cost of each unit of energy produced.

Furthermore, performance degradation and fuel cost are inherently linked since degradation causes reduction in fuel conversion efficiency. Reduction in fuel conversion efficiency leads to a rise in fuel consumption for producing the same unit of energy. Rise in fuel consumption increases fuel cost to producing the same unit of energy, thereby increasing the cost of that unit of energy produced by the Electric Vehicle.

Thus, estimating performance loss with considerable accuracy becomes crucial to the development of financial models for computing cost of Vehicle to Grid energy. Following this, market models could then define the price of the energy produced by taking into account the cost incurred.

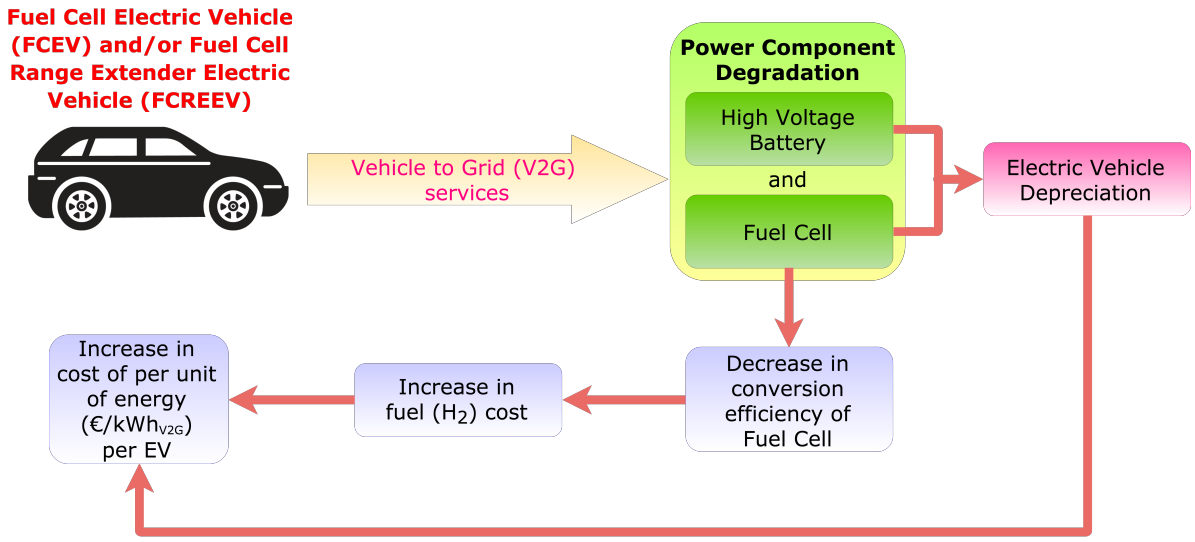

Figure 1.3: Schematic describing the impact of Vehicle to Grid services on Fuel Cell and Fuel Cell Range Extender Electric Vehicles and the impact on the cost of V2G energy delivered

1.4. Need for conducting simulated Vehicle to Grid experiments

Within the Car as Power Plant project at The Green Village in The Netherlands, The Technical University of Delft (TU Delft) has purchased a Hyundai Tuscon ix35 Hydrogen Fuel Cell Electric Vehicle (FCEV). This vehicle is used to help study the effects of real-world operation and to fully understand and develop the potential of FCEVs [35]. Figure 1.4 schematically represents the electrical architecture and the modification made to the Hyundai FCEV, to allow it to also operate in V2G mode. The FCEV's power components consists of a 100kW PEM Fuel Cell stack and 24kW High Voltage Battery connected through a Bi-directional High Voltage DC-DC converter (BHDC) to the High Voltage Junction Box (HVJB) which houses the internal components and also to the electric motor which drives the wheels.

With the assistance of Hyundai, the vehicle was modified to have a Direct Current (DC) outlet plug (V2G Type 1 socket) from the High Voltage Junction Box. This gives the Hyundai FCEV the added ability to operate in vehicle-to-grid (V2G) mode by connecting the V2G Type 1 socket to a external discharge unit. The discharger unit serves as a simulated grid load and also performs the DC $\rightarrow$ AC conversion before delivering the electricity to the Dutch national electricity grid. The desired V2G load

(AC) needed to be delivered by the FCEV operating in V2G mode, is therefore controlled via the discharger unit, and is user defined. Figure 1.5 schematically represents the electrical architecture of the discharger unit. The interested reader is referred to [34] for detailed understanding of the TU Delft Fuel Cell Electric Vehicle to Gird (FCEV2G) setup.

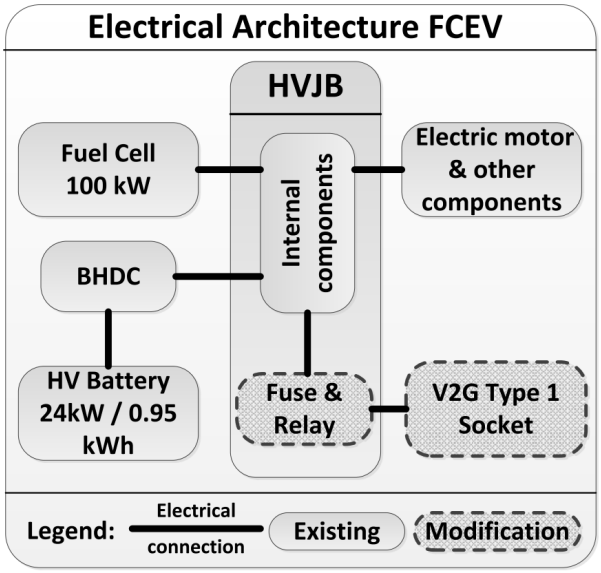

Figure 1.4: Electrical architecture schematic of the Hyundai ix35 FCEV modified for Vehicle to Grid capabilities [34]

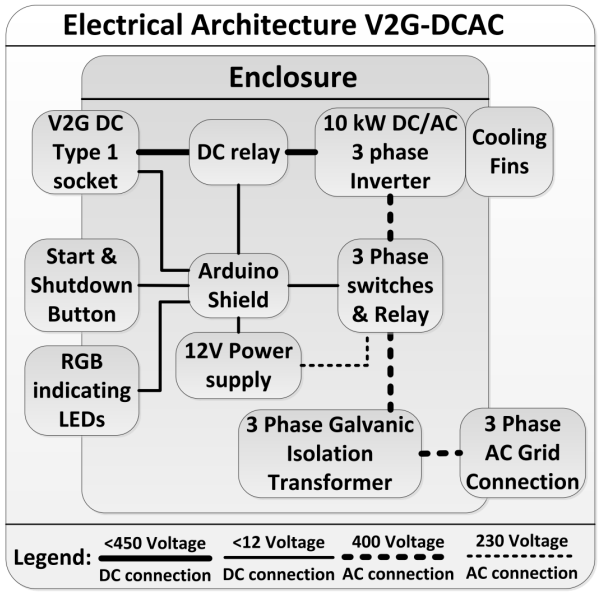

Figure 1.5: Electrical architecture schematic of the discharger unit connecting the FCEV to the National Grid [34]

Figure 1.6 shows the Hyundai ix35 FCEV connected to the discharger unit (white box) while operating in V2G mode at the TU Delft Green Village site. The FCEV is also equipped with a CAN bus data logger and 63 sensor channels that constantly record important parameters such as Fuel Cell (FC) Voltage, FC Current, FC Coolant Temperature, High Voltage Battery (HVB) DC Voltage, HVB DC Current, etc. This data is then analyzed to understand the effect of operation on the various components of the FCEV [33]. It is therefore theoretically possible to estimate Fuel Cell performance degradation caused by V2G operation, using an actual FCEV2G setup. But doing this is not practical, since the

setup has a few limitations. These limitations result in the need to conduct simulated V2G experiments on a laboratory test bench. The limitations will be discussed in the following sub-sections.

Figure 1.6: Hyundai ix35 Fuel Cell Electric Vehicle operating in V2G mode in a actual V2G set-up at the TU Delft Green Village site

1.4.1. Inability to perform long-term Vehicle to Grid experiments using Hyundai Fuel Cell Electric Vehicle

Long term testing is required to quantify Fuel Cell performance degradation due to Vehicle to Grid operation. Performance loss may be split into recoverable and irreversible performance losses [13, 22]. The standardized definition of the term “degradation” according to the norm set by EN 13306 [2] is: “An irreversible process in one or more characteristics of an item with either time, use or an external cause.” Since degradation itself is irreversible, only the magnitude of irreversible performance loss due to Vehicle to Grid applications is of interest. Ref. [4, 7, 39, 43] state that if the duration of an undesired condition is short, then the performance loss is usually recoverable, otherwise system degradation occurs.

The reversible or recoverable losses occur during approximately the first 20 hours of continuous operation, whereas irreversible losses occur subsequently [22]. Furthermore, authors of Ref. [37] state that the main cause for reduction in Remaining Useful Lifetime (RUL) of PEMFCs is the accumulation of degradation and aging effects over time. As shown in Figure 1.7 the time scale of hours to days is required to accurately simulate and quantify aging effects and permanent performance losses. Therefore, it is imperative that accurate quantification of irreversible performance losses caused due to V2G operation can only be achieved through long-term testing.

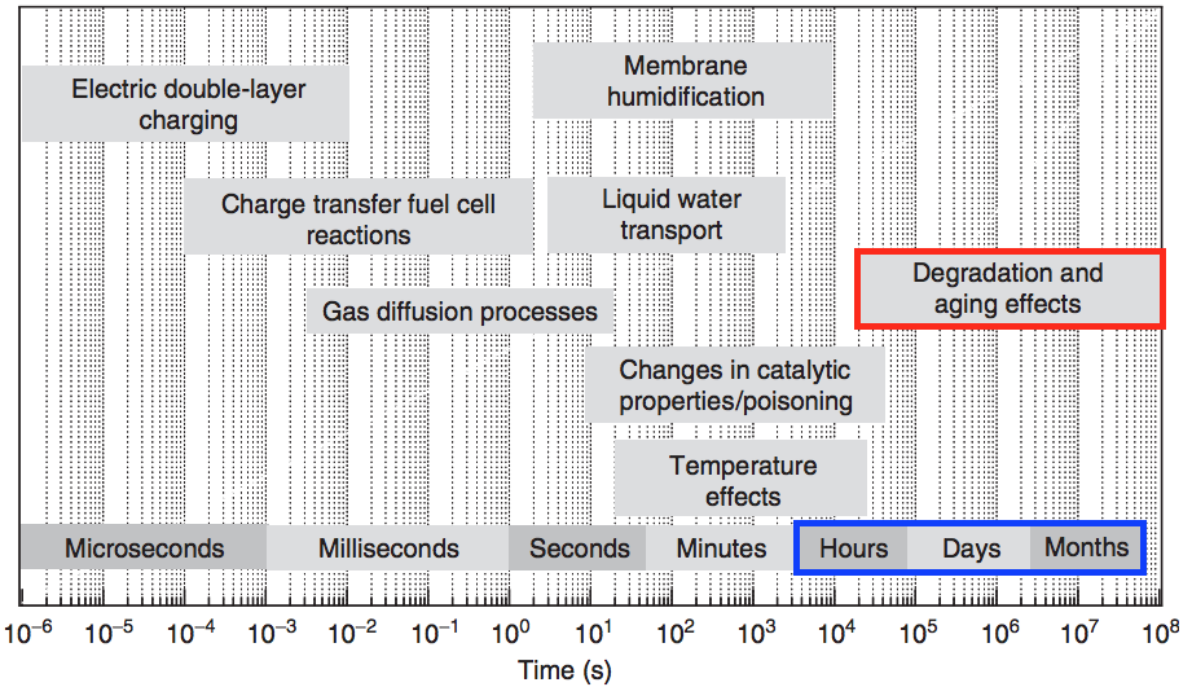

Figure 1.7: PEMFC processes and their time scales [51]

Volume limitation of the fuel tank in the Hyundai Fuel Cell Electric Vehicle: The Hyundai FCEV's fuel-tank volume restriction does not permit for long-term experiments. Accurately quantifying degradation only due to V2G operation, using recorded data from the FCEV, is difficult. The fuel tank is designed to hold 5.64 kg of Hydrogen [14]. Figure 1.8 represents the inverse relation between energy delivered by the Hyundai FCEV in V2G mode (at constant power) with the mass of Hydrogen in the fuel tank of the FCEV. Both, the energy delivered and mass of hydrogen present were computed using data recorded in the FCEV during 1 $hour$ of V2G operation at two different discharger rating (load simulated by the discharger unit) of 9.5kW AC and 7kW AC. The FCEV delivers 9.5kWh of electrical energy in 1 $hour$ at constant power of 9.5kW and 7kWh of electrical energy in 1 $hour$ at constant power of 7kW.

It can be seen that as the energy delivered by the FCEV increases, the mass of Hydrogen in the tank decreases. Assuming 90% of the fuel may be used for FCEV2G operation, the duration of the actual Vehicle to Grid experiment is limited to approximately 8.5 hours of continuous operation at a discharger rating (or simulated load) of 9.5kW AC (Figure 1.8(a)) at a fuel consumption rate of 0.6 kgh^{-1}. The same mass of fuel would last for 12.7 hours at discharger rating of 7kW AC (Figure 1.8(b)) at a fuel consumption rate of 0.4 kgh^{-1}.

Conducting Fuel Cell Vehicle to Grid experiments of 200 hours at discharger rating of 9.5kW AC, would therefore require a minimum of 24 refueling trips. The degradative effects occurring during these driving trips, due to Fuel Cell start-stop sequences, idling, high load operation and driving load ramps

[38] *etc.* cannot be discounted and separated from the pure Vehicle to Grid data. Therefore, because of the duration limitations of the actual Fuel Cell Vehicle to Grid experiments, it is proposed to simulate Vehicle to Grid operating conditions on a laboratory test bench in order to study the impact of Vehicle to Grid operation on Fuel Cell durability.

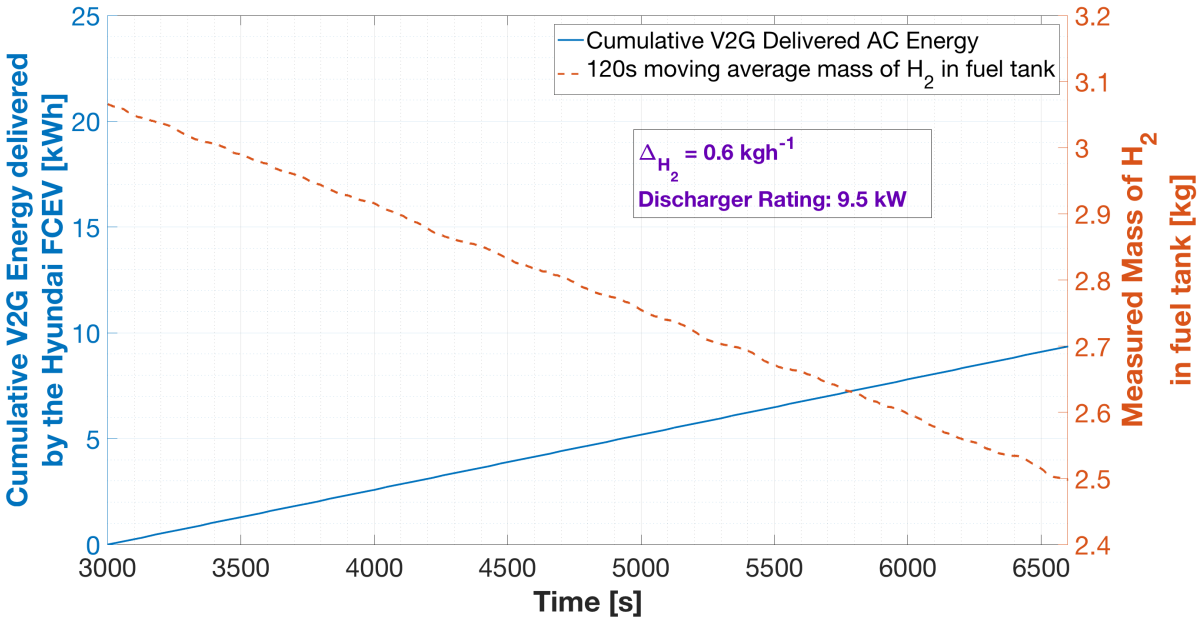

(a) Fuel and Energy Relation during 1 hour of FCEV2G operation at 9.5kW discharger rating

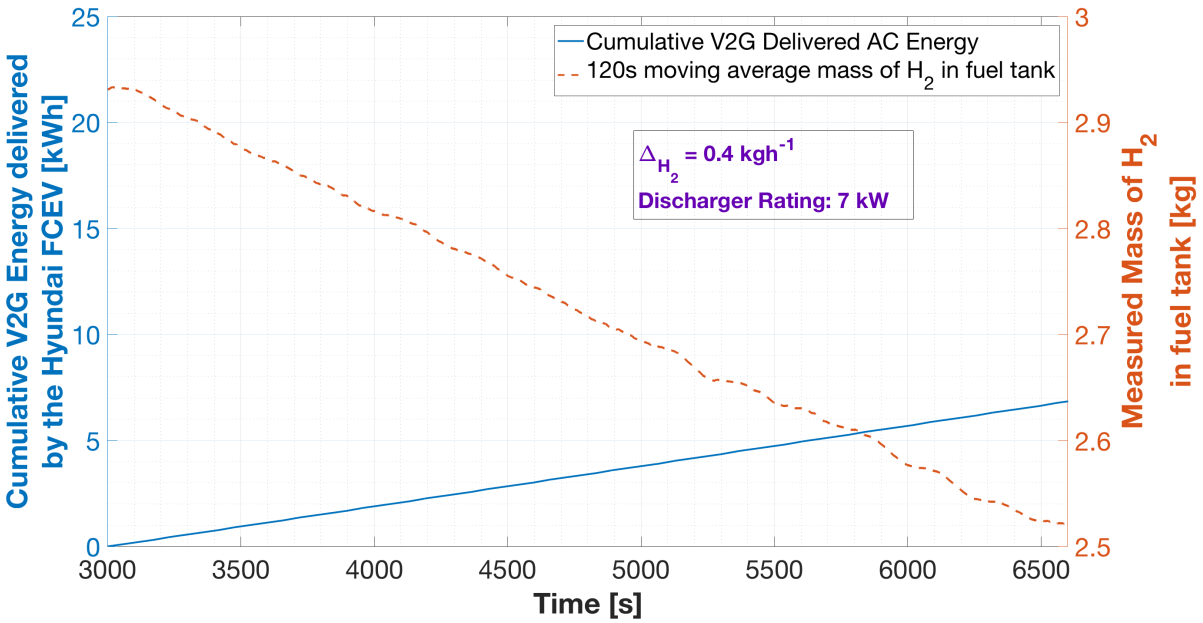

(b) Fuel and Energy Relation during 1 hour of FCEV2G operation at 7kW discharger rating

Figure 1.8: Fuel and Energy Relation during Hyundai FCEV2G operation

1.4.2. Variety of applicable power management strategies

Another reason for conducting simulated Vehicle to Grid experiments on a laboratory test bench is limited control over the programmed power management strategy employed during Vehicle to Grid operation, to distribute the Vehicle to Grid load between the Fuel Cell (FC) and the High Voltage Battery (HVB) within the Hyundai Fuel Cell Electric Vehicle.

Power management strategy may be defined as the distribution of load between the power delivery components (FC and HVB) within the Fuel Cell and Fuel Cell Range Extender Electric Vehicle. In Vehicle to Grid mode, the power management strategy depends on the load (power) demanded by the grid (Vehicle to Grid load) and the technical specifications of the FC and HVB combination present inside the Electric Vehicle: FC power rating, HVB capacity rating and allowable depth of discharge range of the HVB. Furthermore, the power management strategy also depends on the drivetrain architecture in which these power components (FC and HVB) are connected electrically. The technical specifications and the drivetrain architecture are Electric Vehicle (FCEV and/or FCREEV) specific.

Drivetrain architecture describes the method in which the Fuel Cell and High Voltage Battery are connected electrically: FC and HVB connected in series or parallel. Figure 1.9 schematically represents how the power delivery components (Fuel Cell and High Voltage Battery) are connected in different types of drivetrain architecture, to deliver power for automotive operations (driving and/or Vehicle to Grid). In series drivetrain architecture, the Fuel Cell charges the High Voltage Battery, while only the HVB powers all automotive operations. In parallel drivetrain architecture both, the Fuel Cell and High Voltage Battery operate asynchronously or simultaneously to provide power for automotive operations. It should be noted that the electric motor is actually present within the vehicle's body and is responsible for delivering torque to the wheels, while the V2G discharger unit is present externally.

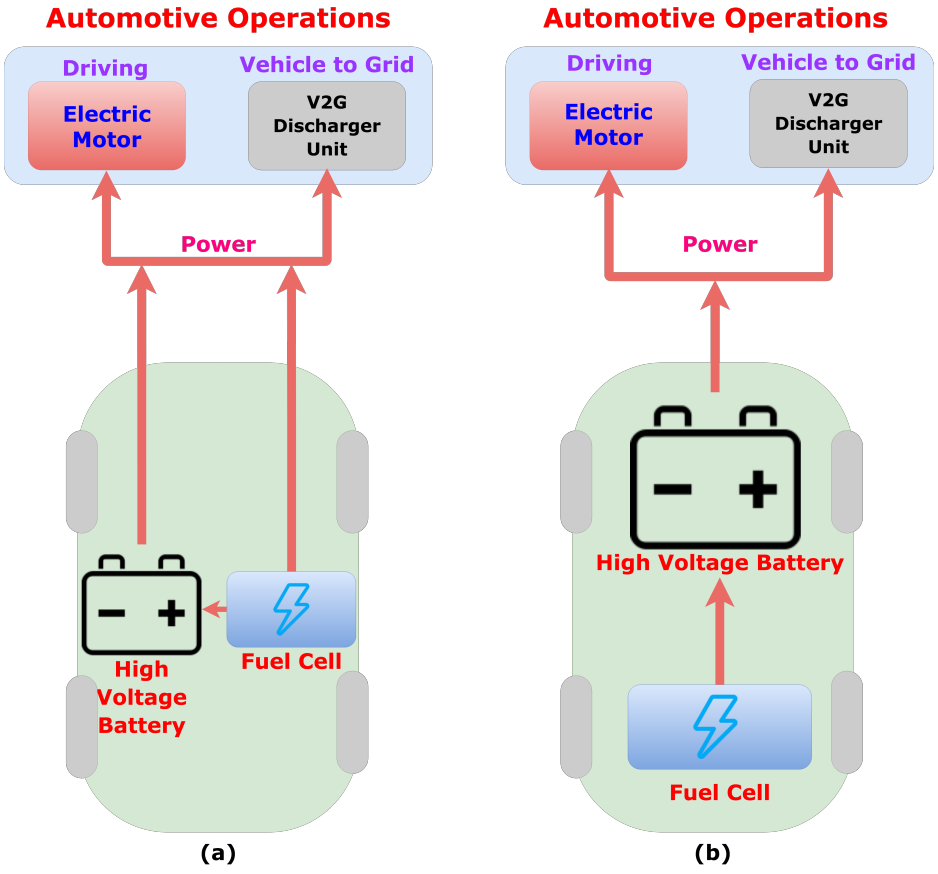

Figure 1.9: Types of drivetrain architecture in Fuel Cell Electric Vehicles and Fuel Cell Range Extender Electric Vehicles
(a) Parallel drivetrain architecture (b) Series drivetrain architecture

Today, Fuel Cell Electric Vehicles and Fuel Cell Range Extender Electric Vehicles are available with a variety of FC-HVB combinations, with varying ***technical specifications***. These variations may be grouped in 3 major categories [29, 44, 46, 47, 59]:

1. ***High Power FC with Low Capacity HVB (FC dominant)*** -
   Hyundai ix35, Toyota Mirai, Honda FCV Clarity, Mercedes Benz GLC F-CELL
2. ***Low Power FC with High Capacity HVB (HVB dominant)*** - Renault kangoo BEV
3. ***High Power FC with High Capacity HVB or Low Power FC with Low Capacity HVB (equally dominant)*** - Toyota FC Heavy Truck, UPS Fuel Cell delivery truck

The drivetrain architecture for these also vary depending on the type of Electric Vehicle. Fuel Cell Electric Vehicles (FCEVs) are usually Fuel Cell dominant with the Fuel Cell and the High Voltage Battery connected in parallel drivetrain architecture; whereas Fuel Cell Range Extender Electric Vehicles (FCREEVs) are High Voltage Battery dominated with the Fuel Cell and the High Voltage Battery connected in series drivetrain architecture. The Electric Vehicles in the equally dominant category may consist of either a series or parallel drivetrain architecture.

Translation of Grid load to Fuel Cell load cycle inside the Electric Vehicle: Figure 1.10 describes schematically how a combination of the power management strategy and the number of Electric Vehicles available for delivering Vehicle to Grid Power, define how the load demanded by the grid (V2G load serviced by the vehicle) translates to the load cycle for the Fuel Cell in the Electric Vehicle (FCEV and/or FCREEV). This Fuel Cell load cycle has an influence on the degradation of the Fuel Cell in Vehicle to Grid operation [5, 38].

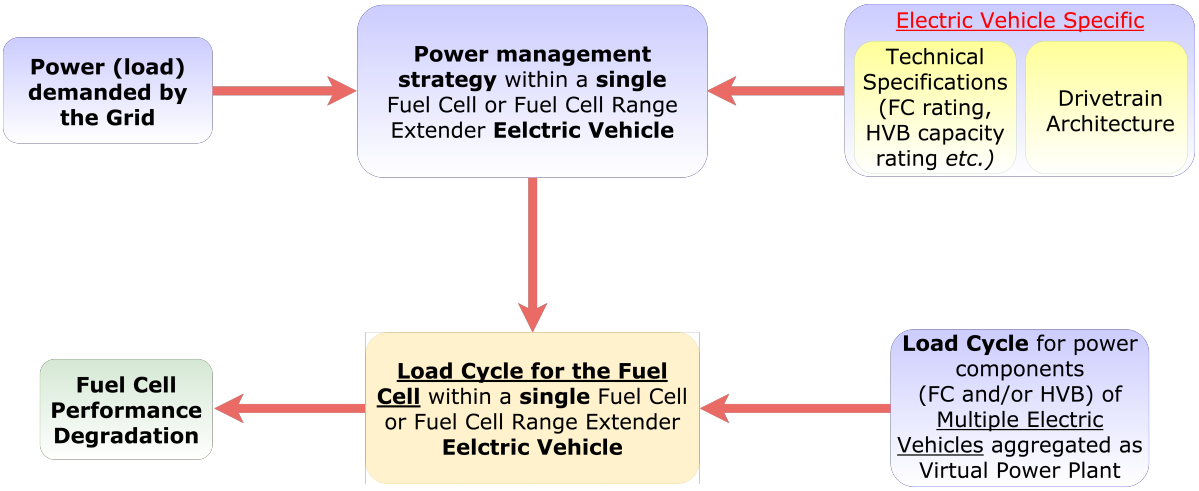

Figure 1.10: Schematic describing Translation of Grid load to Fuel Cell load cycle inside the Electric Vehicle

In the following paragraphs, a 5-case (hypothetical) example is used to illustrate how a certain grid load can be serviced by 5 different FC-HVB combinations connected in different drivetrain architectures within a single Electric Vehicle; and how these variations result in different Fuel Cell load cycles while servicing the same grid load. Each load cycle would cause a different magnitude of performance degradation in the Fuel Cell.

Figure 1.12 shows the power management strategy that could be employed to service the same Vehicle to Grid load, depending on the type of FC-HVB combinations (FC, HVB or Equally dominated) and the drivetrain architecture in which they are connected within an Electric Vehicle. The Vehicle to Grid load is a constant load of $5kW$ as shown in Figure 1.11. The period for which the Electric Vehicle would be expected to service the load is 1 $hour$ ($3600s$).

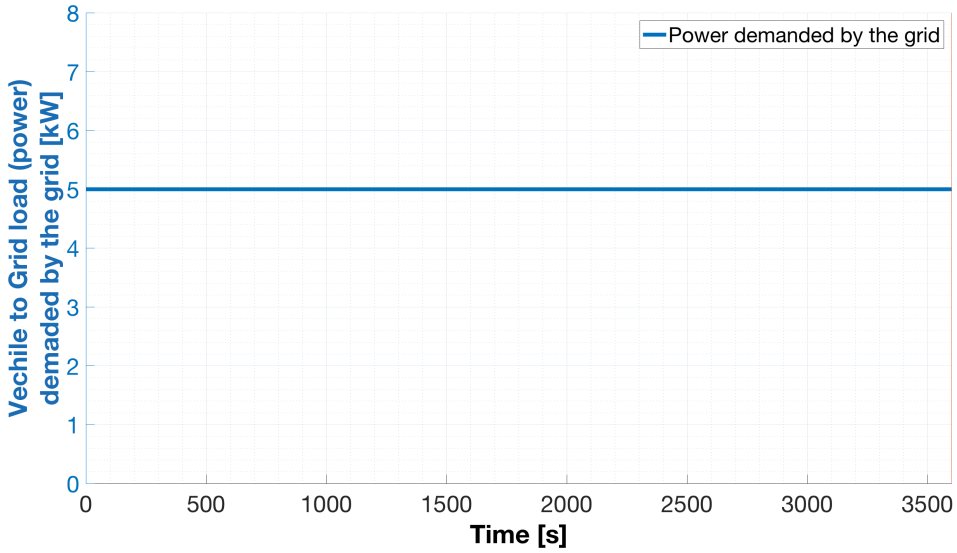

Figure 1.11: Constant Load needed to be serviced by the Electric Vehicle

Case 1: Figure 1.12 (a) shows the power management strategy employed by an Electric Vehicle with a Fuel Cell dominated FC-HVB combination connected in parallel drivetrain architecture. The power management strategy involves periodic operational switching between the Fuel Cell and the High Voltage Battery, to service the constant load of 5kW demanded by the grid (Vehicle to Grid load). The duration for which the High Voltage Battery operates (150s) is shorter as compared to the Fuel Cell (450s) because of it's lower capacity rating (Low capacity High Voltage Battery). Higher Fuel Cell Power (6.67kW) as compared to the Vehicle to Grid power demanded by the Grid (5kW) represents the excess power required to charge the High Voltage Battery while simultaneously delivering the required Vehicle to Grid power to the grid. During discharging, the High Voltage Battery is observed to deliver $\left(5kW \times \frac{150}{3600}h\right) = \frac{5}{24}\ kWh$ of energy. Assuming perfect charging and discharging, the Fuel Cell would have to deliver the same magnitude of energy to the High Voltage Battery in 450s of operation, while also servicing the Vehicle to Grid load of 5kW. This therefore results in the Fuel Cell needing to operate at 6.67kW for 450s. Figure 1.12 (b) shows only the Fuel Cell load cycle for this type of power management strategy.

Case 2: For an Electric Vehicle with a High Voltage Battery dominated FC-HVB combination connected in parallel drivetrain architecture, due to it's higher capacity rating, the duration for which the High Voltage Battery can service the demanded load is higher (450s). This causes the Fuel Cell to operate for a shorter duration (150s) in a power management strategy where periodic operational switching occurs between the Fuel Cell and the High Voltage Battery. This type of power management strategy is shown in Figure 1.12 (c). Figure 1.12 (d) shows only the Fuel Cell load cycle for this type of power management strategy. Similar to Case 1, the higher power for the Fuel Cell also represents power required to charge the High Voltage Battery in the given operating duration (150s).

Case 3: Figure 1.12 (e) shows the power management strategy employed by an Electric Vehicle with a Fuel Cell dominated FC-HVB combination connected in parallel drivetrain architecture, but where the HVB is disconnected and thus does not participate in Vehicle to Grid operation. This strategy could be applicable to avoid load cycling in the Fuel Cell and the High Voltage Battery as load cycling is known to cause degradation of these components, especially the Fuel Cell [5, 38]. This type of power management strategy therefore involves constant operation of the Fuel Cell to service the constant load of 5kW demanded by the grid. Figure 1.12 (f) shows only the Fuel Cell load cycle for this type of power management strategy.

Case 4: For an Electric Vehicle with a High Voltage Battery dominated FC-HVB combination connected in series drivetrain architecture, it could be possible to service the entire Vehicle to Grid load by only operating the High Voltage Battery while disconnecting the Fuel Cell completely. This power management strategy can only be employed when the energy capacity rating of the High Voltage Battery is high, and it is able to constantly service the entire grid load (power) demand without requiring to be recharged by the Fuel Cell. This type of power management strategy is shown in Figure 1.12 (g). Figure 1.12 (h) shows only the Fuel Cell load cycle for this type of power management strategy. The power drawn from the Fuel Cell in this case would constantly be $0kW$.

Case 5: Figure 1.12 (i) represents a power management strategy for an Electric Vehicle with an Equally dominated FC-HVB combination connected in series drivetrain architecture. Here the constant Vehicle to Grid load is serviced by the High Voltage Battery while the Fuel Cell simultaneously replenishes the energy delivered by the High Voltage Battery to the grid. Figure 1.12 (j) shows only the Fuel Cell load cycle for this type of power management strategy. The Fuel Cell load cycle in this case is similar to the Fuel Cell load cycle in the power management strategy employed by an Electric Vehicle with a Fuel Cell dominated FC-HVB combination connected in parallel drivetrain architecture, but where the HVB is disconnected (Figure 1.12 (e) and (f)).

From the 5 Cases described above it can be seen that the Fuel Cell load cycle in Vehicle to Grid operation strongly depends on the type of the FC-HVB combination, the drivetrain architecture in which they are connected and how the power management strategy is programmed.

Moving further, in order to avoid uncertainty in terms of vehicle availability for driving purposes and those required for servicing a desired grid load, and also to increase financial incentives for Vehicle to Grid operation, it is likely that in the future multiple Electric Vehicles would be aggregated to operate as a Virtual Power Plant[17, 26]. In such a case, the Fuel Cell load cycle in a single Electric Vehicle, would vary further since the Vehicle to Grid load would now be shared among multiple vehicles. This would create further variations in possible power management strategies and Fuel Cell load cycles; where each load cycle causes a different magnitude of performance degradation in the Fuel Cell.

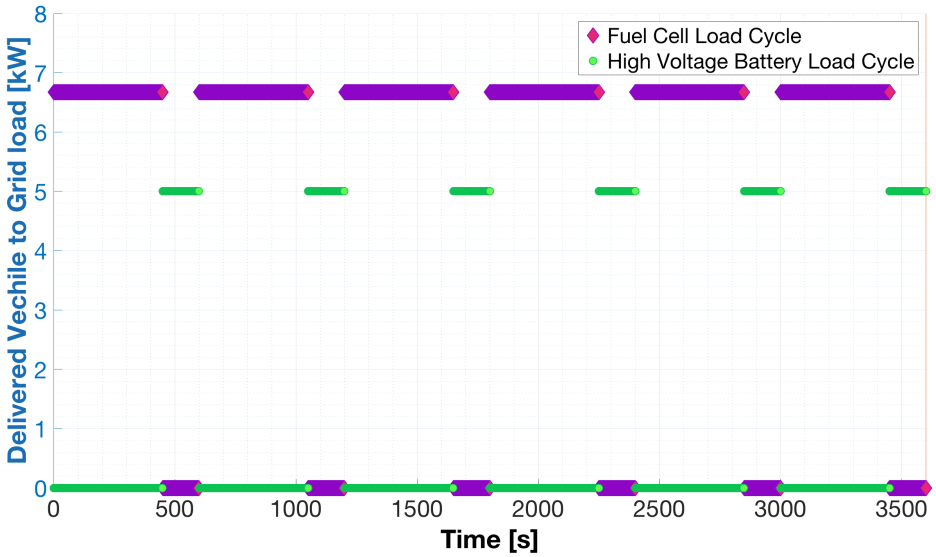

(a) **Case 1:** FC dominated FC-HVB combination in parallel drivetrain achitecture

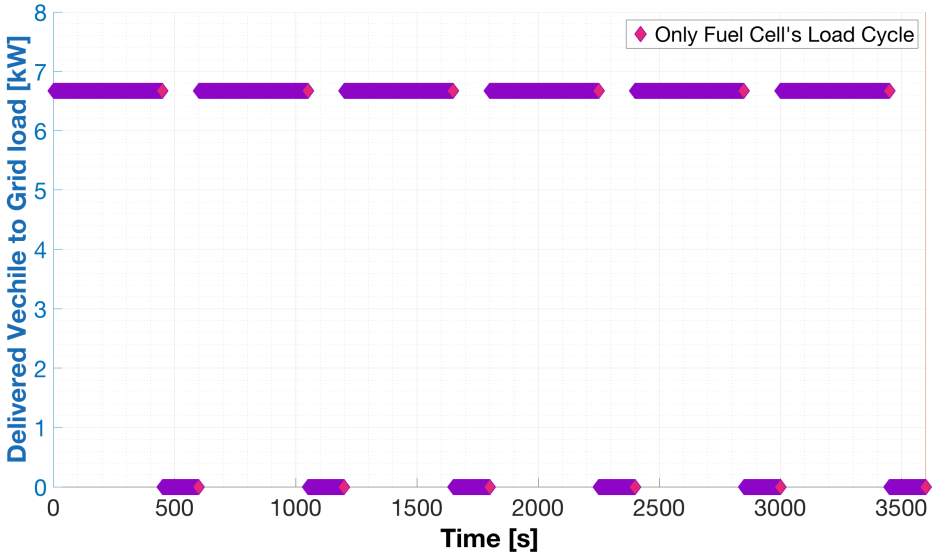

(b) **Case 1:** Equvalent FC load cycle for FC dominated FC-HVB combination in parallel drivetrain achitecture

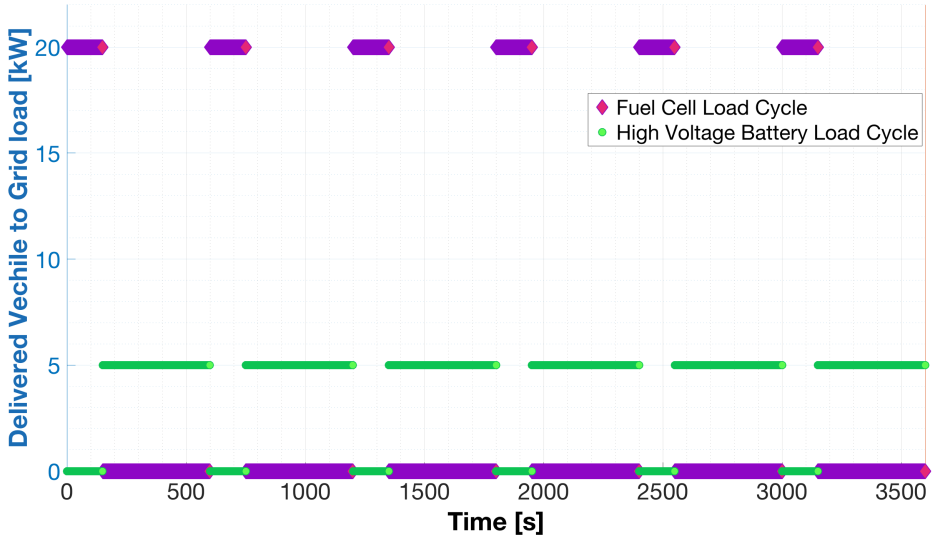

(c) **Case 2:** HVB dominated FC-HVB combination in parallel drivetrain achitecture

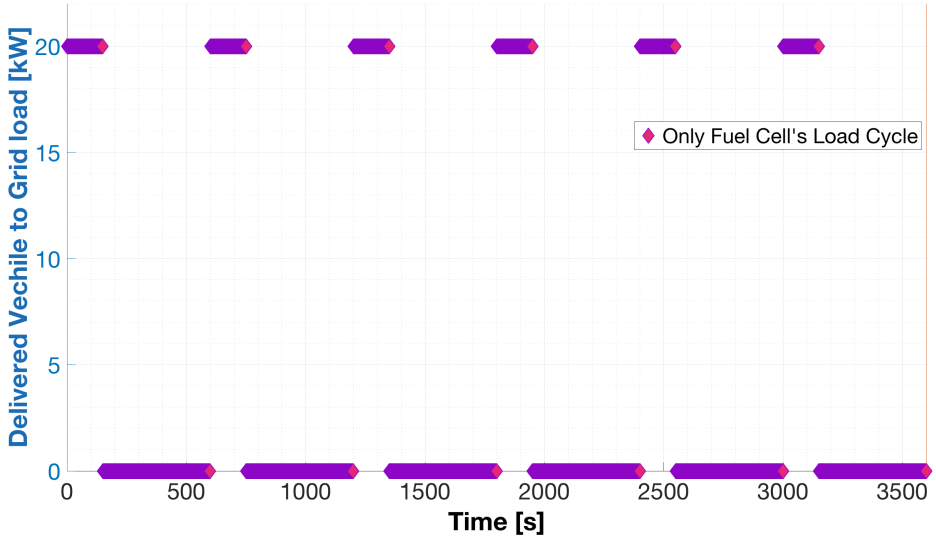

(d) **Case 2:** Equvalent FC load cycle for HVB dominated FC-HVB combination in parallel drivetrain achitecture

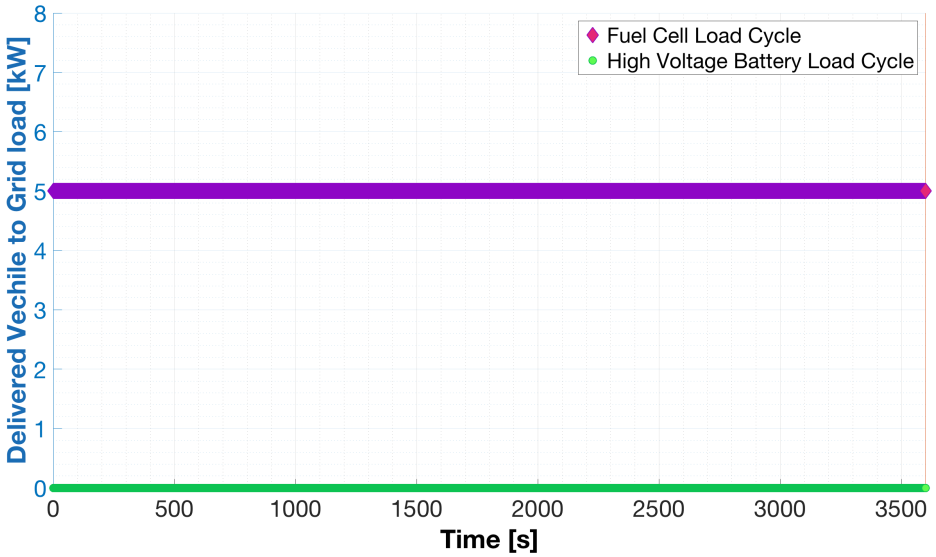

(e) **Case 3:** FC dominated FC-HVB combination in parallel drivetrain achitecture, with disconnected HVB

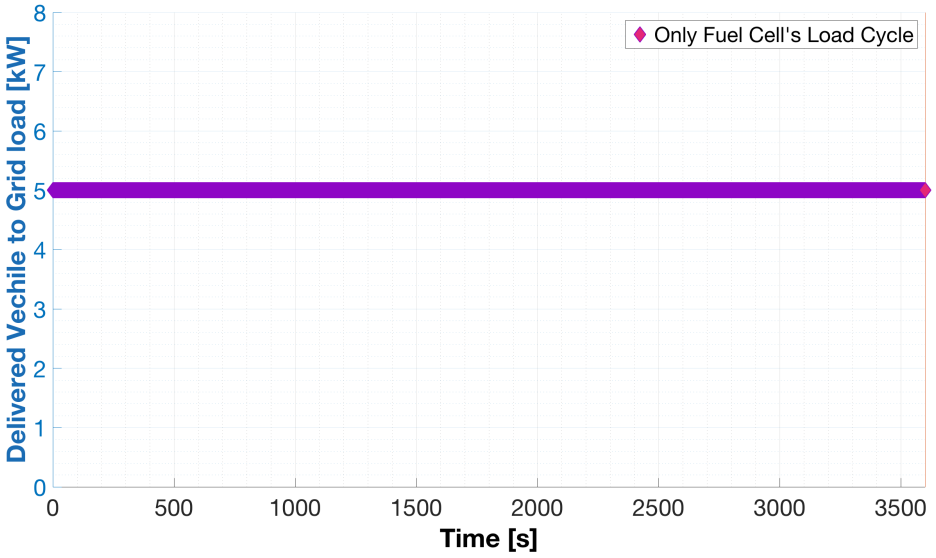

(f) **Case 3:** Equvalent FC load cycle for FC dominated FC-HVB combination in parallel drivetrain achitecture, with disconnected HVB

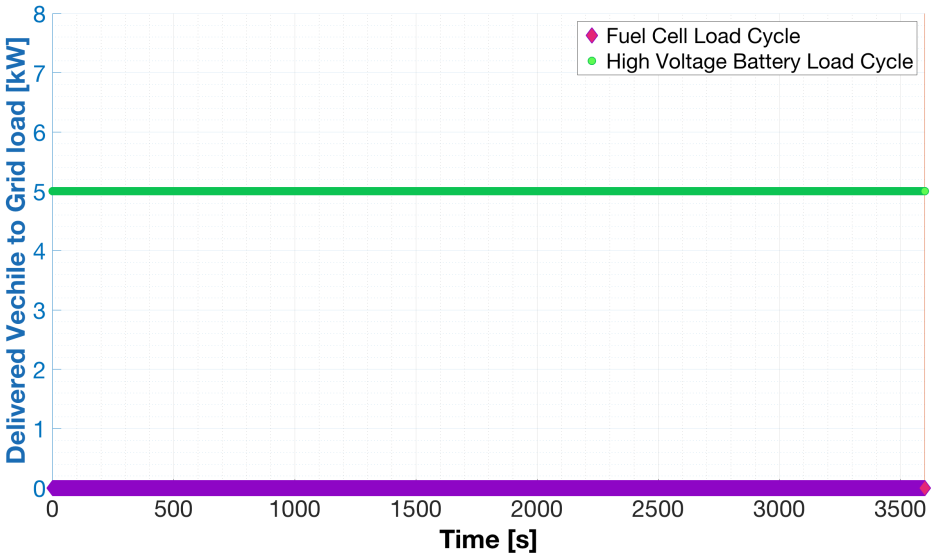

(g) **Case 4:** HVB dominated FC-HVB combination in series drivetrain achitecture, with disconnected FC

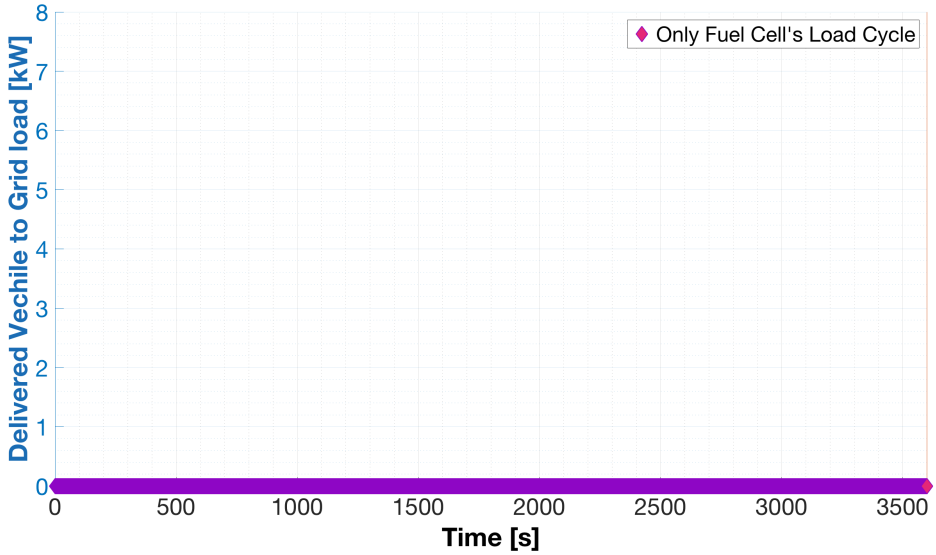

(h) **Case 4:** Equvalent FC load cycle for HVB dominated FC-HVB combination in parallel drivetrain achitecture, with disconnected FC

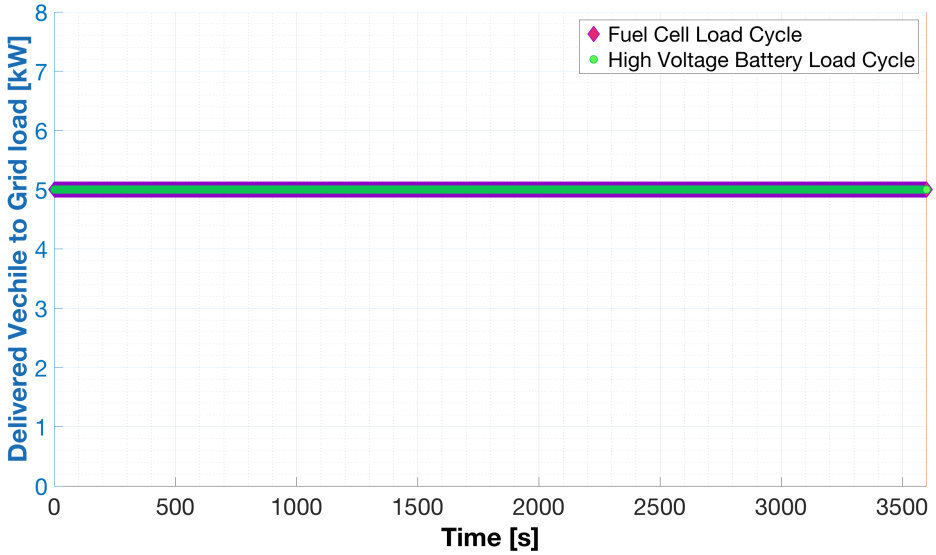

(i) **Case 5:** Equally dominated FC-HVB combination in series drivetrain achitecture, with FC constantly charging the HVB

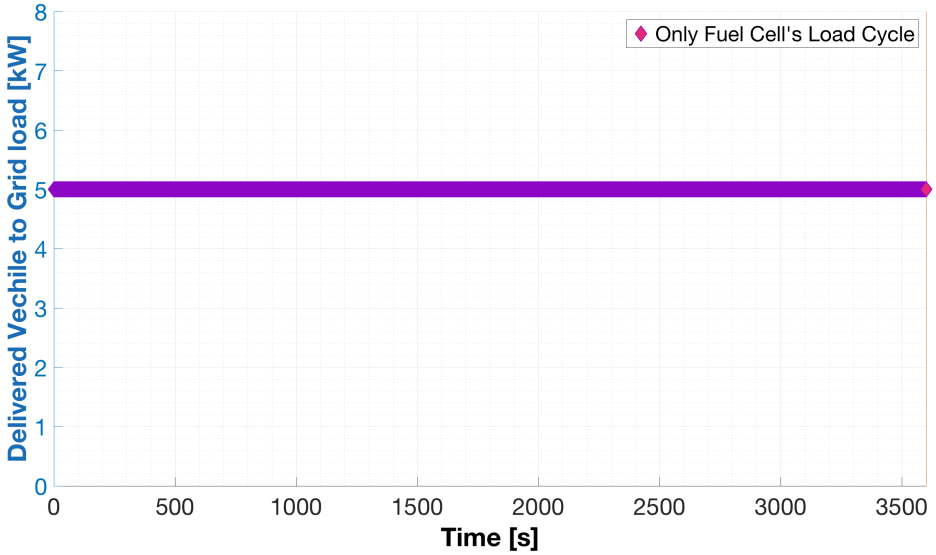

(j) **Case 5:** Equvalent FC load cycle for an Equally dominated FC-HVB combination in series drivetrain achitecture, with FC constantly charging the HVB

Figure 1.12: Power management strategy employed to service a given grid load, by some types of FC-HVB combinations connected in series or parallel drivetrain architecture

1.4.3. Inability to change power management strategy programmed in Hyundai Fuel Cell Electric Vehicle:

The power management strategy described in Case 1 is also observed in the Hyundai Fuel Cell Electric Vehicle, which is a typical Fuel Cell dominated FCEV with parallel drivetrain architecture. Figure 1.13 was produced using recorded unfiltered data from Vehicle to Grid operation of the Hyundai FCEV. It graphically represents the power management strategy employed to service a constant Vehicle to Grid load of 9.5kW AC. The power management strategy consists of operational transitioning between the High Voltage Battery and the Fuel Cell of the FCEV.

In a single transition cycle, the Fuel Cell first services the constant Vehicle to Grid load, while simultaneously charging the High Voltage Battery. Following this, in the same transition cycle, the Fuel Cell idles at 0kW while only the High Voltage Battery services the Vehicle to Grid load. The time of transition is determined by the state of charge (SOC) of the High Voltage Battery, and is periodic because of the constant nature of the Vehicle to Grid load. At the lower SOC threshold (42%) the Fuel Cell takes over while at the higher SOC threshold (57%) the Fuel Cell is disconnected by drawing a current of 0A (idling), and only the High Voltage Battery services the Vehicle to Grid load. High Voltage Battery charging is represented by increasing State of Charge (SOC), and discharging by decreasing SOC.

During it's operation, the power delivered by the Fuel Cell is higher than the constant Vehicle to Grid load (9.5kW) because it also charges the High Voltage Battery. Furthermore, the Fuel Cell power reduces as the State of Charge of the High Voltage Battery increases, since the rate of charging for batteries decreases as State of Charge increases.

Furthermore, the DC power delivered by the High Voltage Battery ($\approx$ 10.75kW AC) is higher than the Vehicle to Grid load (9.5kW AC) to accommodate for DC $\rightarrow$ AC conversion efficiency of the inverter. It is expected that this conversion efficiency is also taken into account when only the Fuel Cell services the Vehicle to Grid load.

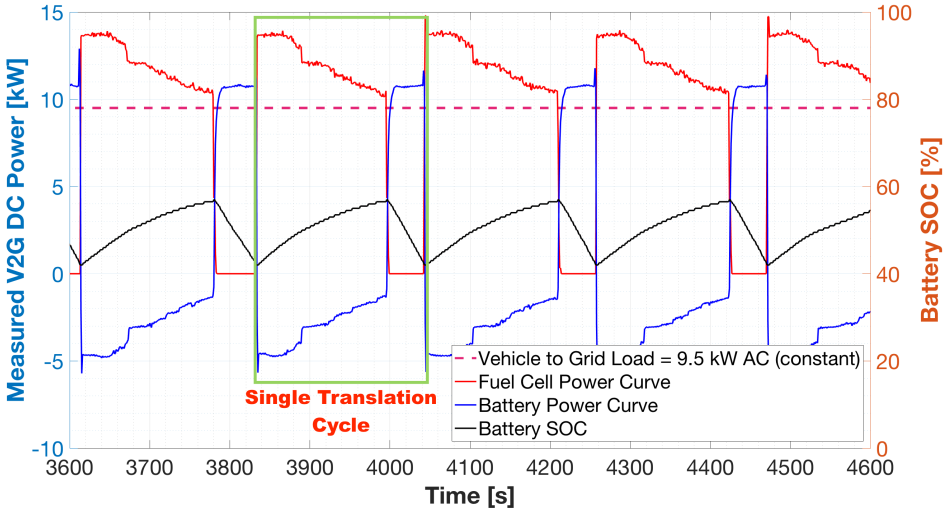

Figure 1.13: Power management strategy of the Hyundai FCEV operating in Vehicle to Grid mode at 9.5kW Vehicle to Grid load

Figure 1.14 shows the power management strategy in the Hyundai FCEV while servicing a constant Vehicle to Grid load of 7kW AC. It was also produced using data recorded in the Hyundai. Operational switching between the Fuel Cell and the High Voltage Battery is observed once again, but the Fuel Cell load cycle is different compared to the load cycle at 9.5kW Vehicle to Grid load. Figure 1.15 shows only the Fuel Cell load cycle for the Hyundai FCEV operating in Vehicle to Grid mode to service Vehicle to Grid loads of 7kW and 9.5kW. The difference in the Fuel Cell load cycles can be seen by comparing the operating durations of the Fuel Cell and the High Voltage Battery. At 9.5kW AC Vehicle

to Grid load, the Fuel Cell operates for approximately 170s after which it idles for 49s. At 7kW, the Fuel Cell operates for approximately 160s after which it idles for 70s. At 7kW the larger idling time for the Fuel Cell is because the same High Voltage Battery is able to service the lower Vehicle to Grid load for a longer duration. At 9.5kW the longer operating time of the fuel cell is because the High Voltage Battery takes longer to charge; since a larger percentage of the fuel cell power is consumed to service the higher Vehicle to Grid load.

Each of these Fuel Cell load cycles would cause a different magnitude of Fuel Cell performance degradation in the Hyundai FCEV. This power management strategy consisting of operational transitioning between the High Voltage Battery and the Fuel Cell of the FCEV, is fixed and is difficult to change without the assistance of Hyundai.

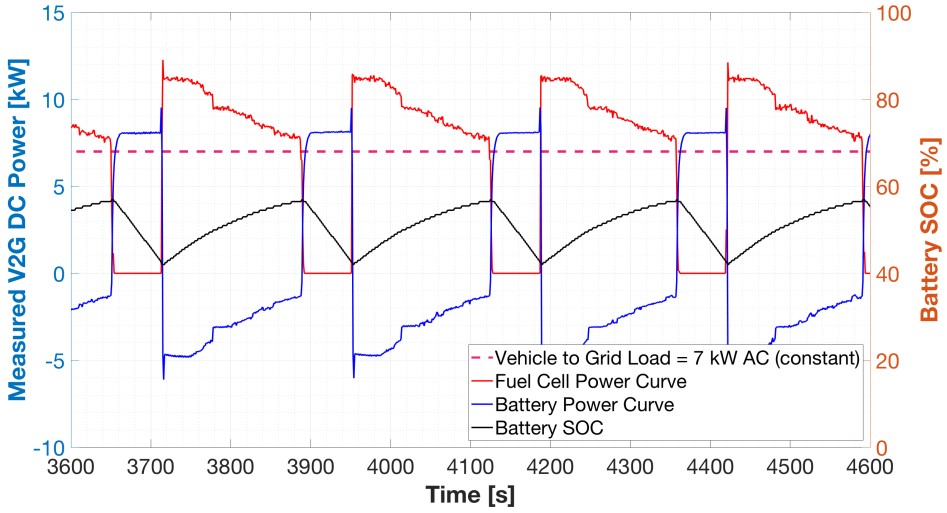

Figure 1.14: Power management strategy of the Hyundai FCEV operating in Vehicle to Grid mode at 7kW Vehicle to Grid load

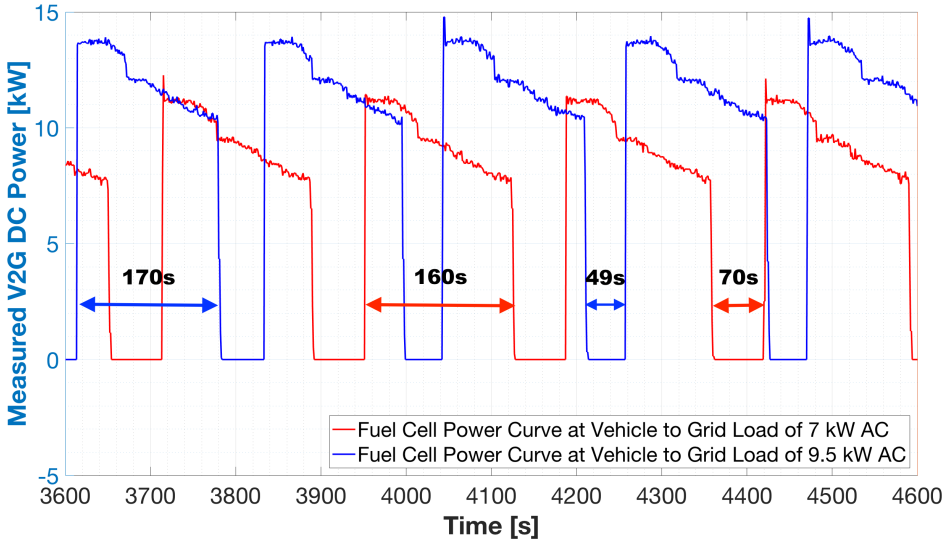

Figure 1.15: Fuel Cell load cycle of the Hyundai FCEV while servicing two different Vehicle to Grid loads

Conducting actual Vehicle to Grid experiments using the Hyundai Fuel Cell Electric Vehicle therefore limits the power management strategy that can be tested, since it has been programmed into the vehicle and is difficult to change. Furthermore, the Hyundai FCEV represents only a single type of FC-HVB combination connected in only one type of drivetrain architecture. Therefore, there is a need to ensure that Fuel Cell degradation studies for Vehicle to Grid operation are applicable to all types of power management strategies, FC-HVB combinations and drivetrain architectures. Simulating Vehicle to Grid operation on a laboratory test bench therefore permits easy testing of these variations.

1.4.4. Advantages of small-scale experiments

Compared to actual Vehicle to Grid experiments, small-scale laboratory experiments have some advantages. Conducting laboratory based simulated Vehicle to Grid experiments allows more control over the operating conditions within the fuel cell. Through higher control, it becomes possible to derive the optimal operating conditions for Vehicle to Grid operation of PEM Fuel Cells.

Furthermore, conducting small scale experiments leads to the possibility of understanding the degradative phenomenon (such as pin-hole and crack formation and propagation) that occur through in-situ electrochemical analysis and in-situ analysis using sensors on the active area; and also through ex-situ postmortem analysis techniques using Transmission and Scanning Electron Microscopes. Identifying these degradative phenomenon on a full-scale automotive Fuel Cell is challenging due to the vast size of the active area on which the appearance of these phenomenon might be spread out.

Finally, conducting long-term Vehicle to Grid experiments on the laboratory scale would be inexpensive as compared to conducting long-term experiments using the actual Hyundai FCEV, assuming the volume limitation of the fuel-tank is overcome.

1.5. Research Question and Outline

This research focuses on answering the question: ***How can the performance loss of the Fuel Cell in Electric Vehicle to Grid operation be estimated?***

To answer the main research question, the following sub questions need to be answered:

1. Can Vehicle to Grid experiments using the actual Vehicle to Grid set-up be used to quantify performance degradation in Fuel Cell due to Vehicle to Grid operation? Or is there a need to conduct simulated Vehicle to Grid experiments on a laboratory PEMFC test bench in order to accurately quantify performance degradation?
2. How can a small-scale simulated Vehicle to Grid experiment be designed and what Vehicle to Grid Fuel Cell load cycles should be simulated?

In **Chapter 1** it was first concluded that there is a need for conducting simulated Vehicle to Grid experiments on a laboratory PEMFC test bench; because of the inability to conduct long-term dedicated Vehicle to Grid experiments using the TU Delft Hyundai Fuel Cell Electric Vehicle and actual Vehicle to Grid set-up. Furthermore, it was described how limited control over the power management strategy programmed into the Hyundai Fuel Cell Electric Vehicle leads to the need for conducting simulated Vehicle to Grid experiments on a laboratory test-bench.

In **Chapter 2** the experimental PEMFC set-up on which Vehicle to Grid operation was simulated has been described. Furthermore, the experimental conditions for the simulated Vehicle to Grid experiments has been derived using data collected in the Hyundai FCEV during actual Vehicle to Grid operation. The Vehicle to Grid Fuel Cell load cycles, specific to the TU Delft Hyundai Fuel Cell Electric

Vehicle, that were simulated in the laboratory-based experiments have also been defined here. This was done using a literature survey and by envisioning Vehicle to Grid scenarios in which Fuel Cell Electric Vehicles are likely to operate. Finally, a method to translate the Fuel Cell load cycle, that was unique to the TU Delft Hyundai FCEV, to an equivalent Fuel Cell Current Cycle unique to the laboratory test-bench PEMFC has also been proposed.

In **Chapter 3** a description of the experimental methodology followed and the method used to compute the performance degradation of the test-bench PEMFC under simulated Vehicle to Grid operation, can be found. In **Chapter 4** the results of performance degradation measured for the test-bench PEMFC under simulated Vehicle to Grid operation have been presented and discussed. Finally, the conclusions drawn from this thesis and recommendation for future works can be found in **Chapter 5** and **Chapter 6** respectively.

1.6. Summary

While developing financial models to price Vehicle to Grid services it is important to include the impact of Vehicle to Grid operation on the power-delivery components of these Electric Vehicles. Considerable amount of academic research has been focused on understanding the impact of Vehicle to Grid operation on Battery Electric Vehicles (BEVs). However, information about the impact of Vehicle to Grid operation on the fuel cells (FCs) of Fuel Cell Electric Vehicles (FCEVs) and Fuel Cell Range Extender Electric Vehicles (FCREEVs) is scarce.

Long term tests are required to asses the impact of Vehicle to Grid operation on these fuel cells. The fuel tank volume limitation of the TU Delft Hyundai FCEV does not allow for long term Vehicle to Grid experiments using the operational Vehicle to Grid set-up at the TU Delft Green Village site. Furthermore, there exist limited control over the power management strategy programmed in the Hyundai FCEV; the power management strategy defining the load cycle it's Fuel Cell undergoes in Vehicle to Grid operation. This study therefore proposes a method to conduct simulated long term Vehicle to Grid experiments on a laboratory test bench.

2

Experiment

2.1. Set-up for simulated Vehicle to Grid experiments

Figure 2.1 shows a schematic of the PEMFC test-bench on which simulated Vehicle to Grid experiments were conducted. The sub-sections that follow describe some of the important components in detail.

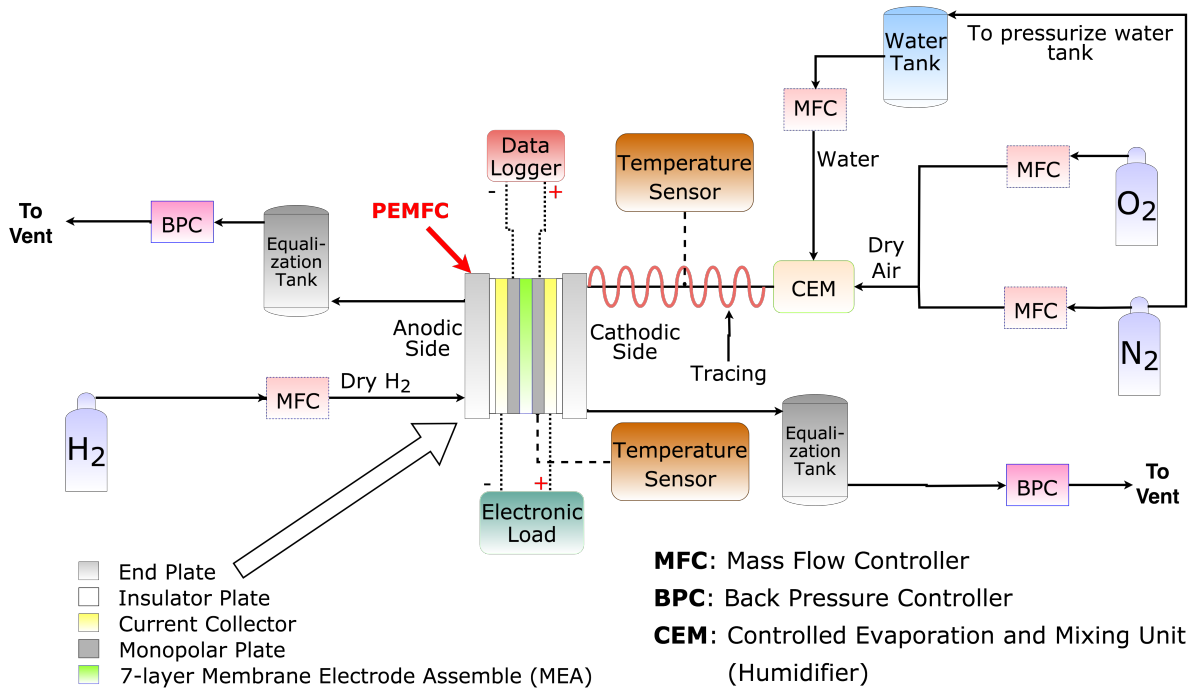

Figure 2.1: Schematic of the laboratory PEMFC set-up on which all simulated Vehicle to Grid experiments were conducted

2.1.1. Fuel Cell

The experiments for investigating Fuel Cell performance degradation in simulated Vehicle to Grid operation were performed on a single cell Proton Exchange Membrane Fuel Cell (PEMFC) with 5 cm^2 active area. Figure 2.2 shows the components of a generic single cell PEMFC. The single cell PEMFC used during this research consisted of a 7-layer Membrane Electrode Assemble - MEA (Figure 2.3 (a) and (b)), monopolar plates with single serpentine flow fields (Figure 2.3 (c)), current collectors (Figure 2.4 (a)), insulators (Figure 2.4 (b)), o-ring gaskets (Figure 2.4 (b)) and end plates with inlet and outlet apertures for reactants (Figure 2.4 (b)). All components were held together using nuts and bolts which were uniformly tightened.

Figure 2.5 shows the different views of the single cell PEMFC used during this research and Figure 2.6 shows the single cell PEMFC connected in the PEMFC set-up used during this research.

The 7-layer MEA comprised of a single Nafion 212 perfluorinated membrane of 50 μm thickness, two electrodes (anode and cathode) constructed from 70% Pt/C where carbon served as the support structure with a catalyst loading of 0.5 $\frac{mg}{cm^2}$, two gas diffusion layers (GDLs) made of non-woven carbon material with micro-porous layer (MPL) and two 48 microns thick Mylar or Silicon reinforced sub-gaskets. Ultrasonic spraying was the process employed to load the electrodes on the membrane.

Each Vehicle to Grid Fuel Cell load cycle was simulated on a new 7-layer MEA, following activation and electrochemical characterization of each MEA. The monopolar plates, current collectors, insulators, o-ring gaskets and end plates of the fuel cell were reused.

The experimental setup consists of all components including the fuel cell. Besides the fuel cell itself, the experimental apparatus includes mass flow controllers, back pressure controllers, temperature controllers, electronic load, data logger, humidifier, reactant tanks, pipes, flow valves etc. A brief desription of some important components has been provided in the following sub-sections. The Piping and Instrumentation Diagram (P&ID) and the parts list for the setup can be found in the Appendix C.

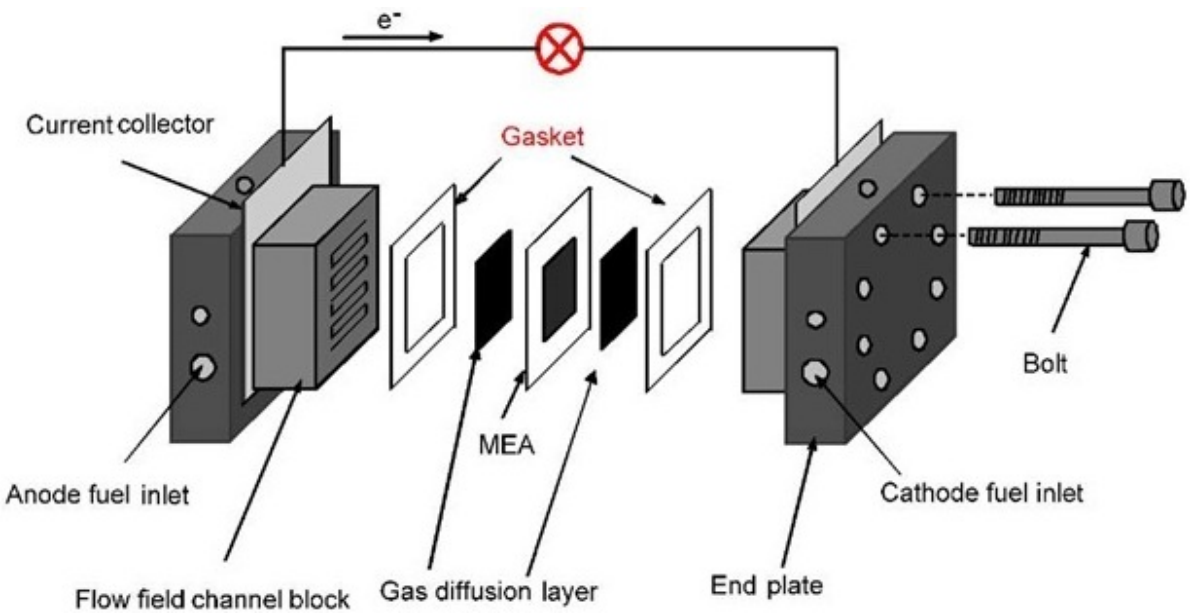

Figure 2.2: Generic single cell PEMFC construction [30]

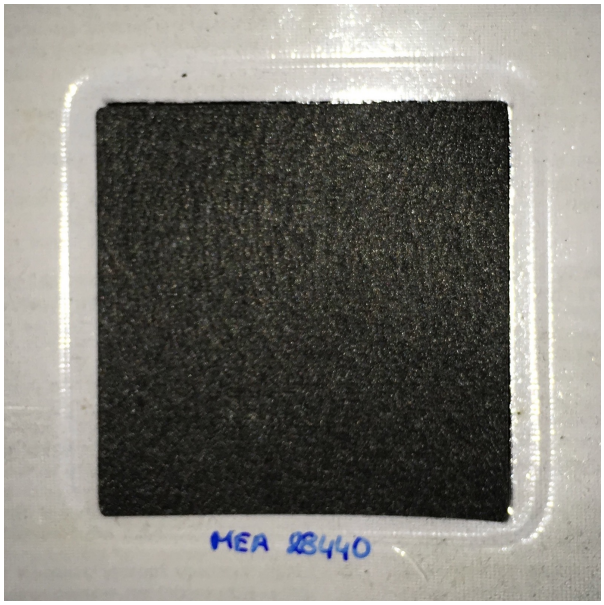

(a) 5-layer MEA (1 Membrane, 2 Electrodes, 2 GLDs)

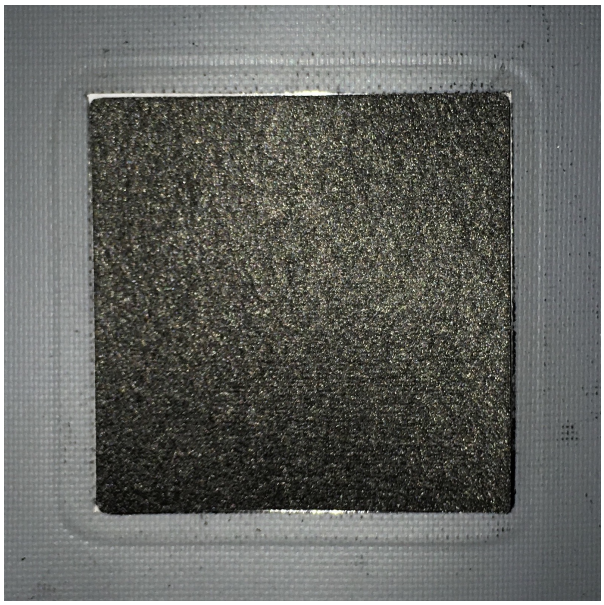

(b) 7-layer MEA (1 Membrane, 2 Electrodes, 2 GLDs with 2 additional Sub-gaskets (gray)

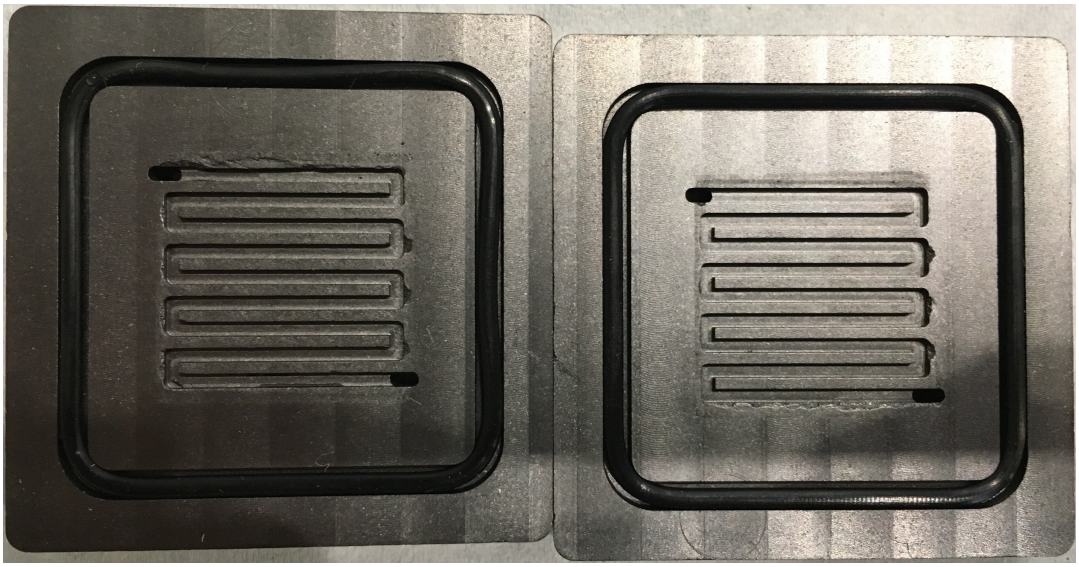

(c) Monopolar plates with single serpentine flow field, reactant inlet and outles, and gasket

Figure 2.3: MEA and Monopolar plates of laboratory PEMFC used during this research

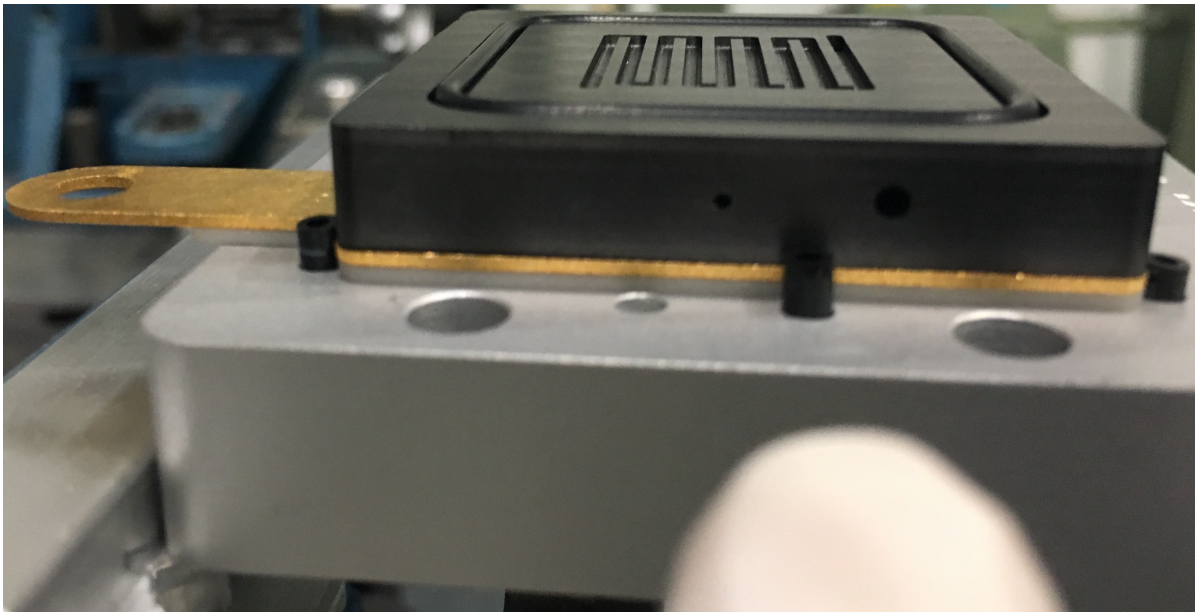

(a) Current collector (gold) between monopolar plate and insulator plate

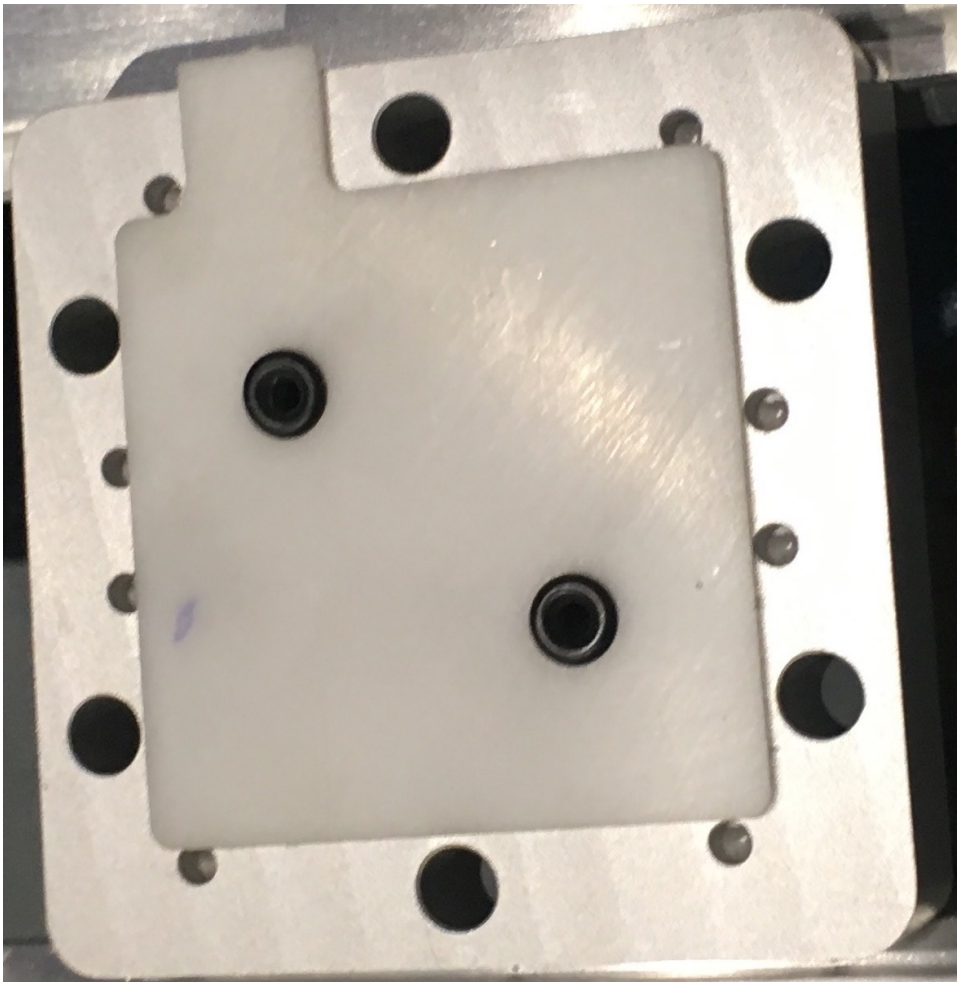

(b) Insulator plate (white) with o-ring gasket (black) on the end plate (silver/gray)

Figure 2.4: Half-cell PEMFC assembly without MEA

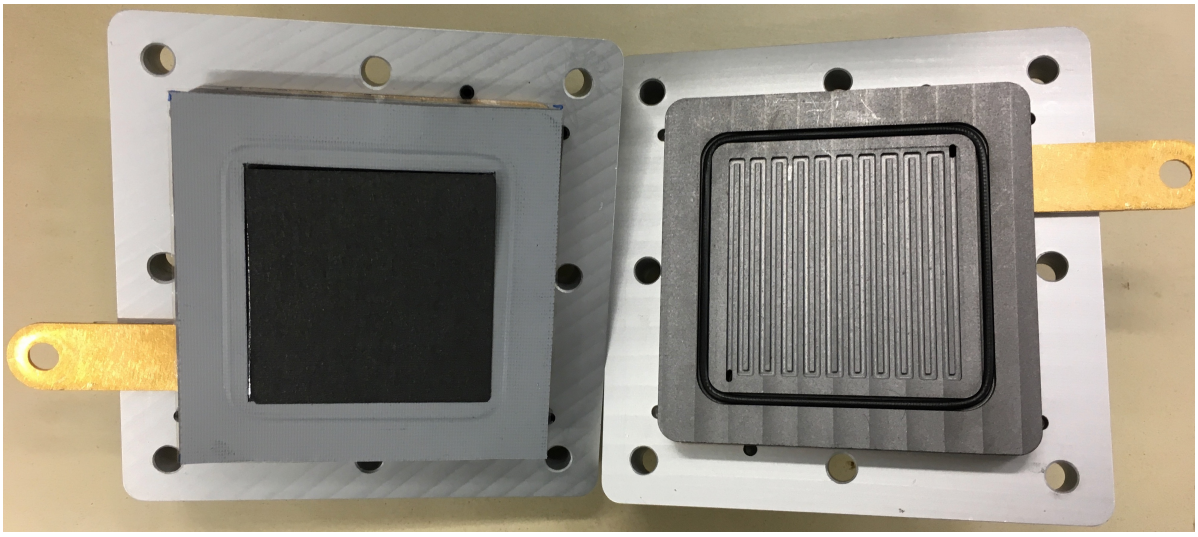

(a) Opened PEMFC view

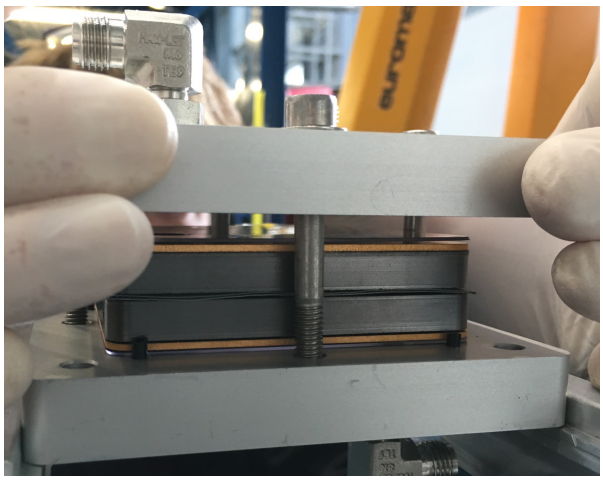

(b) PEMFC assembly (with bolts) side view

(c) Assembled (with bolts) PEMFC top view

Figure 2.5: Assembled PEMFC used during this research

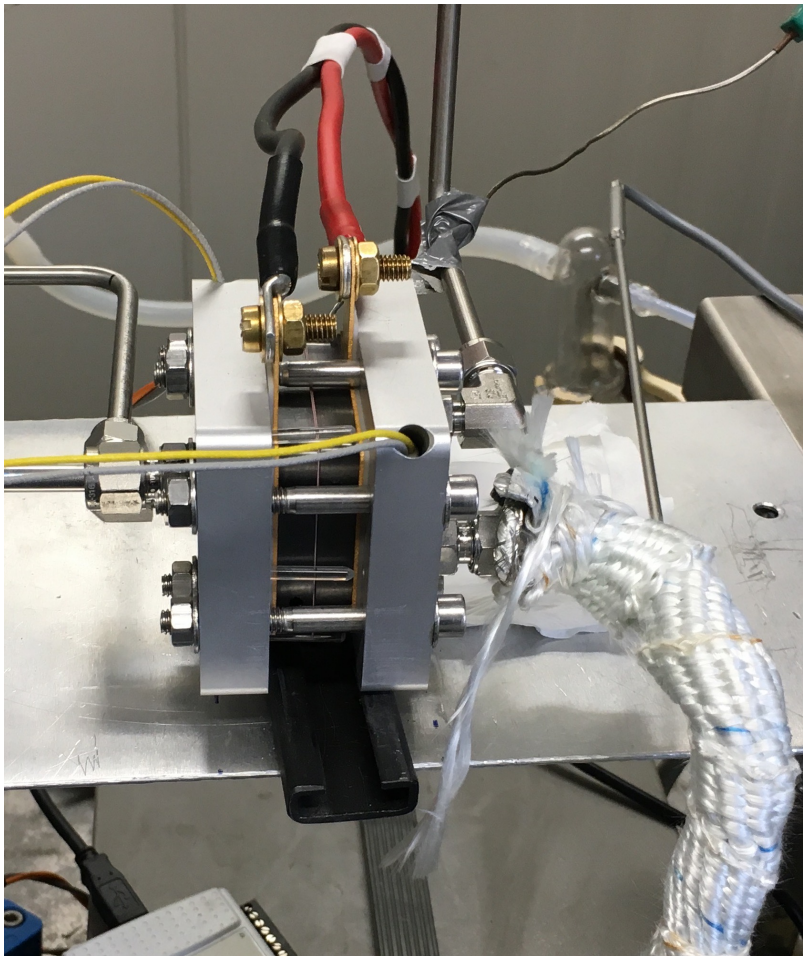

Figure 2.6: Assembled PEMFC connected in the set-up used during this research

2.1.2. Supporting Equipment

Mass Flow and Back Pressure Controllers: To control the mass flow of the reactants such that the required stoichiometric ratio is maintained, mass flow controllers (HI-TEC MFC) from Bronkhorst BV, The Netherlands were used. The unit of measurement of these MFCs was $\frac{mln}{min}$. The set value of the MFC was entered using digital PID controllers from Shimaden. The MFCs used for Hydrogen and Oxygen had a maximum flow rate of 100 $\frac{mln}{min}$ and that used for Nitrogen had a maximum flow rate of 500 $\frac{mln}{min}$.

Although the experiment was conducted at atmospheric pressure, activation of a new MEA before starting each experiment required a system pressure of 3 $Bar(a)$. Back Pressure Controllers (BPCs) from Bronkorst BV, The Netherlands were used for this purpose. The unit of measurement of these BPCs was Bar. The set value of the controller was entered using the software FlowDDE® and FlowView®. The maximum pressure rating of these devices was 20 Bar. The BPCs were connected downstream to the equalization tank before the vent. The equalization tank dampened short-term pressure fluctuations in the system.

Temperature Control: The FC membrane temperature measurement was *ex-situ*. A T-type thermocouple was inserted into the cathode side monopolar plate to measure the temperature of the fuel cell. The temperature of the fuel cell was controlled using heating rods provided by the FC supplier, PaxiTech®. These heating rods were inserted into the end plates. The unit of measurement for these devices was ℃. The temperature was set using a digital PID controller and display unit.

The cathode side reactants needed to be heated and humidified before they were fed to the fuel cell. This was done using a tracing element that was wound around the pipe leading from the outlet of the humidifier to the inlet of the fuel cell. The tracing element was constantly maintained at a temperature that was 10 ℃ higher than the required fuel cell inlet temperature. Doing this compensated for the temperature difference between the pipe surface and the reactant itself, thus ensuring that the reactants were heated sufficiently. Furthermore, this also made sure that no condensation occurred between the outlet of the humidifier and the inlet of the fuel cell, thereby guaranteeing that the reactant humidity conditions at the fuel cell inlet were as required. A T-type thermocouple was also used to measure the temperature of the tracing element. The temperature was set using a digital PID controller and display unit.

Electronic Load: For conducting the activation procedure, applying the experimental simulated load profile and to visually monitor the electrochemical performance of the fuel cell, an electronic load (PLZ 1004WZ) from Kikusui Electronics, Yokohama, Japan was used. The experiments were performed in constant current (CC) mode while the activation procedure was performed at constant voltage (CV) mode. The loader was also equipped to operate in constant power (CP) and constant resistance (CR) mode, although these modes were never used.

Humidifier: A Controlled Evaporation and Mixing (CEM) system was used to maintain the required relative humidity of the reactants. Since only the cathode reactants had to be humidified, the CEM was only attached before the reactant inlet of the cathode. The CEM operates by drawing distilled water from the water tank before atomizing and mixing it with the reactant stream at the required temperature. The CEM was procured from Bronkorst BV, The Netherlands. The water tank was fabricated from stainless steel by the lab technicians. In order to facilitate liquid flow from the tank to the CEM, the tank was pressurized to 8-10 $Bar(g)$ using Nitrogen.

The CEM requires two inputs: Dew Point Temperature and Mass Flow of liquid water. A combination of these two values define the output relative humidity of the reactant flowing through. The set values of these two parameters were calculated using relations from [49].

Data Logger: A data logger (USB DAQ6009®) from National Instruments *Ltd.* was used to measure the voltage across the membrane and log it simultaneously. The logging frequency of the data was 1Hz with an average of 10 scans/second. The voltage channels were connected to probes that were inserted into the side of the mono-polar plate. Although the experiments were conducted at constant current, the data logger was also used to log the current drawn by the load. This was done to verify that there were no fluctuations in the current drawn during the entire duration (200+ continuous hours) of the experiment.

Reactants Used: The Nitrogen, Oxygen and Hydrogen used during the course of this experiment were procured from Linde Group. The Hydrogen and Oxygen were stored at 200 $Bar(g)$ in 50L bottles; therefore, every new bottle contained 10,000 Liters of these reactants. The respective bottles were replaced as and when required. The purity of the reactants in the bottles was 5.0. The Nitrogen was stored as a liquid in bulk storage vessels at the TU Delft campus. This meant that Nitrogen replacement was not required throughout the course of this thesis. The Nitrogen was not only used as a reactant for the experiment but was also used as an inert gas to pressurize the stainless steel water tank. Details of the Nitrogen purity are unknown, but is is not expected that it would be lower that 4.9. The delivery pressure of all reactants was constantly maintained at slightly above 5 $Bar(g)$, well below the safety limit of the MFCs and the pipes, which was 8 $Bar(g)$. 5 $Bar(g)$ was selected in order to maintain an over-pressure considering the specified pressure drop of 1.1 $Bar(g)$ across the MFCs and the need to achieve a system pressure of 2 $Bar(g)$ during activation.

Figure 2.7 shows a picture of some of the supporting components connected to the laboratory PEMFC on which all simulated Vehicle to Grid experiments were conducted.

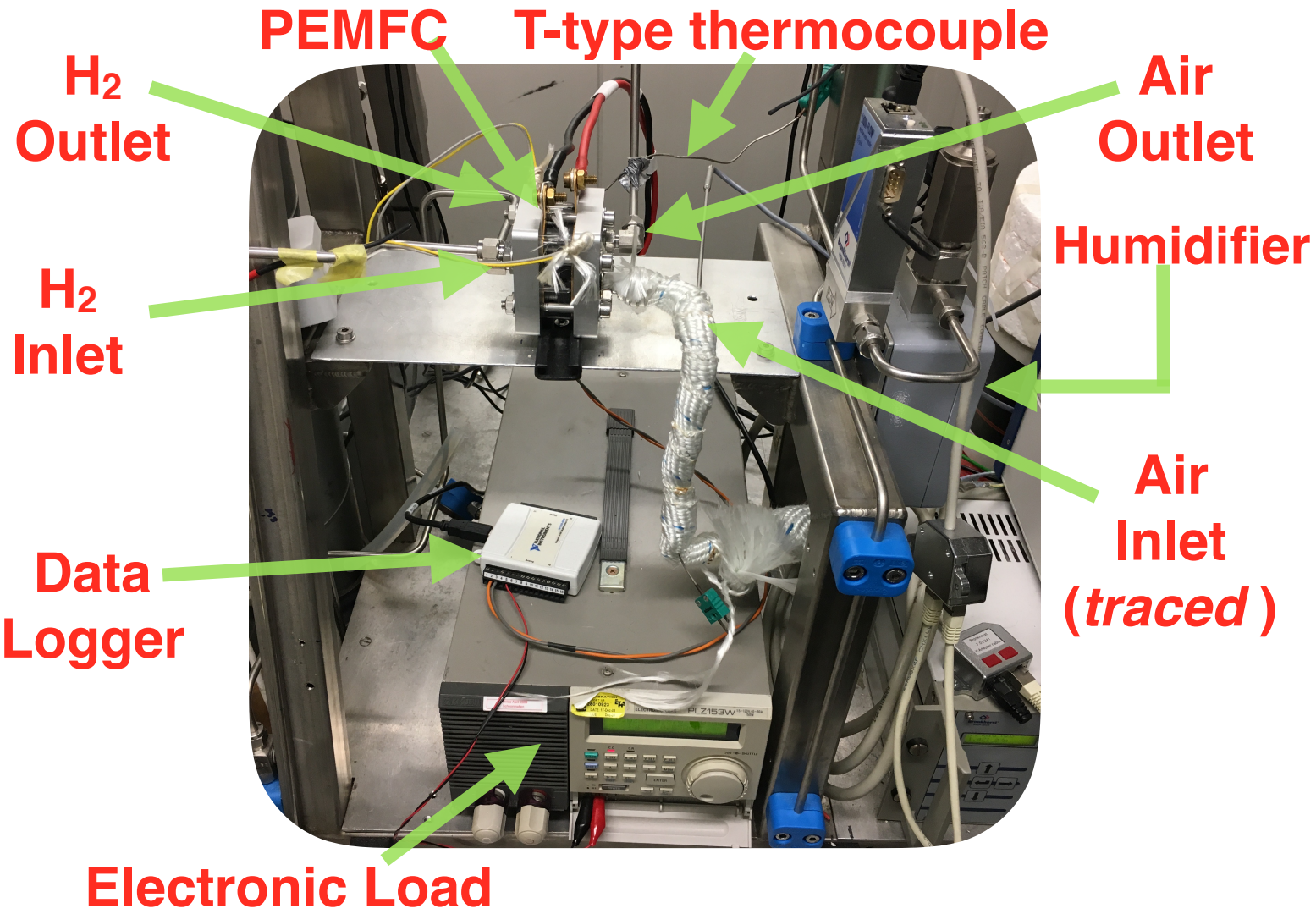

Figure 2.7: Picture of the laboratory PEMFC set-up on which all simulated Vehicle to Grid experiments were conducted

2.2. Determining experimental conditions for simulated Vehicle to Grid experiments

The experimental conditions that should be implemented during the simulated Vehicle to Grid experiments are derived from actual data recorded in the Hyundai ix35 Fuel Cell Electric Vehicle operating in Vehicle to Grid mode. Mimicking actual Fuel Cell Electric Vehicle operating conditions on the experimental setup ensure that the results obtained at the experimental scale would be applicable with greater accuracy to the Fuel Cells in Fuel Cell Electric Vehicle and Fuel Cell Range Extender Electric Vehicle.

1. **Pressure:** The operating pressure of the Fuel Cell Electric Vehicle in Vehicle to Grid application was obtained from the pressure sensor data of the Fuel Cell Electric Vehicle (Figure 2.8). The pressure in the Fuel Cell is observed to be constant at slightly above 1 $Bar(a)$. Therefore, the simulated Vehicle to Grid experiments may be conducted at ambient pressure.

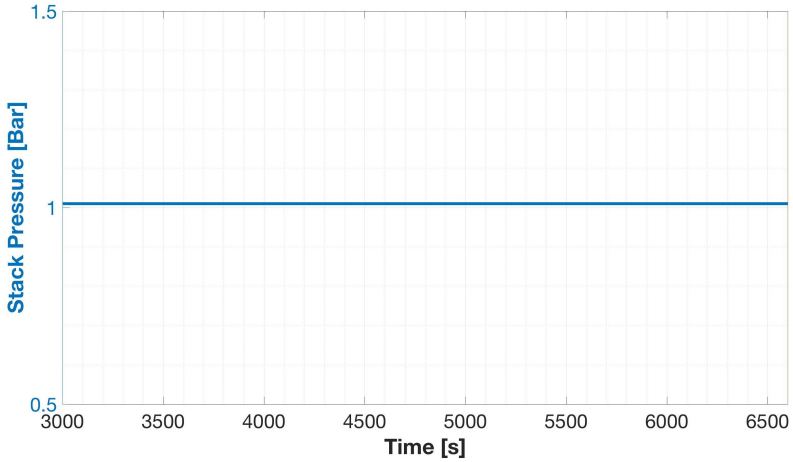

Figure 2.8: Fuel Cell Pressure measured in the Hyundai during 1 hour of Vehicle to Grid operation

2. **Temperature:** The Hyundai Fuel Cell Electric Vehicle's Fuel Cell temperature was extracted from the Fuel Cell coolant outlet temperature data channel. The coolant outlet temperature was observed to fluctuate between 57℃ to 62℃ (Figure 2.9) during 1 hour of Vehicle to Grid operation. The Fuel Cell temperature in the simulated Vehicle to Grid experiment should therefore be constantly maintained at 70℃. The experimental Fuel Cell temperature is set slightly above the measured coolant outlet temperature to accommodate for temperature difference required to drive heat transfer between the Fuel Cell Electric Vehicle's Fuel Cell and the coolant.

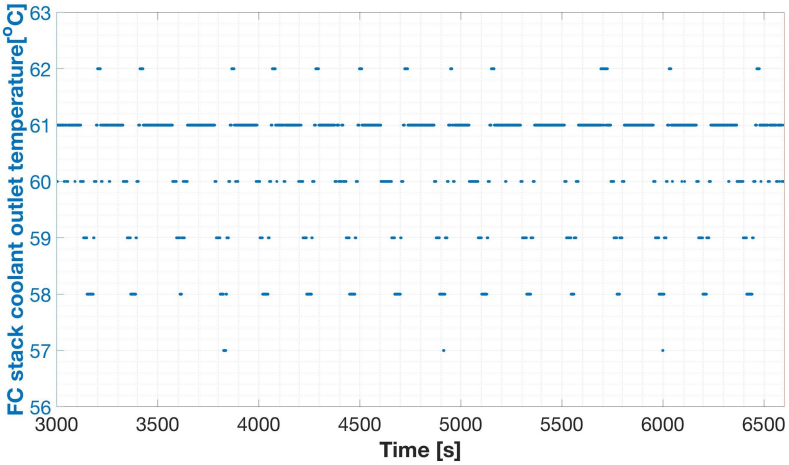

Figure 2.9: Fuel Cell Coolant outlet temperature measured in the Hyundai during 1 hour of Vehicle to Grid operation

3. **Relative Humidity:** The relative humidity (RH) of the cathode reactant flow should be maintained at 80% at 70℃. This is an approximated value as the humidification in actual Vehicle to Grid operation of the Hyundai Fuel Cell Electric Vehicle is dynamic and the minimum inlet humidification requirement has been claimed to be confidential by Hyundai. Furthermore this RH value is selected as an educated guess to ensure a balance between avoiding drying and avoiding flooding of the fuel cell. Finally, it is expected that the Hydrogen delivered to the Fuel Cell in the Hyundai Fuel Cell Electric Vehicle is dry. Therefore, dry hydrogen should be used as the anode reactant in the simulated Vehicle to Grid experiments.

4. **Anode Stoichiometry:** Stoichiometry may be defined as the ratio between reactant feed and, the reactant consumption to produce a certain magnitude of current in a given fuel cell. The magnitude of stoichiometry is always above 1 to ensure that the performance requirement of a cell is maintained. The anode stoichiometry for the simulated Vehicle to Grid experiments should be maintained at 1.2. The Hyundai Fuel Cell Electric Vehicle is equipped with an anode recycle blower that helps improve fuel efficiency by recycling the unreacted Hydrogen at the outlet of the Fuel Cell stack, back to the inlet. Lack of information due to non-measurement of the recycle blower recirculating flow rate, makes it difficult to accurately calculate the reactant (fuel) stoichiometry at the anode inlet. Therefore, a stoichiometry of 1.2 has assumed for simulated Vehicle to Grid experiments in this study, based on conditions for automotive FC lifetime tests that were found in literature [5, 38].

5. **Cathode Stoichiometry:** The cathode stoichiometry in the simulated Vehicle to Grid experiments should be maintained at 3. This value is derived by using relations from [19] and the Hyundai Fuel Cell Electric Vehicle cathode reactant data in constant power application. Stoichiometry range of 2.5 to 3 has been was selected for the simulated Vehicle to Grid experiments because it corresponds to 12 kW, which is the magnitude of constant load for the first load cycle simulated in this study (Figure 2.10). It must also be pointed out that the Fuel Cell Electric Vehicle uses filtered and conditioned air draw from the atmosphere as cathode reactant. But during the course of the simulated Vehicle to Grid experiments conducted in this study, cathode reactant was considered to be only a mixture of 79% Nitrogen and 21% Oxygen respectively. Nevertheless, it is expected that the results would not vary considerably if actual conditioned atmospheric air or a mixture of simulated atmospheric air was used instead of a simple mixture of Nitrogen and Oxygen in the specified proportion.

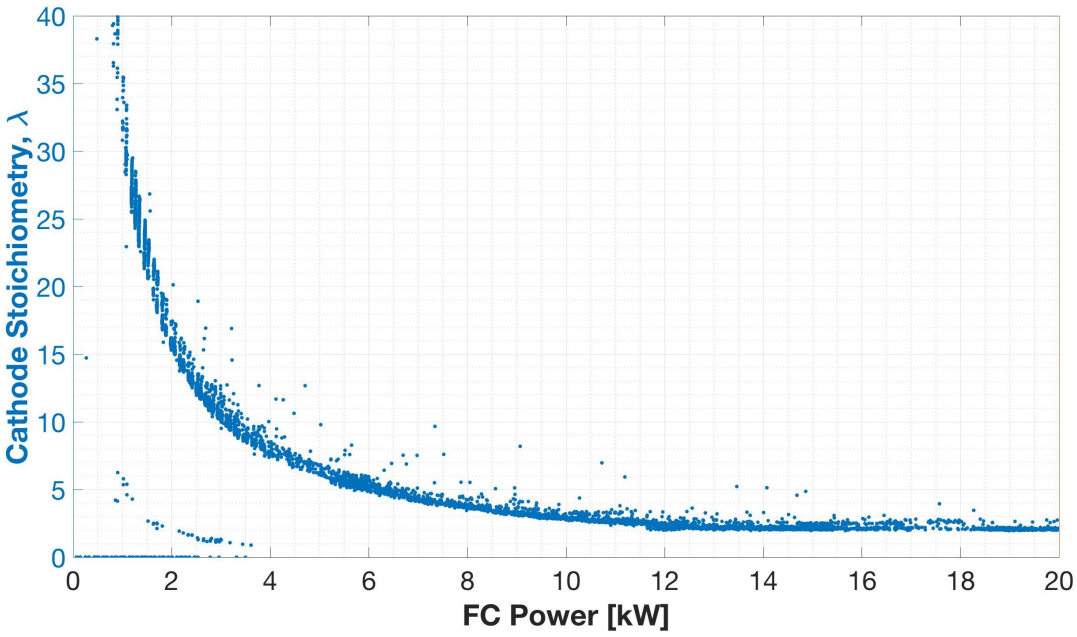

Figure 2.10: Cathode stoichiometry in the region of interest (0kW to 20kW), for the 100kW Fuel Cell in the Hyundai FCEV during constant power application

Summarizing, all the experimental conditions that should maintained while conducting simulated Vehicle to Grid experiments have been presented in Table 2.1. Furthermore, the reactant conditions for these experiments have been presented in Table 2.2.

Table 2.1: Experimental conditions for simulated Vehicle to Grid experiments

Experimental Condition	**Magnitude**	**Unit**	**Remark**
Pressure	1	Bar (a)	Derived from V2G data
Temperature	70	℃	Computed from V2G data
Relative humidity	80	%	Estimated
Anode Stoichiometry	1.2	-	Estimated
Cathode Stoichiometry	3	-	Computed from V2G data

Table 2.2: Reactant conditions for simulated Vehicle to Grid experiments

Reactant	**Composition in mixture** $\left[\%\right]$	**Temperature** $\left[℃\right]$	**Humidity Content**
Hydrogen	100	Ambient	Dry
Nitrogen	79	70	80 % RH at 70℃
Oxygen	21		

Since reactant flow conditions are a function of current density, all reactant volumetric flow rates were calculated at the current density of 0.34 $\frac{A}{cm^2}$ and at STP, using relations from [19] and [49]. 0.34 $\frac{A}{cm^2}$ is the maximum current density of the first MEA on which Vehicle to Grid operation was simulated. This current density was measured at a voltage of 0.6V just after activation of the MEA. This metric of maximum current density corresponding to a voltage of 0.6V was defined similar to what was suggested by authors in [48] in their protocol to asses the impact of on-off load cycling on automotive PEMFCs.

A current density of 0.34 $\frac{A}{cm^2}$ resulted in flow rates of 14.2 $\frac{mLn}{min}$, 17.8 $\frac{mLn}{min}$ and 66.2 $\frac{mLn}{min}$ for Hydrogen, Oxygen and Nitrogen respectively. A water flow rate of 1.319 $\frac{gH_2O}{h}$ was required to humidify the Dry air mixture (Nitrogen+Oxygen) to 80% Relative Humidity at 70℃.

The experimental and reactant conditions and the reactant flow rate was the same for all types simulated Vehicle to Grid Fuel Cell load cycles. This was done to ensure uniformity of conditions between tests, which in turn ensured that the performance decay measured is only a consequence of the load cycle applied. Furthermore, the flow rates were calculated for maximum current density because if the flow rates were computed for actual applied current densities, the error induced by virtue of the flow measurement equipment operating in its lower operating region would be very high. The accuracy of the test results would therefore reduce drastically for such flow rates.

An overview of the exact steps followed while conducting the simulated Vehicle to Grid experiments can be found in Appendix D.

2.3. Fuel Cell load cycles simulated

2.3.1. Literature Survey

Causes for degradation in Electric Vehicle Fuel Cells can be classified according to type of operation or according to the processes occurring during operation. If not used for Vehicle to Grid applications, only driving constitutes the type of operation that the Fuel Cells undergo. The processes occurring during driving operations include load cycles or dynamic operation and start-stop sequences. Pei *et al* have satisfactorily reviewed the main factors affecting the lifetime of automotive PEM fuel cells [37]. They conclude that load cycling is the main cause of fuel cell degradation in vehicular application, as it could lead to water management and dynamic response problems. Pei *et al* have also studied automotive fuel cell performance degradation, in driving cycles of real PEMFC buses, at the different cycles and loads that typically occur during operation: load changing cycles, start-stop cycles, idling time (low or no power operation) and high power loads [38]. They deduce that 56.6% of total degradation can be linked to load changes, 33% to start-stop sequences, 5.6% to high power operation and 4.7% to idling operation. From their study it can be seen that load cycling and start-stop sequences cause higher performance degradation as compared to constant high or low load operation. This conclusion may also be true for light passenger vehicles (which are more likely to deliver Vehicle to Grid services) because of the similarity in their materials of construction.

Chen *et al* used real-life driving cycles of a PEM Fuel Cell, in a High Voltage Battery dominated Fuel Cell Bus, to develop a load cycle to test on a laboratory set-up [5]. They report degradation rates of 8.662 μVh^{-1} and 10 μVh^{-1} at idling and high power load respectively. They also report a degradation rate of 0.4185 $\mu Vcycle^{-1}$ and 13.79 $\mu Vcycle^{-1}$ due to load cycling and start-stop cycling respectively. They report an overall rate of degradation of 42.16 μVh^{-1} due to a combined driving cycle. In their study of heat and water management on automotive fuel cells, Nandjou *et al* implemented the New-European Driving Cycle (NEDC/RH) cycling test and report a degradation rate of 27 μVh^{-1} [27]. Li *et al* report degradation rates varying from 18 μVh^{-1} to 390 μVh^{-1} at different current densities and various stages of operation for a fuel cell city bus [23]. Therefore, the measured performance loss strongly depends on the experimental conditions and the type of load cycles; where the type of load cycle describes the type of operation the Fuel Cell undergoes.

As seen in the Vehicle to Grid operation of the Hyundai Fuel Cell Electric Vehicle's Fuel Cell (Figure 1.13), the Fuel Cell idles at $0A$ when the High Voltage Battery services the Vehicle to Grid load. Idling at $0A$ may be referred to as operation at Open Circuit Voltage (or Potential). Open Circuit Voltage operation has been reported to cause performance degradation in the Fuel Cell. Kundu *et al* report degradation rates of 83 μVh^{-1} and 141 μVh^{-1} at high temperature-high pressure and low temperature-low pressure conditions for long term open circuit voltage durability tests [22]. Lim *et al* evaluated combined mechanical and chemical durability of the membrane by developing a cyclic open circuit voltage (COCV) accelerated stress test (AST). The AST was designed to exert chemical and mechanical stresses cyclically and comprised of an OCV phase at high temperature/low RH condition followed by a series of wet/dry cycles in N_2. They report a decay rate of 0.7 mVh^{-1} up to the first 7 cycles, followed by a high decay rate of 3.9 mVh^{-1} after the 10^{th} cycle. The magnitude of Fuel Cell degradation reported in the two studies above is considerably high as compared to those reported by Chen *et al* [5] as described in the previous paragraph; albeit the experimental conditions were different.

Nandjou *et al* in their study also performed a reference stationary test at constant current density of 0.4 Acm^2, to compare with performance loss measured under driving load, and report a degradation rate of 18 μVh^{-1} at constant current operation [27]. This is lower than the performance loss of 27 μVh^{-1} measured for the New-European Driving Cycle (NEDC/RH) cycling test. Furthermore, Kocha *et al* report that the rate of performance decay is lower for constant current (or load) operation as compared to cyclic current profiles, for the same range and duration [21].

Therefore operating Fuel Cell Electric Vehicles at constant load while avoiding load cycling, start-stop sequences and Open Circuit Voltage operation may potentially be less harmful to the Fuel Cell of these Fuel Cell Electric Vehicles. In such a scenario Fuel Cell degradation caused due to constant load operations becomes more relevant. However, Electric Vehicle Fuel Cell degradation due to long-term constant load operation has not been studied and reported much in literature, since constant load operation is unlikely to occur for extended periods of time in real-world Electric Vehicle Fuel Cells. Nevertheless, results of performance losses at constant load application of stationary fuel cells may serve as a good reference for comparison.

Pahon *et al* studied a μ-CHP load profile that simulates the behavior of a stationary PEMFC application throughout the year. The conducted tests of 2 durations: Long-term (1000h) and Short-term (500h). The load cycle for the short-term test was obtained by scaling the load cycle for the long-term test in the time domain. They report degradation rates of 170 μVh^{-1} and 180 μVh^{-1} for constant load operation durations of 147 and 125 $hours$ in each type of test respectively [36]. In the same experiment they also studied the impact of cyclic loads with intermediate operation at OCV and at maximum and 50% of maximum power. They report an overall degradation rate of 75 μVh^{-1} and 76 μVh^{-1} after total test duration of 1000 and 500 $hours$ respectively. They suggest that the constant load degradation is higher than the overall degradation rate because some of the degradation occurring during constant load operation was recovered due to load cycling and OCV operation in the subsequent cyclic load applied on the same fuel cell immediately. This further highlight the impact that the load cycle, and the manner in which it is applied on the Fuel Cell, has on the performance degradation measured.

From the sources mentioned above it is evident that the rate of degradation strongly depends on the aim of the experiments, type of load cycle and the experimental conditions. The values can be as low as 8.662 μVh^{-1} to as high as 3.9 mVh^{-1}. For ease of analysis, Figure 2.11 below represents graphically the range of reported rate of degradation organized according to type of application. Table 2.3 shows the reported values and their sources; which were used to develop the figure. From Figure 2.11 it can be observed that driving (or load cycling) can cause higher degradation as compared to constant load operation and therefore operating the Electric Vehicle Fuel Cell at constant load and avoiding driving and start-stop sequences could potentially reduce Fuel Cell degradation.

It should be noted that the degradation rate measured for combined Driving and Vehicle to Grid operation, shown in Figure 2.11, was computed from the data recorded in the TU Delft Hyundai Fuel Cell Electric Vehicle over a duration of approximately 9 months. The vehicle was used for driving as well as short-term Vehicle to Grid experiments (less than 12-15 $hours$ of continuous Vehicle to Grid operation), during this 9 month duration. The two values represent two different fitting algorithms that were used to analyze the recorded data to measure performance loss. These results have only been presented here to serve as a reference for comparison with the results of this study. These values have not been published in the given form, but were used to compute the net stack percentage voltage drop for the Hyundai Fuel Cell Electric Vehicle in [32].

Furthermore, it should also be noted that the results of performance loss reported are for varying experimental aims, type of load cycles and experimental conditions. This further highlights the need to conduct simulated Vehicle to Grid experiments to estimate performance losses in Fuel Cells specifically due to Vehicle to Grid operation.

Nevertheless, based on the literature survey it may be safe to conclude that constant load operation could potentially cause lesser performance degradation in Electric Vehicle Fuel Cells.

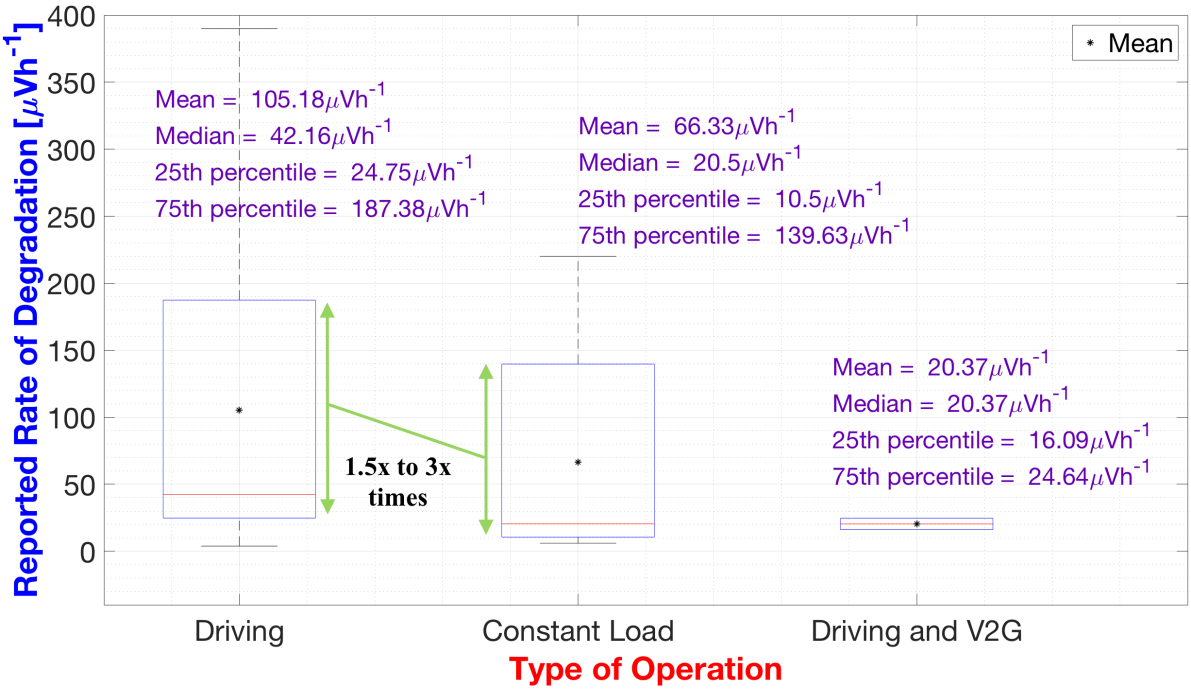

Figure 2.11: Reported Degradation Results

Table 2.3: Reported Degradation Results

Source	Reported Rate of Degradation ($\mu Vh^{-1}cell^{-1}$)	Type of Operation
Shan *et al* [45]	27	Driving
Nandjou *et al* [27]	27	
Chen *et al* [5]	42.16	
Liu *et al* [25]	70	
Lin *et al* [24]	209.5	
Li *et al* [23]	18	
	13	
	180	
	230	
	360	
	390	
Vincent et al	31.11	
	31.35	
	6.73	
	3.83	
	75.15	
	73.24	
Pahon *et al* [36]	170	Constant Load
	180	
Nandjou *et al* [27]	18	
Fowler *et al* [12]	11	
Yu *et al* [55]	22	
Vincent et al	24.64	Driving + V2G
	16.09	

2.3.2. Power management strategy selected for simulation

In Vehicle to Grid operation, the power management strategy programmed into the Hyundai Fuel Cell Electric Vehicle involves operational switching between the Fuel Cell and High Voltage Battery (Figure 1.13,1.14 and 1.15). During it's operation, the Fuel Cell not only services the external Vehicle to Grid load but also simultaneously charges the High Voltage Battery. It may be concluded that the external Vehicle to Grid load is essentially serviced by the Fuel Cell only; but by periodically employing the High Voltage Battery as an intermediate capacitor.

As described in the literature survey, fuel cell load cycling and idling operation causes performance degradation. Furthermore, load cycling of the High Voltage Battery during charging and discharging cycles are also known to cause degradation of the Battery [40, 53]. Therefore, a power management strategy in which only the Fuel Cell of the Hyundai FCEV is assumed to be participating in Vehicle to Grid services was selected for the simulated Vehicle to Grid experiments. The High Voltage Battery was assumed to be disconnected and therefore not participate in Vehicle to Grid services. Figure 2.12 shows this power management strategy schematically. This strategy is similar to the strategy described in Case 3 of Section 1.4.2 - Fuel Cell dominated FC-HVB combination connected in parallel drivetrain architecture, but where the High Voltage Battery disconnected during Vehicle to Grid operation.

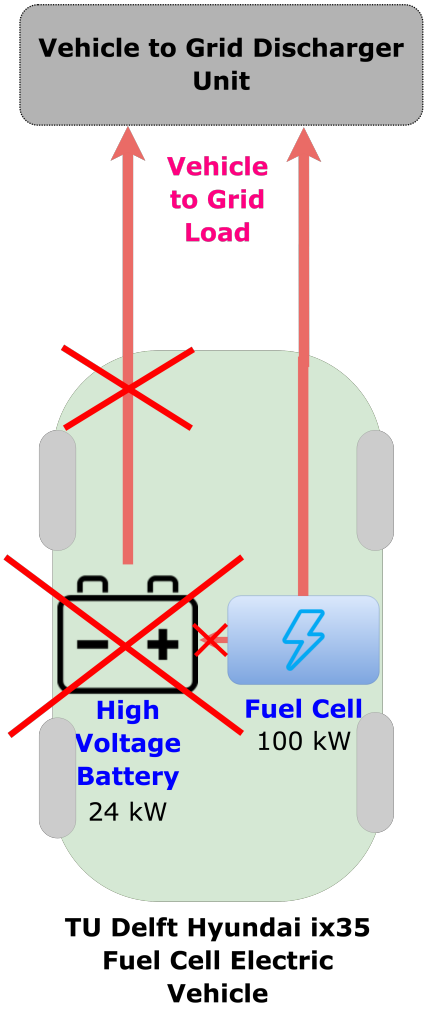

Figure 2.12: Selected power management strategy for simulated Vehicle to Grid experiments

2.3.3. Types of Fuel Cell load cycles selected for simulation

The Vehicle to Grid load cycles, that were simulated in this study, were developed based on the literature survey and the selected power management strategy. They were developed specific to the TU Delft Hyundai FCEV's Fuel Cell, since the simulated Vehicle to Grid experiments were specific to this Electric Vehicle.

1. **Constant-load Fuel Cell operation at 12kW:**

   Based on the literature survey, it is seen that operating the Fuel Cell of the Electric Vehicles at constant load while avoiding load cycling, start-stop sequences and Open Circuit Voltage operation may potentially cause lesser degradation. A constant load cycle for the Fuel Cell would mean that the Vehicle to Grid load[1] would need to be constant. Such a constant Vehicle to Grid load would occur in a scenario where the Electric Vehicle behaves as a back-up to other renewable energy sources by delivering constant, non-load-following power[2].

   The magnitude of this constant Vehicle to Grid load was assumed to be an arbitrary magnitude of 12kW AC. Assuming 100% DC $\rightarrow$ AC conversion efficiency would result in the constant AC Vehicle to Grid load translating to a constant DC load of 12kW for the Fuel Cell in the Hyundai Fuel Cell Electric Vehicle (FCEV). A Fuel Cell load of 12kW correlates to approximately a constant vehicle speed of 30kmh^{-1} to 60kmh^{-1} (see Appendix Figure E.1). This speed is a nominal vehicle speed and it would be acceptable for the Hyundai FCEV's Fuel Cell to operate in Vehicle to Grid mode at this constant power, if the operating conditions would be adapted to minimize Fuel Cell degradation in this type of Vehicle to Gird operation. Therefore, the first Fuel Cell load cycle selected for simulating Vehicle to Grid operation, was a constant load cycle of 12kW DC.

   For ease of identification, this load cycle will be labeled as Load Cycle 1 **(LC1)**. Figure 2.13 graphically represents LC1 during Vehicle to Grid operation of 1 $hour$.

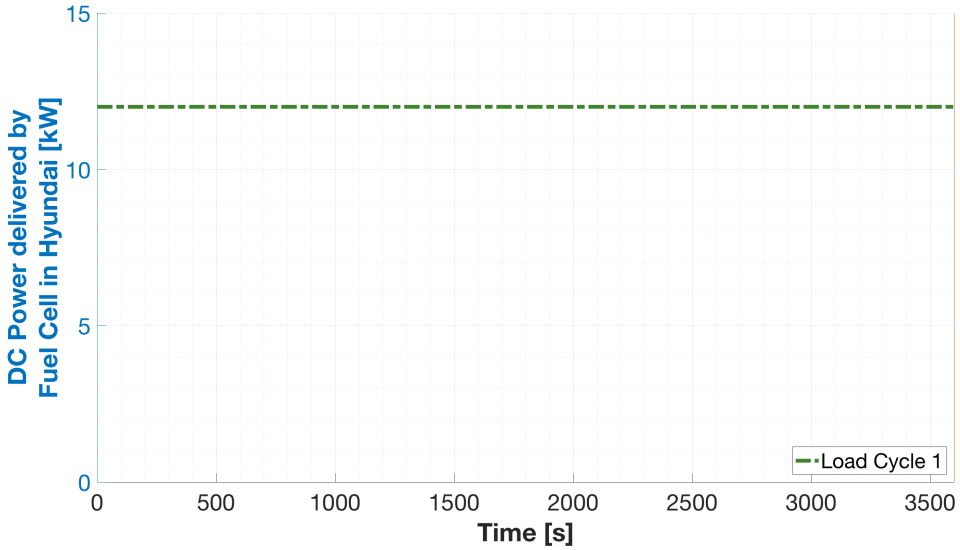

Figure 2.13: First type of Fuel Cell load cycle simulated in this study (LC1)

Besides **LC1**, 2 other load cycles were selected to be applied in the laboratory based simulated Vehicle to Grid experiments.

[1] Load demanded by the grid

[2] The Vehicle to Grid load serviced by the Electric Vehicle would be non-constant when they would be operating as spinning reserves responsible to servicing sudden power demand ramps in the grid i.e the Vehicles would need to be operating in load following Vehicle to Grid mode

2. **Constant-load Fuel Cell operation at 5kW:**

   For the second load cycle, the Vehicle to Grid load was assumed to be a constant load of 5kW AC. This translates to a constant load of 5kW DC for the Fuel Cell in the Hyundai FCEV, assuming 100% DC $\rightarrow$ AC conversion efficiency.

   This load cycle was selected to assist in making a comparison between the impact of high load and low load operation on the test-bench Fuel Cell, for the same simulated Vehicle to Grid experimental conditions. The results from such a load cycle would be useful in a future scenario while making decisions regarding the number of Electric Vehicles required to service a certain Vehicle to Grid load *i.e.* from a Fuel Cell degradation perspective, to service the same electric energy demand, would it be advisable to operate fewer Fuel Cell and Fuel Cell Range Extender Electric Vehicles at higher load, or *vice-versa*? The answer to this question would also have an impact on the availability of these Electric Vehicles for normal (driving) operation.

   The load cycle has been graphically represented in Figure 2.14. This load cycle for the Hyundai FCEV's Fuel Cell operating at constant load of 5kW DC in Vehicle to Grid mode, will be labeled as Load Cycle 2 **(LC2)**.

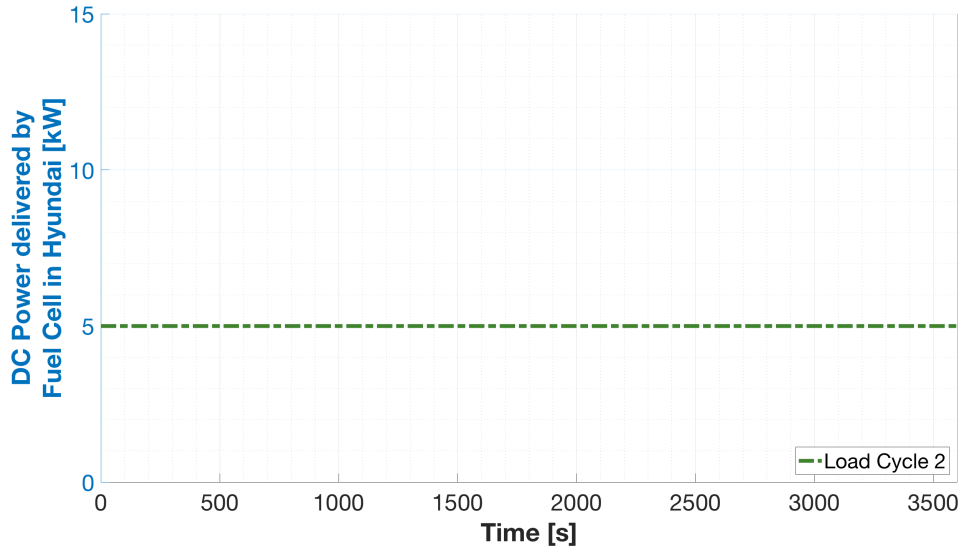

Figure 2.14: Second type of Fuel Cell load cycle simulated in this study (LC2)

3. **Cyclic-load Fuel Cell operation between 12kW and 5kW:**

   The price of electricity includes cost of generation, profit for the grid operator and the cost of the infrastructure required to deliver the energy. Electric Power is defined as the rate at which energy is consumed (kW). Electric Energy is the total energy consumed (kWh). Energy consumption contributes to the cost of generation whereas power demand contributes to the cost of infrastructure required for delivery.

   Pricing for residential energy consumers are constant since power demand and energy consumption does not vary from house to house [28]. But this is not the case for commercial and institutional energy consumers. For such a consumer, the energy consumption and the power demand differ vastly from consumer to consumer [28]. Power-peak demand periods occur at different times for each consumers. The prices for each unit of energy is higher during these peak demand periods. Variable pricing aids in providing adequate reimbursement for the grid operator

who maintains the infrastructure to service the peak power demand of each consumer.

Fuel Cell and Fuel Cell Range Extender Electric Vehicles (FCEVs and FCREEVs) operating in Vehicle to Grid mode are proposed to assist in peak shaving [10, 15]. Peak shaving is the ability of these Electric Vehicles to quickly service the peak in power demand from the grid. This is a consequence of the quick start-up and ramp-up capabilities of these Electric Vehicles. Therefore it would be useful to quantify the impact of such operation on the Fuel Cell of these Electric Vehicles.

For the third simulated load cycle, the Vehicle to Grid load was assumed to be cycling between $5kW$ AC and 12 kW AC. $5kW$ AC represents the base load of the grid that is also delivered by the Electric Vehicle, and $12kW$ AC represents the peak demand. The period for which the peak demand lasted was defined as 15 minutes. This was done to mimic the industry practice of selling power in 15-minute blocks, during peak demand. Assuming 100% DC $\rightarrow$ AC conversion efficiency, this Vehicle to Grid load cycle translates to a cyclic load cycle of $5kW$ DC and $12kW$ DC in 15 minute blocks, for the Fuel Cell in the Hyundai Fuel Cell Electric Vehicle.

The load cycle has been graphically represented in Figure 2.15. This load cycle will be labeled Load Cycle 3 **(LC3)**.

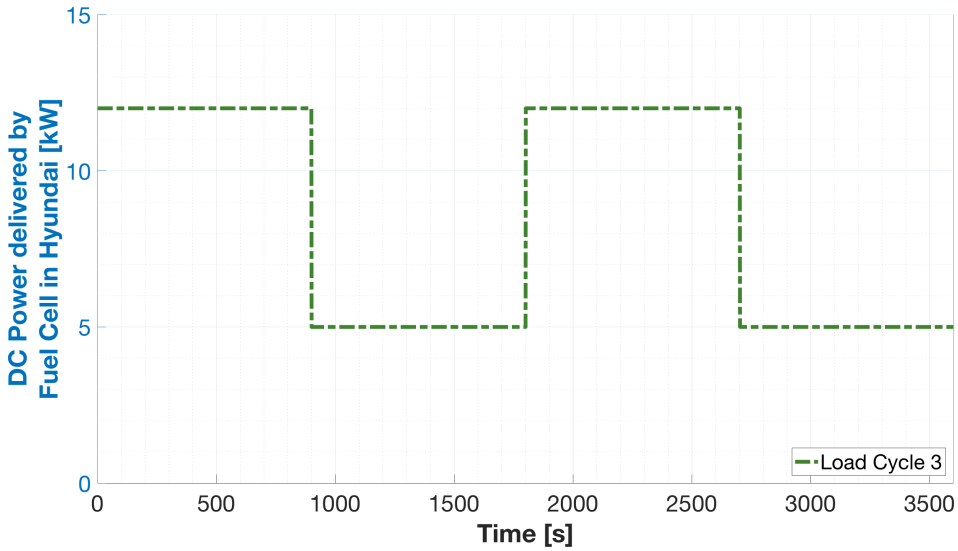

Figure 2.15: Third type of Fuel Cell load cycle simulated in this study (LC3)

Figure 2.16 shows the three different types of Fuel Cell load cycles representing three different kinds of Vehicle to Grid operation of the Hyundai FCEV's fuel cell stack. These load cycles are unique to the power management strategy selected, the Hyundai FCEV's Fuel Cell stack technical specifications ($100kW$ rating) and the Vehicle to Grid load that were assumed. These load cycles can then be translated to a cycle unique to the test-bench PEMFC stack before imposing them on the test-bench under the specified experimental conditions for simulated Vehicle to Grid experiments.

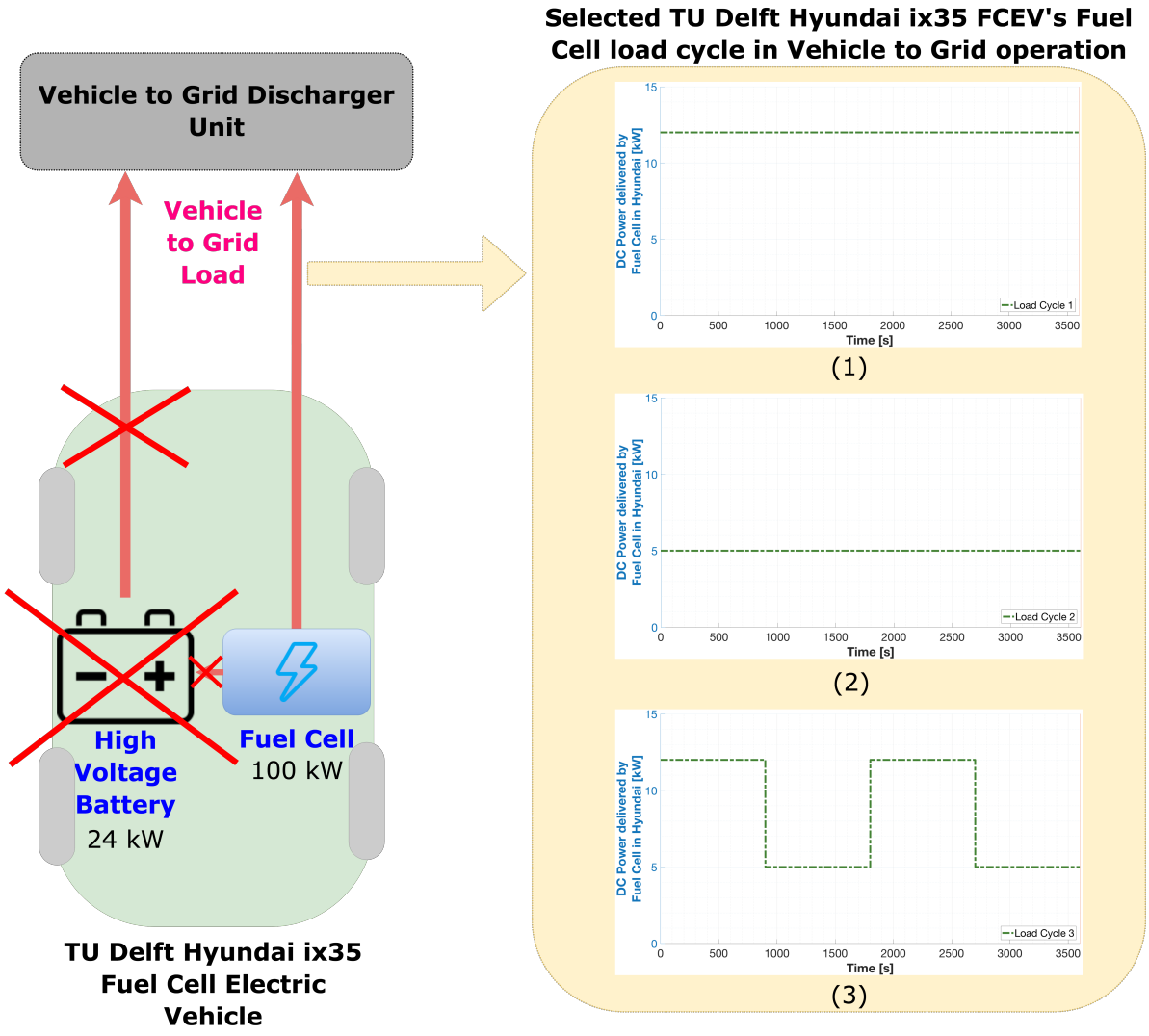

Figure 2.16: Load cycles selected to be simulated: (1) **LC1:** Constant Fuel Cell operation at 12kW (2) **LC2:** Constant Fuel Cell operation at 5kW (3) **LC3:** Cyclic operational switching between 12kW and 5kW

2.3.4. Translating selected Hyundai FCEV specific Fuel Cell load cycle to equivalent current cycle specific to the laboratory PEMFC used for simulated Vehicle to Grid experiments

Implementing the selected load cycles (LCs) described in subsection 2.3.3 on the laboratory PEMFC is not possible because the single cell laboratory PEMFC set-up is unable to deliver the same magnitude of power as the 100 kW Fuel Cell stack inside the Hyundai Fuel Cell Electric Vehicle. This is because the total active area of the 424 single cells in the Hyundai's Fuel Cell stack is more than three orders of magnitude larger than the active area of the single-cell in the PEMFC set-up (5cm^2). It would therefore be efficient to translate the selected load (power) cycles specific to the Hyundai FCEV's Fuel Cell to equivalent cycles specific to the PEMFC set-up. The translated cycle represents equivalent Vehicle to Grid operation of the PEMFC stack.

Instead of translating the selected load cycles specific to the Hyundai FCEV's Fuel Cell to equivalent load (power) cycles specific to the PEMFC set-up, the selected load cycles have been translated to equivalent current cycles specific to the PEMFC set-up. Imposing a load (power) cycle on the laboratory PEMFC would result in a large range of current densities for each of which the performance decay would have to be quantified. This is because the current drawn from the laboratory PEMFC would constantly need to be adapted to suit the highly dynamic voltage delivered by the PEMFC. Adapting current according to drawn voltage ensures that the power condition imposed on the PEMFC is constantly satisfied. Therefore, the selected load cycles specific to the Hyundai FCEV's Fuel Cell is translated to an equivalent current cycle specific to the PEMFC of the laboratory set-up. This current cycle can then be imposed on the PEMFC while recording the voltage delivered at the unique current density that define the current cycle. The performance degradation can then be computed at each unique current density.

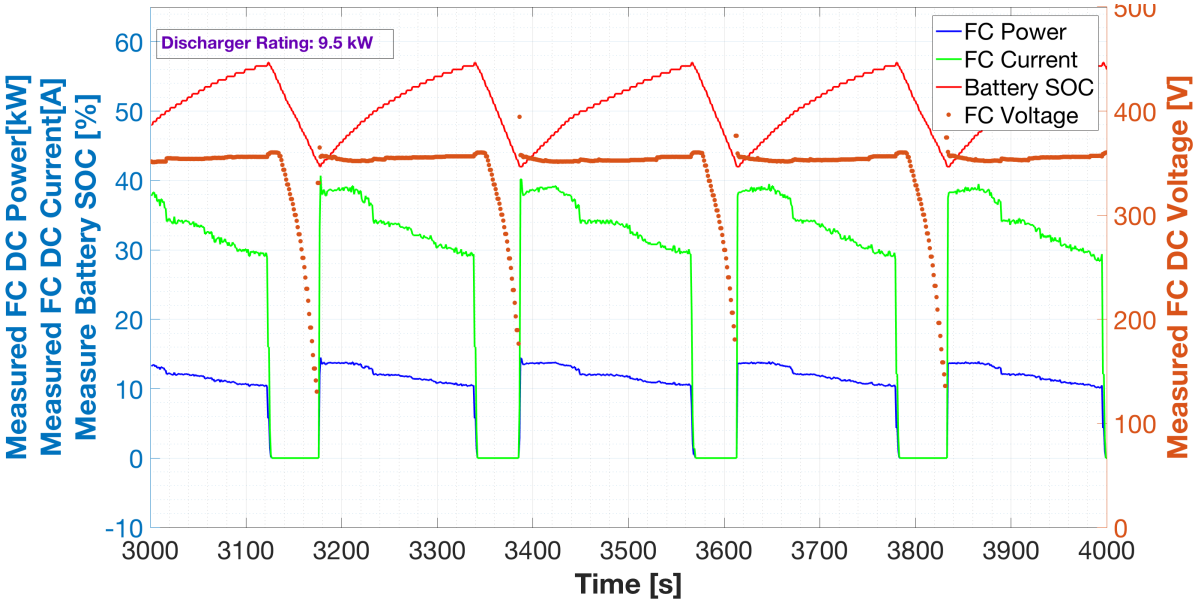

Figure 2.17: Fuel Cell Power, Current and Voltage relation during 1000s of Vehicle to Grid operation at 9.5kW AC using the Hyundai FCEV

To demonstrate that translating the load cycles specific to the Hyundai that were selected for simulation (LC1 - 12kW, LC2 - 5kW and LC3 - cyclic) to their equivalent current cycle specific to the PEMFC of the test-bench is valid, Figure 2.17 has been developed from recorded data in the Hyundai Fuel Cell Electric Vehicle during Vehicle to Grid operation. From Figure 2.17 it can be observed that the Fuel Cell stack operation in Vehicle to Grid occurs at almost constant voltage. Since the Vehicle to Grid load is constant (9.5kW AC), the current would have also been constant if recharging of the High Voltage Battery was not required. The recharging of the High Voltage Battery can be identified by the increasing State of Charge (SOC) of the Battery. The dynamic current and power delivered by the Fuel Cell is only a consequence of adapting charging current to the increasing SOC of the High Voltage Battery, during charging. This is because, as the High Voltage Battery in the Hyundai approaches it's upper SOC threshold (as it completes charging), the power delivered by the Fuel Cell for charging the Battery decreases. The power is decreased by keeping the voltage delivered by the Fuel Cell almost constant while decreasing the current drawn from the Fuel Cell. Thus, it could be said that the the current delivered by the Fuel Cell also describes the load (or power) cycle of the Hyundai's Fuel Cell in Vehicle to Grid operation.

Therefore translating the load cycle (LC) specific to the Hyundai's Fuel Cell stack to an equivalent current cycle (CC) specific to the laboratory PEMFC is valid since in the power management strategy selected for simulation, the High Voltage Battery of the Hyundai is assumed to be disconnected in

Vehicle to Grid operation. Thus, the Fuel Cell is not required to charge the Battery. Which means that the current delivered by the Hyundai's Fuel Cell can be constant (at constant voltage) for the assumed constant Vehicle to Grid Load (constant power demanded by the grid).

The steps followed to conduct this translation have been described in this section.

The first step for translation is to express the magnitude of the Fuel Cell DC power in the load cycles selected for simulation (LC1 - 12kW, LC2 - 5kW and LC3 - cyclic) as a function of the maximum power rating of the Hyundai Fuel Cell Electric Vehicle's Fuel Cell stack. This aids in developing a relation between the actual automotive Fuel Cell stack and the laboratory test bench PEMFC.

$$P_{FC\%} = \frac{P_{FC}}{P_{FC-rating}} \times 100\% \tag{2.1}$$

where P_{FC} is the magnitude of the Fuel Cell DC power constituting the selected load cycle and $P_{FC-rating}$ is the maximum power rating of the Hyundai FCEV's Fuel Cell stack.

The Hyundai ix35 has a Fuel Cell stack with a power rating of 100 kW [18]. Therefore, the load magnitude of LC1 (12 kW) can be expresses as 12% of maximum power rating and that of LC2 (5 kW) may be expressed as 5% of maximum power rating. Analogously, LC3 can be interpreted as load cycling between 12% and 5% of maximum power rating, in 15-minute blocks.

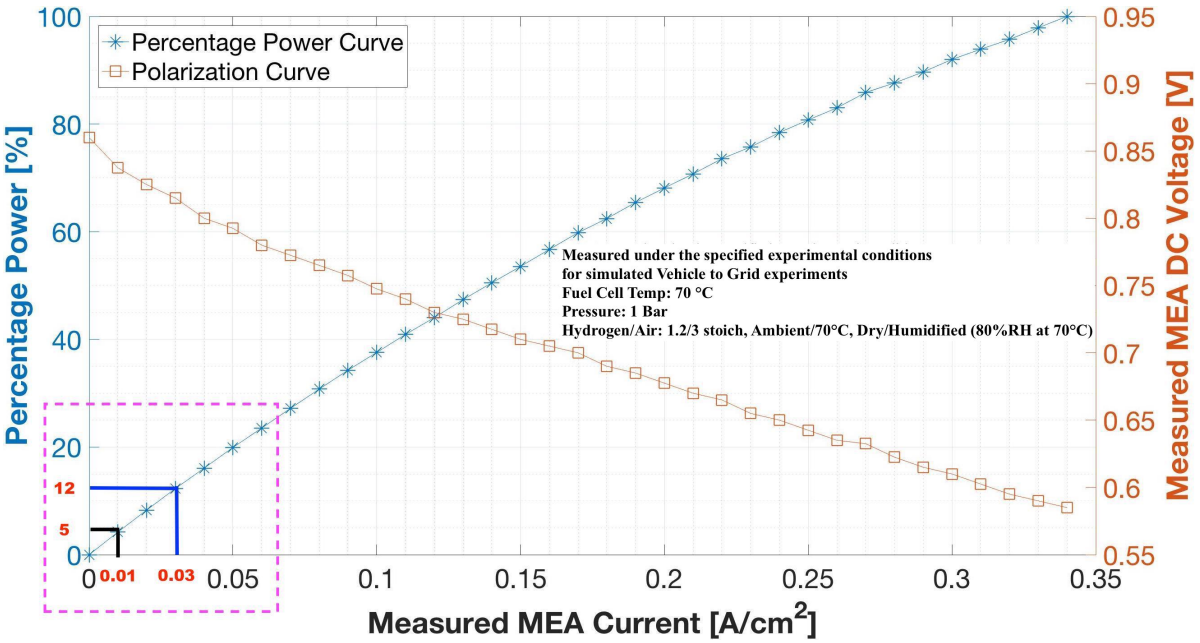

Figure 2.18: Polarization and Percentage Power curve for MEA1 in the test-bench PEMFC

Following this, from the percentage power curve of the test bench PEMFC, the current density corresponding to the same $P_{FC\%}$ can be extracted. This is a translation step which links the percentage-power ($P_{FC\%}$) for the Hyundai's Fuel Cell with it's equivalent percentage-power unique to the laboratory test-bench PEMFC. It should be noted that the power curve for the laboratory test bench PEMFC is first developed from the polarization curve measured under experimental operating conditions for simulated Vehicle to Grid experiments, as described in section 2.2. The percentage power curve is then developed from the power curve by considering maximum power occurs at a current density which results in a cell voltage of around 0.6V. This metric of 0.6V was defined similar to what was suggested by authors in [48] in their protocol to asses the impact of on-off load cycling on automotive PEMFCs.

Figure 2.18 shows the polarization curve along with the percentage-power curve, for the first Membrane Electrode Assembly (MEA - see section 2.1) that was tested in this research. It can be observed that approximately 12% of the maximum power delivered by MEA1 corresponds to a current density of 0.03 $\frac{A}{cm^2}$ and 5% of maximum power occurs at 0.01 $\frac{A}{cm^2}$. Therefore, it may be concluded that the power magnitude for load cycle LC1 (12% of maximum FC rating) would occur at 0.03 $\frac{A}{cm^2}$ and that for LC2 (5% of maximum FC rating) would occur at 0.01 $\frac{A}{cm^2}$ in the test bench PEMFC. It should be noted that the magnitude of the current density for the corresponding percentage power did not vary for all other subsequent MEAs used for simulated Vehicle to Grid experiments.

The Load Cycle (LC) for the Hyundai Fuel Cell Electric Vehicle's Fuel Cell stack, can thus be translated into the corresponding equivalent Current Cycle (CC) for the test bench PEMFC.

Table 2.4 shows the translation of each type of Load Cycle from its power magnitude specific to the Hyundai ix35 Fuel Cell Electric Vehicle's Fuel Cell stack to it's equivalent Current Cycle specific to the laboratory PEMFC set-up on which simulated Vehicle to Grid experiments were conducted.

Table 2.4: Translating load cycle specific to the Hyundai FCEV's Fuel Cell stack to it's equivalent current cycle specific to the test bench PEMFC

Selected Load Cycle (Hyundai specific)	P_{FC} [**kW**]	$P_{FC\%}$ [**%**]	**Equivalent Current Cycle (PEMFC specific)**	C_{FC} $[\frac{A}{cm^2}]$
LC1	12	12	CC1	0.03
LC2	5	5	CC2	0.01
LC3	12 - 5 - 12 (15-minute blocks)	12 - 5 - 12 (15-minute blocks)	CC3	0.03 - 0.01 - 0.03 (15-minute blocks)

Figure 2.19 illustrates the equivalent current cycles that were imposed on the laboratory PEMFC set-up to simulate Vehicle to Grid operation of the Hyundai Fuel Cell Electric Vehicle's Fuel Cell stack in the selected load cycles.

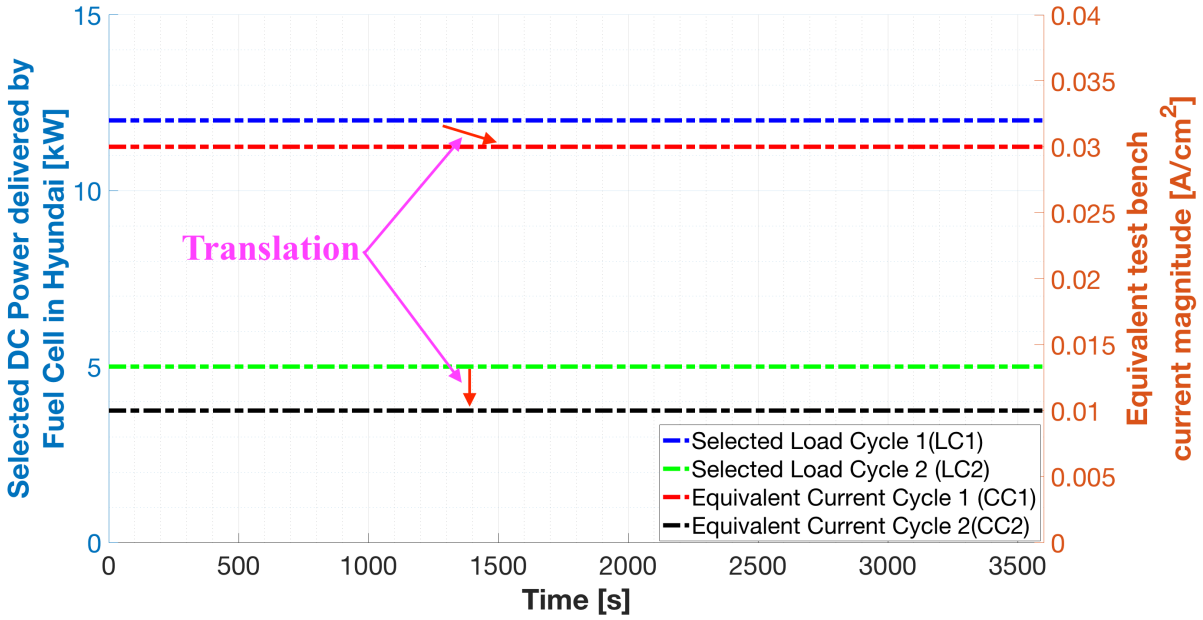

(a) Equivalent test-bench current cycles of the two selected constant-load load cycles of the Hyundai FCEV's Fuel Cell stack (CC1 and CC2)

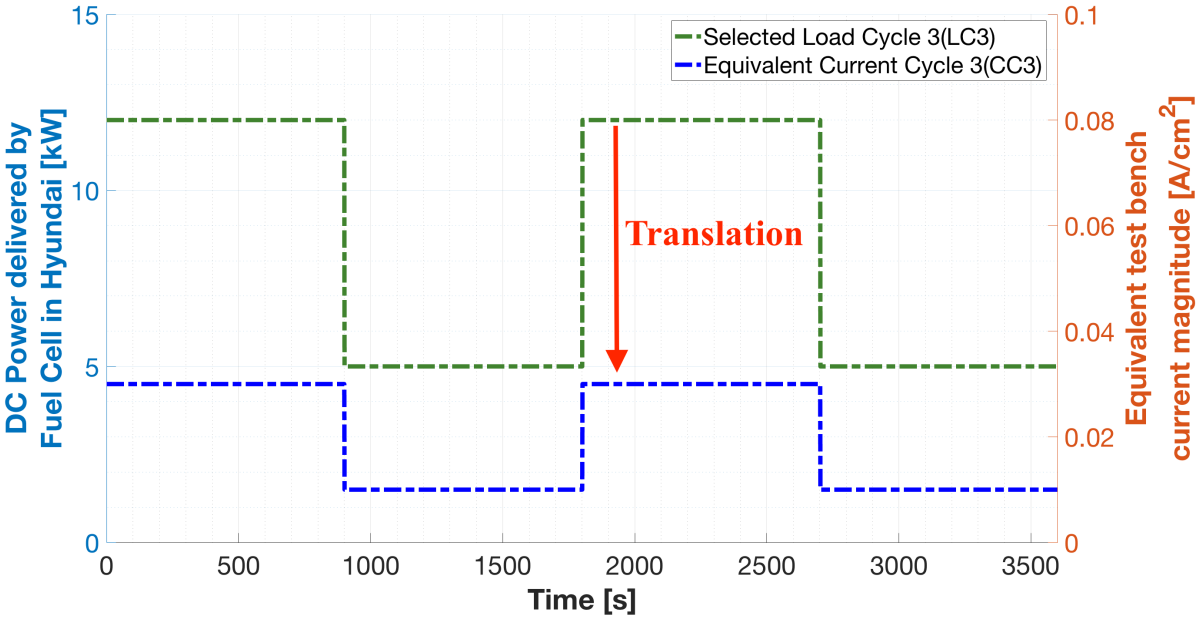

(b) Equivalent test-bench current cycle of the third selected cyclic-load load cycle of the Hyundai FCEV's Fuel Cell stack (CC3)

Figure 2.19: All Translated Current Cycles unique to the laboratory PEMFC set-up which were tested during this research

2.4. Summary

A small-scale experiment has been designed to simulate Vehicle to Gird operation of the 100kW Fuel Cell stack in the TU Delft Hyundai Fuel Cell Electric Vehicle (FCEV), on a laboratory PEMFC test-bench of 5cm^2 active area. The Hyundai's Vehicle to Grid mode Fuel Cell load cycle that was simulated on the laboratory PEMFC during this study was developed based on a literature survey and considering Vehicle to Grid scenarios in which the Vehicle is likely to operate. Three load cycles for the Hyundai's Fuel Cell were selected to be simulated: 1. LC1 - Fuel Cell operation at constant load of 12kW 2. LC2 - Fuel Cell operation at constant load of 5kW and 3. LC3 - Cyclic load fuel cell operation between 12kW and 5kW in 15 minute blocks. Following this, a method has been proposed to translate the selected load cycles (LC1, LC2 and LC3) specific to the Hyundai FCEV's Fuel Cell to equivalent current cycles specific to the PEMFC set-up on which Vehicle to Grid operation is simulated. This resulted in three equivalent current cycles (CCs) that were then imposed on the test-bench PEMFC. The three equivalent current cycles were: 1. CC1 - PEMFC operation at constant current of 0.03$\frac{A}{cm^2}$ 2. CC2 - PEMFC operation at constant current of 0.01$\frac{A}{cm^2}$ and 3. CC3 - Cyclic current PEMFC operation between 0.03$\frac{A}{cm^2}$ and 0.01$\frac{A}{cm^2}$ in 15 minute blocks.

Furthermore, the operating conditions that occur in the Hyundai FCEV's Fuel Cell was also derived from data recorded in the Vehicle during actual Vehicle to Grid operation. These conditions have a strong impact the performance loss of the Fuel Cell, and therefore need to be simulated on the test bench PEMFC on which the equivalent current cycles were imposed. This would ensure that the results obtained at the laboratory PEMFC was applicable to the actual Fuel Cell with greater accuracy.

3

Experimental Methodology

Here a brief description of what is Fuel Cell performance decay and how it has been measured and expressed while conducting this particular study, has been provided.

3.1. MEA activation procedure applied before staring simulated Vehicle to Grid experiments

The Membrane Electrode Assembly (MEA) strongly determines the performance of a PEM fuel cell. The MEA is composed of the anode where fuel oxidation occurs, a cathode where oxygen reduction takes place and a membrane which is responsible for protonic transportation. To improve the kinetics of the reduction and oxidation reaction, noble metal catalyst such as platinum are mixed in the carbon support structure of the two electrodes. Thus, the loading of the catalyst has an influence on the performance of the fuel cell.

To improve the catalyst utilization, the MEA is first exposed to high pressure, temperature and humidity conditions. This helps break-into the catalyst reaction sites thereby improving membrane performance at relatively milder conditions. The process of exposing the MEA to harsh conditions for a short period of time (approximately 2-3 hours) in order to facilitate reaction site break-in is known as membrane activation procedure.

During the course of this research, a new MEA was used for each simulated Vehicle to Grid experiment. This eliminated the probability of degradative effects of previous experiments contaminating the results of the new experiment. Therefore, before simulating each equivalent current cycle, the new MEA had to be activated before electrochemical characterization followed by conducting the long-term experiment. The membrane activation procedure was provided by the supplier of the MEA.

The MEA activation was conducted at a system pressure of 3 $Bar(a)$. The temperature of the Fuel Cell was maintained at 70℃. Dry Hydrogen was used at a flow rate of 50 $\frac{mLn}{min}$. Simulated Air (79% Nitrogen + 21% Oxygen) humidified to 50% RH at 70℃ was used at a combined flow rate of 150$\frac{mLn}{min}$. The reactant flow rate values were suggested by the MEA supplier and were chosen to ensure that there was enough reactant gases for the red-ox reactions to occur, even at low current densities, without the drying out the membrane too quickly.

It was then ensured that the Open Circuit Voltage (OCV) at these conditions is between 0.85V and 1V. A lower OCV would signify either leakages around the fuel cell or gas-crossover across the MEA. Once the set conditions had been reached and the OCV was acceptable, a constant voltage of 0.6V was drawn from the fuel cell for a period of approximately 2-3 $hours$; or until the current stabilized instead of constantly increasing. The increasing trend of the current, at constant voltage, represents

the “break-in” process. The metric of $0.6V$ was suggested by the supplier of the MEA.

Following activation, the system was de-pressurized to $1Bar(a)$, which was the pressure at which the simulated Vehicle to Grid experiments were conducted. The reactant flow rates were also adjusted to the values specified for simulated Vehicle to Grid experiments (section 2.2). The polarization curve was then measured after which the simulated Vehicle to Grid experiment was started.

3.2. Computing impact of simulated Vehicle to Grid operation

One of the most common testing modes in Fuel Cell lifetime studies is to control the current density under the desired operating conditions and study the voltage evolution over time. Voltage (or performance) degradation may be defined as the decreased ability of a Fuel Cell to deliver the same voltage at that particular current density, over time and usage. Since the product of current and voltage results in power, studying constant current performance of a Fuel Cell gives insight into the performance evolution of the Fuel Cell over its lifetime. Comparing the constant-current voltage recorded at the beginning of the measurement period (BoM voltage) and at the end of the measurement period (EoM voltage) results in the rate of degradation (RoD). The rate of degradation at a particular constant current is expressed as

$$\boxed{\boldsymbol{RoD_{@\ constant\ current\ density\ (i)}} = \frac{\boldsymbol{\Delta V}}{\boldsymbol{\Delta t}}} \tag{3.1}$$

Where ΔV is the difference in the voltage recording (at current density *i*) at BoM and EoM, in $Volts$ and Δt is the absolute value of the measurement period in $hours$. These result in RoD (or measure of performance loss) being expressed in units of Vh^{-1} or more commonly found units of mVh^{-1} and μVh^{-1}.

3.2.1. Defining measurement period

The measurement period for all the equivalent current cycles (CCs) tested in this study was defined such that the impact of simulated Vehicle to Grid operation under each type of cycle could be quantified accurately, in a relatively shorter duration. The measurement periods during this study ranged from 140 $hours$ to 440 $hours$, depending on the initial performance of each new MEA.

As mentioned before, long-term simulated Vehicle to Grid experiments on a laboratory test bench need to be conducted in order to quantify the irreversible performance loss. Authors of Ref. [22] suggest that irreversible performance losses occur approximately after a period of 20 $hours$. Therefore the start of the measurement period through which the Fuel Cell performance degradation is quantified may be considered to be $20h$. The authors identify the first $20h$ of operation as a exponential voltage evolution period and suggest that the decay occurring during this period should not be mistaken for irreversible degradation. They report that the performance loss caused during the exponential voltage evolution period may be cause by transient processes where the loss in voltage may be recovered by changing the operating conditions. One of the most common causes for recoverable degradation is water flooding within the cell. The performance loss caused due to this may be reversed by drying the cell using dry inert reactants such as dry Nitrogen. Authors of Ref. [22] report a very high performance decay in this exponential voltage evolution period as compared to the subsequent linear voltage evolution period, which they identify as the steady decay period, during which irreversible degradation occurs. An example of irreversible degradation may be mechanical failures such as crack and pin-hole formation and catalyst agglomeration. The performance losses caused due to these are permanent and thus cannot be recovered or reversed.

The voltage evolutions for all the current cycles implemented in this study showed similar evolution characteristics. Figure A.1 shows voltage evolution for Experiment 3. It has been presented in the

Appendix because it is a result of one of the experiments conducted in this study. It has been used to depict the various periods in one experiment, since such a figure with the same terminology and measurement period in a single figure was not available in literature. As seen in Figure A.1, a transient (or exponential) period of voltage decay was observed up to approximately $20h$ which was followed by a period of steady (or linear) decay.

To compute the Fuel Cell performance decay caused by simulated Vehicle to Grid operation under each type of current cycle, the beginning of measurement period in this study has therefore been defined as $20h$. The end of the measurement period was taken to be the end of the first sequence of the experiment (Sequence 1). Therefore, the magnitude of the measurement period, for each simulated Vehicle to Grid experiment, is given by the difference between the length of the simulated Vehicle to Grid experiment and $20h$.

Furthermore, in order to verify that the recoverable voltage evolution indeed occurs under simulated V2G conditions, the recovery procedure suggested by authors of Ref. [13], was implemented at the end of Sequence 1 of the experiment. Details of the steps taken while implementing the recovery procedure can be found in Appendix D. The objective of implementing the recovery procedure was to reverse the transient conditions that caused transient or recoverable performance losses. Implementing a recovery procedure at the end of Sequence 1 resulted in two distinctly separate voltage evolutions. As in [13], these two evolution periods have been termed as voltage evolution in Sequence 1 and voltage evolution in Sequence 2 (Figure A.1). Sequence 1 refers to the part of the voltage evolution before the recovery procedure was implemented and sequence 2 refers to the period after the recovery procedure.

The exponential and linear voltage decay periods can be observed to occur in both sequences. This would mean that the measurement period for performance decay has to be split into 2 periods, namely, measurement period 1 and measurement period 2. Measurement period 1 (MP1) refers to the period of linear voltage decay occurring in sequence 1. The start of MP1 is at 20h and the end is at the end of sequence 1. Similarly, MP2 starts at the 20h after sequence 2 has started and ends at the end of sequence 2.

It should be noted that in the results reported in this study, the impact of simulated Vehicle to Grid operation under the different equivalent current cycles has been quantified only for Measurement Period 1 (MP1). The impact during Measurement Period 2 (MP2) operation was not quantified because the duration of Measurement Period 2 (MP2) was not sufficient to accurately quantify the irreversible performance decay.

3.2.2. Computing rate of voltage decay

The frequency of voltage data recording by the data-logger connected to the test bench PEMFC (NI USBDAQ) during the simulated Vehicle to Grid experiments conducted during this study was 1Hz. Therefore, the slope in the voltage evolution of simulated Vehicle to Grid operation under the different equivalent current cycles was used as a measure of performance decay (or RoD) of the Fuel Cell. The slope of the voltage evolution, through Measurement Period 1 (MP1), was computed from the voltage recordings during this period, using the MATLAB Curve Fitting Toolbox™. The slope was computed by using a polynomial fit of degree 1, through the recorded time-voltage data; the slope of the fitted line being considered an indicator of performance decay over time. The toolbox uses the method of least squares to generate fits through the data and offers multiple types least-square fittings [1]. In this study, the results have been derived using a robust least square (rls) fitting. Since outliers have a strong influence on the results of least square fittings, this type of fit minimizes the influence of these outliers on the fit.

3.3. Summary

Catalyst loading and it's utilization has a strong influence on the performance of the Membrane Electrode Assemblies (MEAs) of PEMFCs. To improve the catalyst utilization, the MEA is first exposed to high pressure, temperature and humidity conditions. This helps break-into the catalyst reaction sites thereby improving membrane performance at relatively milder conditions. The process of exposing the MEA to harsh conditions for a short period of time (approximately 2-3 hours) in order to facilitate reaction site break-in is known as membrane activation procedure. The activation procedure applied on each new MEA used in this study has been described in this chapter.

Furthermore, the method used to analyze the voltage evolution and compute the performance degradation in the measurement period MP1, on applying the equivalent current cycles (CC1, CC2 and CC3) on a laboratory PEMFC set-up under the specified experimental conditions for simulated Vehicle to Grid operation, has also been described in this chapter.

4

Results and Discussions

4.1. Electrochemical characterization of MEAs

4.1.1. Polarization Curve

1. ***Before simulated Vehicle to Grid experiments:***

   Figure 4.1 represents the polarization curves of all Membrane Electrode Assemblies (MEAs) before they were used in the simulated Vehicle to Grid experiments. All polarization curves were measured just after activation, under simulated Vehicle to Grid experimental conditions as specified in section 2.2. It can be observed that, contrary to what is expected, all new activated MEAs do not perform identically. This difference in performance may be linked to the differences in the manufacturing of each MEA, such as difference in size of active area, differences in catalyst loading *etc*.

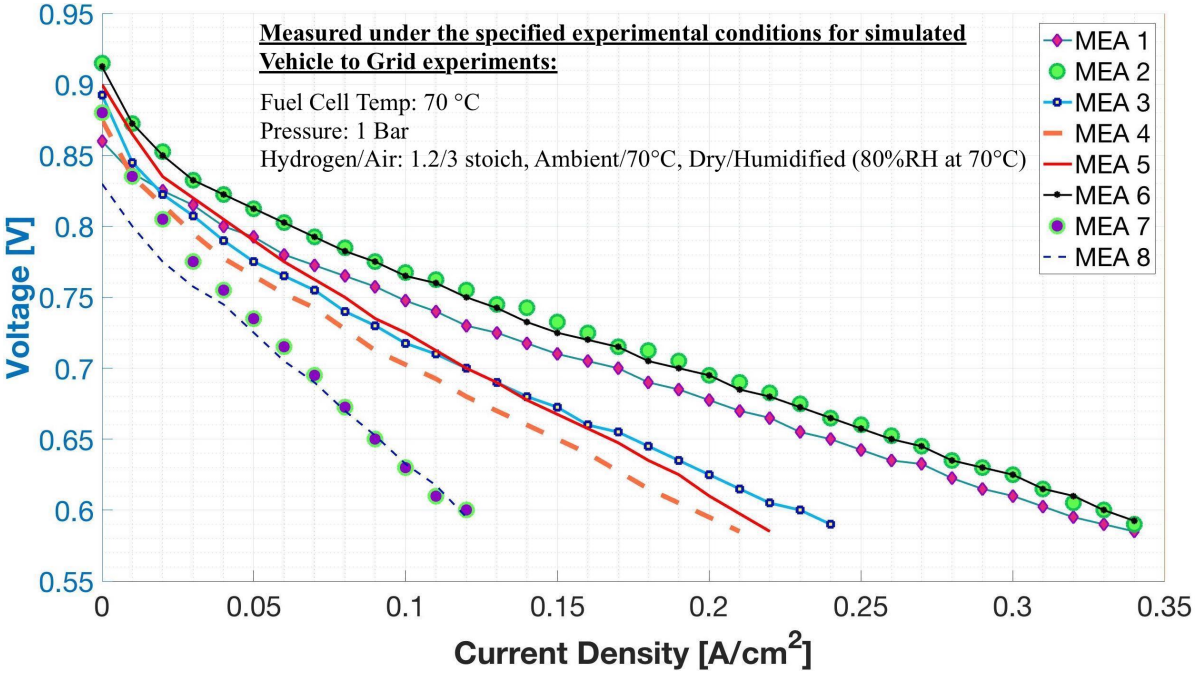

Figure 4.1: Polarization Curve of all MEAs before start of simulated Vehicle to Grid experiments

Furthermore, the difference in performance may have also been caused by the difference in the tightening torque applied during the test-bench PEMFC assembly. Each experiment was conducted using a new MEA which was assembled into the Fuel Cell before the experiment. During assembly, all bolts were first tightened under a tightening torque of 10Nm, applied using a torque wrench. Following this, all bolts were tightened by approximating the torque applied, without using a precision device. This was because the tightening torque of 10Nm, suggested by the PEMFC manufacturer, did not yield a leak proof set-up. Insufficient tightening torque causing increased contact resistance in some assemblies could be one of the reason for difference in performance. It is also possible that due to this approximation, the size of the inter-facial gaps between the Gas Diffusion Layer (GDL) and the flow plates might vary between various assemblies and within a single assembly itself. Excess inter-facial gaps causing water retention could potentially lead to performance loss because of poor mass transport. Thus, the varying assembling torques could have led to varying performance between new MEAs.

Therefore, it is could be concluded that the difference in performance between new MEAs may be caused by the marginal differences in physical properties, manufacturing difference between the MEAs and by the approximations made while assembling the MEAs into the test-bench PEMFC.

Although all MEAs perform differently at the start of the experiments, it does not effect the final computed performance loss result over time. This is because the performance loss in this study is measured by computing the slope of the voltage evolution under each equivalent Current Cycle (CC). Therefore it is independent of the initial performance of the MEA and is only a measure of relative voltage drop between the start and the end of the measurement period; the relative voltage drop being a consequence of continuously operating under the respective equivalent Current Cycles (CCs) and experimental conditions for simulated Vehicle to Grid experiments.

4.2. Description of the recorded voltage evolution data of simulated Vehicle to Grid experiments

4.2.1. Voltage evolution characteristics under each type of equivalent current cycle

Figure 4.2 shows the voltage evolution characteristic for the equivalent constant current aging cycles CC1 ($0.03\frac{A}{cm^2}$) in Experiment 2, where only a single set of voltage evolution data is observed because of constant operation at a single unique current density. All the voltage evolutions under the constant current aging cycles (CC1 and CC2) showed similar evolutionary behavior.

Figure 4.3 shows the voltage evolution characteristic under the equivalent cyclic current aging cycle (CC3) in Experiment 6. The two distinct voltage evolution visible in Figure 4.3 is a consequence of periodic operation at the two distinct current densities of CC3 - $0.03\frac{A}{cm^2}$ and $0.01\frac{A}{cm^2}$ in 15 minute blocks. The voltage evolution with higher absolute magnitude represents Fuel Cell operation at lower current density, and *vice-versa*. The periodic operation at the two separate current densities can be seen in a magnified scale of the voltage evolution data in Figure 4.3. The increasing trend while operating at higher current densities, observed in the magnified voltage evolution plot in Figure 4.3, may be due to the temporary improvement in the humidification characteristics as a consequence of more water being produced at higher current density operation. All the voltage evolutions under the cyclic current aging cycle (CC3) showed similar evolutionary behavior.

Finally, the high frequency of voltage recordings (1 Hz) causes small excursions between two data points recorded in consecutive seconds, as seen in the magnified scale of Figure 4.3. These local fluctuations that are observed between consecutive voltage recordings may be attributed to the chemical reaction kinetics of the re-dox reactions; and also to the local reactant transport resistance caused

by the dynamic humidity distribution across the reaction sites. Moreover, since the voltage measuring probes were inserted into holes on the side of the mono-polar plates, it's location might also have an effect on the voltage recordings. Nevertheless, despite these local voltage excursions that occur on a seconds time scale, the performance degradation over the length of the entire experiment (time scale of hours) could be measured with considerable accuracy.

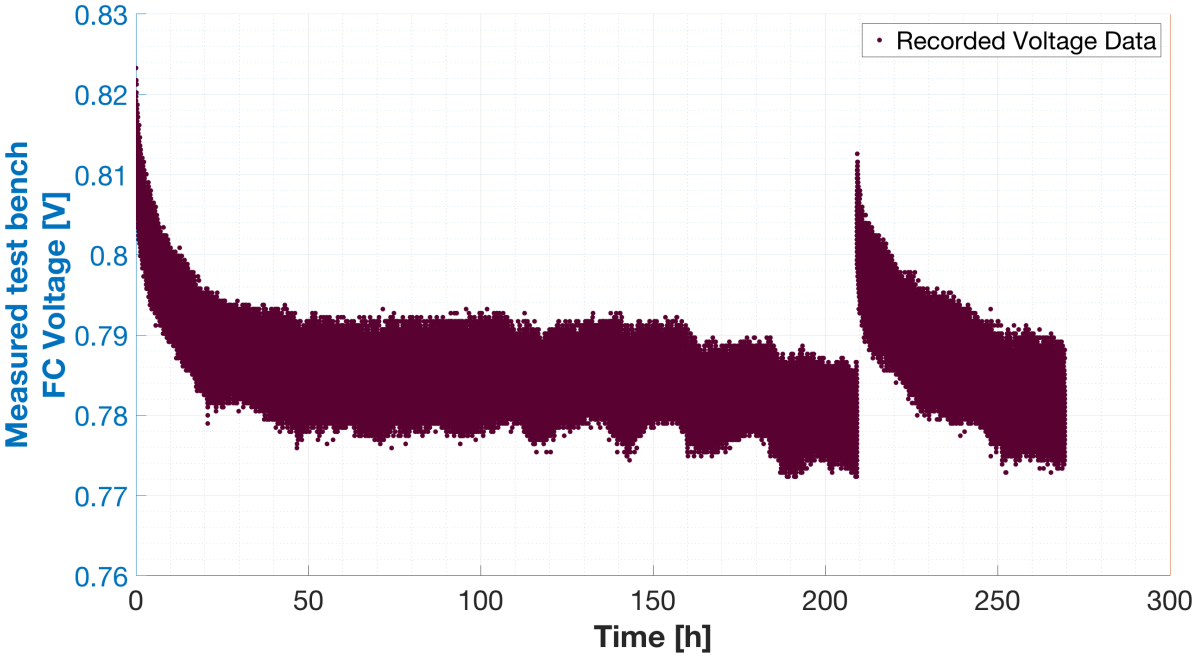

Figure 4.2: Voltage evolution characteristic of test bench Fuel Cell in simulated Vehicle to Grid operation under equivalent constant current aging cycles CC1 in Experiment 2

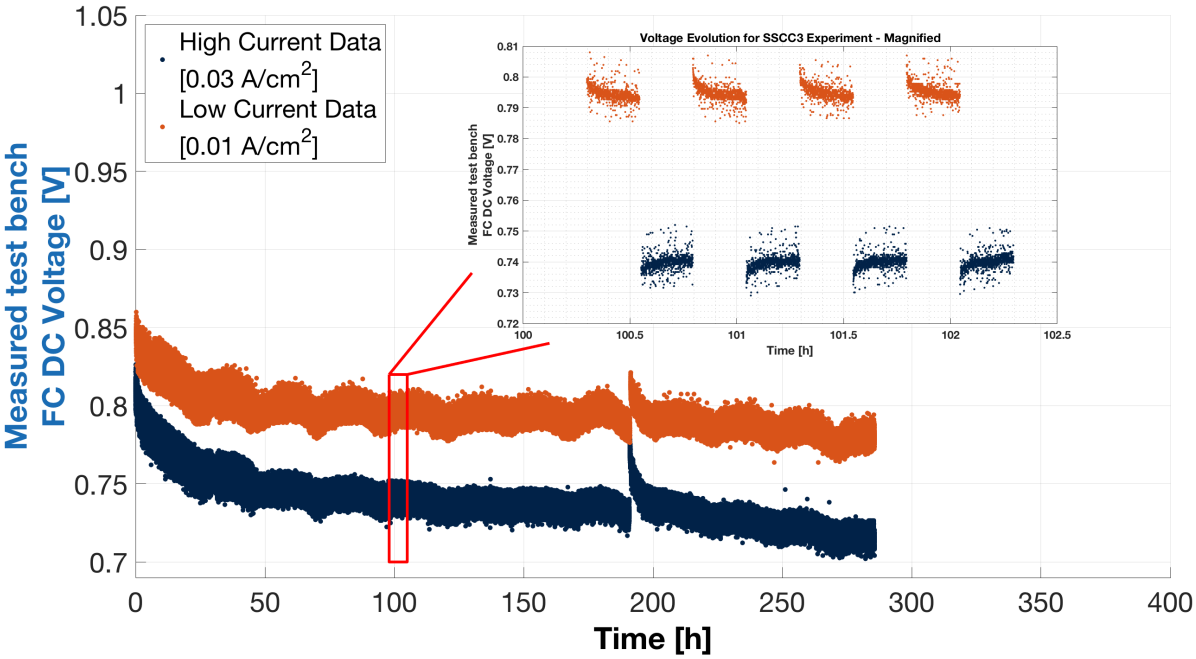

Figure 4.3: Voltage evolution characteristic of test bench Fuel Cell in simulated Vehicle to Grid operation under equivalent cyclic current aging cycle CC3 in Experiment 6

4.2.2. Effect of laboratory temperature on the simulated Vehicle to Grid experiments

Periodic valleys can be seen on observing the voltage evolution in Figures 4.3 and 4.2. These valleys occur approximately every 24 hours. The cause for this behavior of the voltage evolution was found to be the daily fluctuations in the laboratory (ambient/environmental) temperature.

Figure 4.4 shows the inverse relation between laboratory temperature and the voltage measured across the test bench fuel cell during Experiment 3. It is seen that as the temperature rises around mid-day, the voltage shows a corresponding drop. The voltage evolution can be seen to recover overnight, when the ambient temperature reduces. This type of inverse relation was observed in all simulated Vehicle to Grid experiments, but only recordings from one experiment have been presented and discussed here.

Due to its periodic nature, these temperature fluctuations are not expected to impact measured performance loss. It may be said that the periodic voltage valleys are balanced by the periodic voltage peaks that follow them. Furthermore, since FCEVs are most likely to operate in the outdoors, where periodic environmental temperature fluctuations occur naturally, it could be useful to include the effects of these fluctuations while conducting studies related to Fuel Cell Electric Vehicle to Grid operation.

Since the fuel cell, humidifier and the cathodic reactant were all constantly maintained at 70℃, it is likely that the temperature fluctuations have an impact on the temperature of the anodic reactant (hydrogen). It should be specified here that the hydrogen in the Hyundai FCEV is also possibly heated during operation, although this was not actively measured in the FCEV. That is why the Hydrogen was not heated while developing the method for simulating Vehicle to Grid operation on a laboratory test-bench. Therefore, it is likely that tracing the hydrogen inlet pipe of the laboratory set-up, which ensures that the hydrogen fed to the fuel cell is heated, may aid in stopping these periodic voltage excursions.

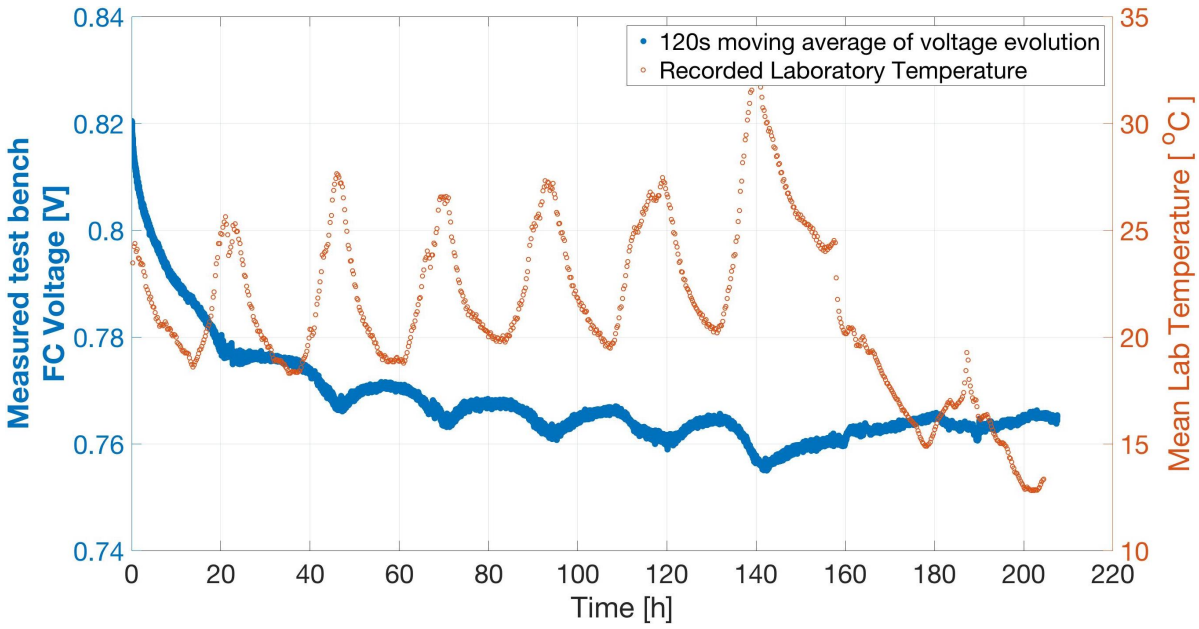

Figure 4.4: Relation between voltage evolution data under simulated Vehicle to Grid operation and the laboratory temperature during Experiment 3

Finally, the water flow rate measured in the Controlled Evaporation and Mixing unit (CEM) was also found to have an impact on the voltage evolution. Figure 4.5 shows the inverse relation between water flow rate measured in the CEM and the voltage measured across the test bench fuel cell during Experiment 3. On comparing Figures 4.4 and 4.5, it can be seen that as the temperature rises, the flow rate of water through the humidifier also shows a corresponding rise. This type of inverse relation was observed in all simulated Vehicle to Grid experiments, but only recordings from one experiment have been presented and discussed here. Finally, it is also likely that temperature fluctuations have an impact on the other supporting equipment such as the Mass Flow Controllers (MFCs) and the Back Pressure Controllers (BPCs), but this was not measured during this study.

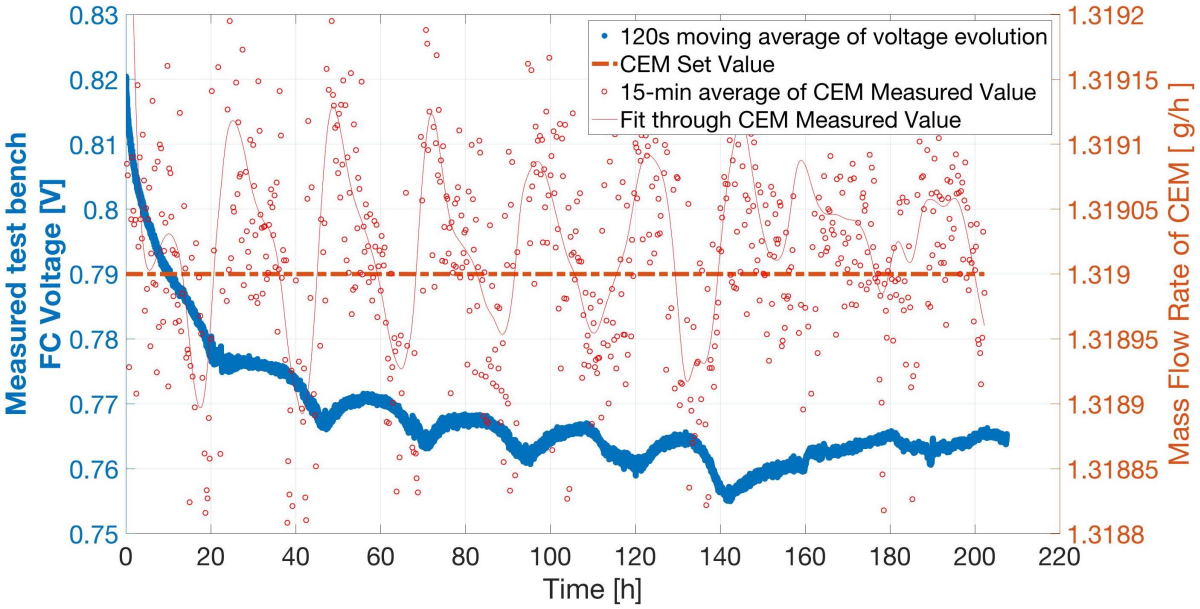

Figure 4.5: Relation between voltage evolution data under simulated Vehicle to Grid operation and the water flow rate measured in the humidification unit (Controlled Evaporation and Mixing unit - CEM) during Experiment 3

4.3. Computed performance loss in simulated Vehicle to Grid Experiments

4.3.1. Performance loss computed from the voltage evolution data recorded during simulated Vehicle to Grid Experiments

The performance loss due to simulated Vehicle to Grid operation under the various equivalent current aging cycle (CCs) have been shown in Figures 4.6, 4.7, 4.8 and Table 4.1.

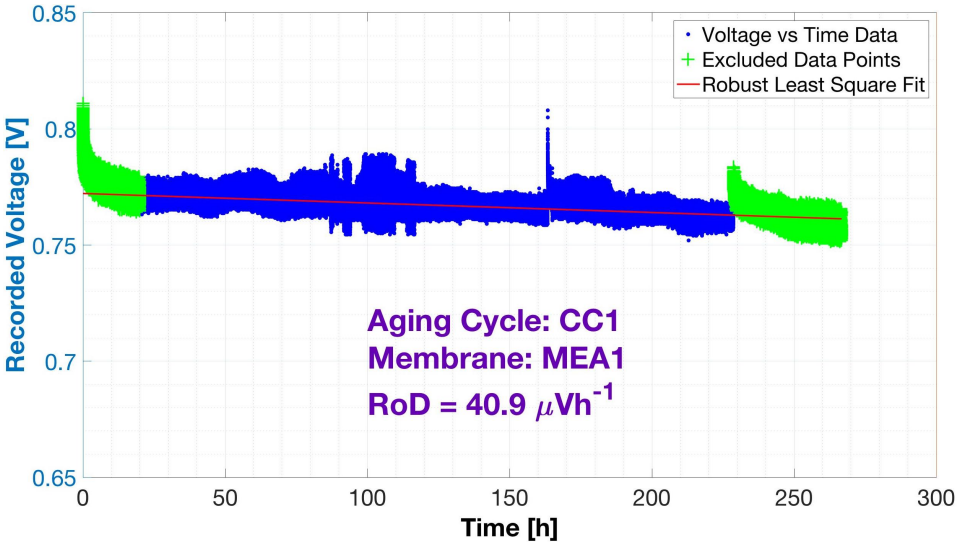

(a) Simulated Vehicle to Grid Experiment 1

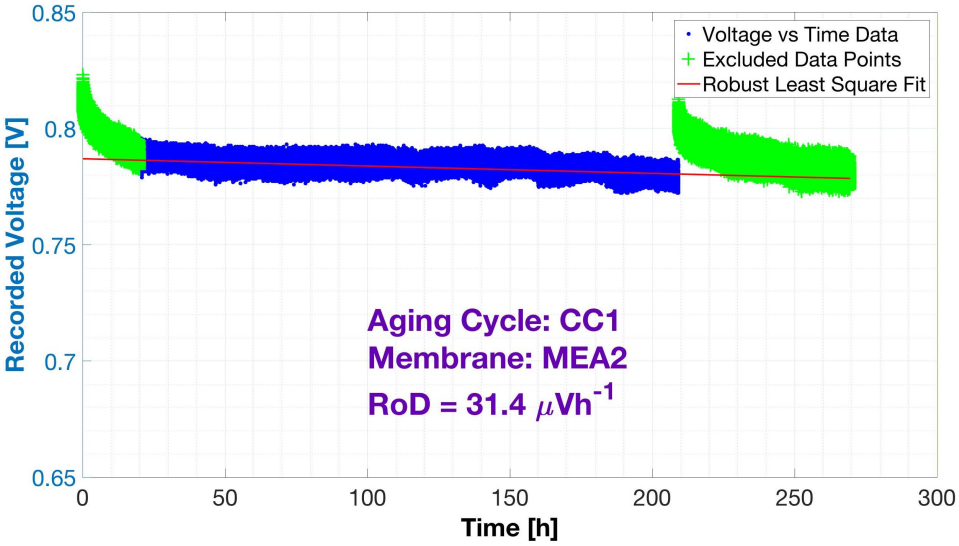

(b) Simulated Vehicle to Grid Experiment 2

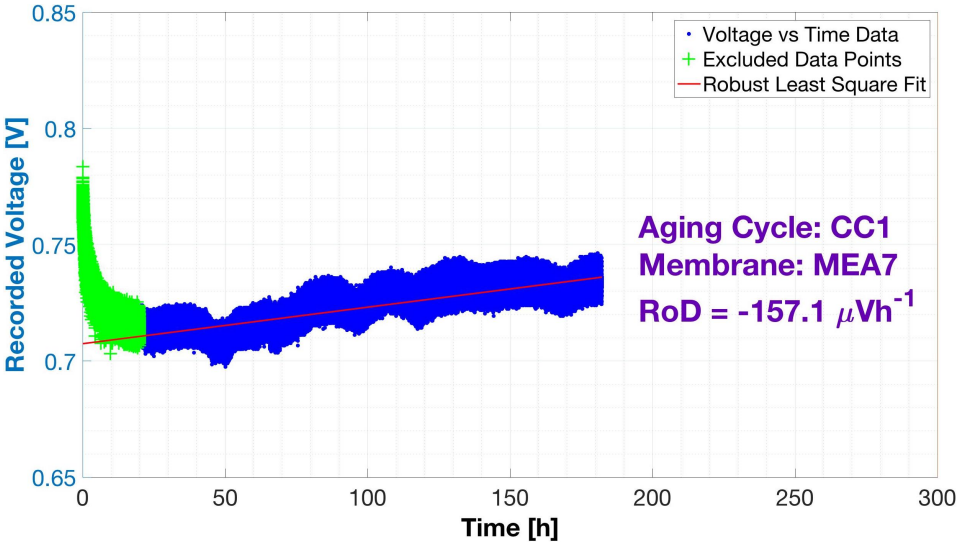

(c) Simulated Vehicle to Grid Experiment 7

Figure 4.6: Computed rate of voltage decay caused by simulated Vehicle to Grid operation under aging cycle CC1 - Constant current cycle of 0.03$\frac{A}{cm^2}$

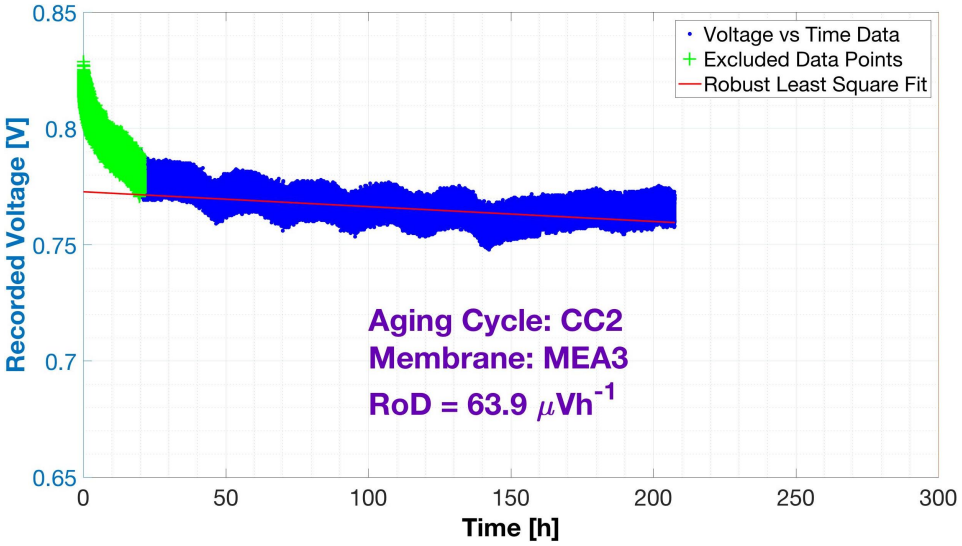

(a) Simulated Vehicle to Grid Experiment 3

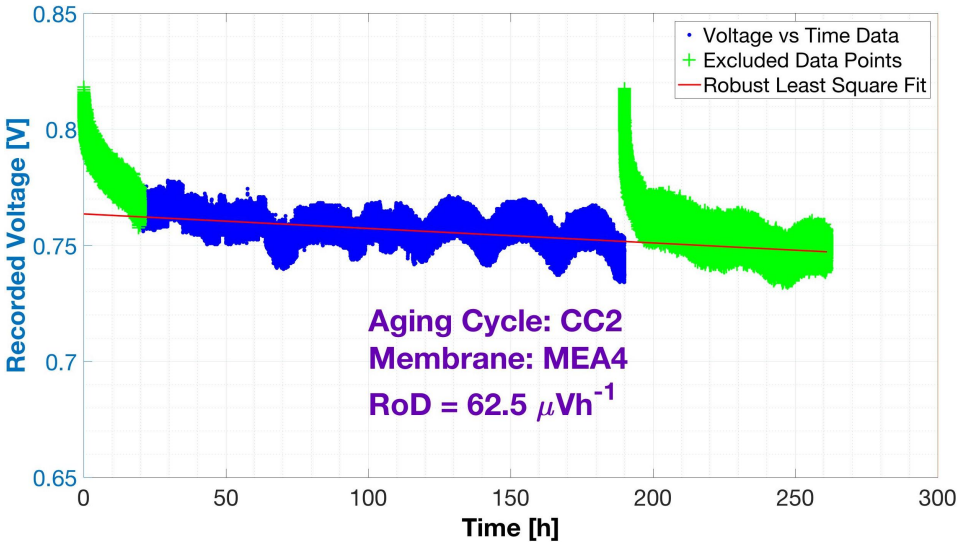

(b) Simulated Vehicle to Grid Experiment 4

Figure 4.7: Computed rate of voltage decay caused by simulated Vehicle to Grid operation under aging cycle CC2 - Constant current cycle of 0.01 $\frac{A}{cm^2}$

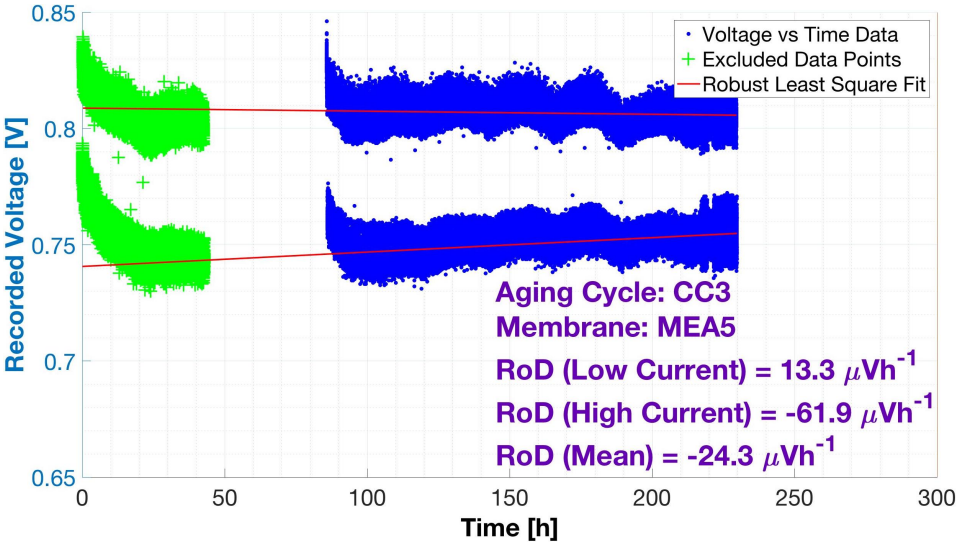

(a) Simulated Vehicle to Grid Experiment 5

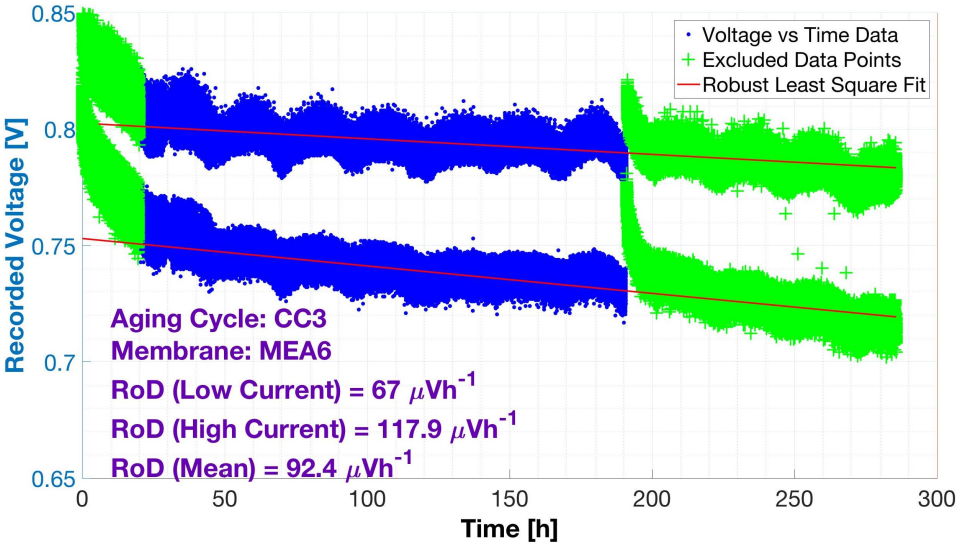

(b) Simulated Vehicle to Grid Experiment 6

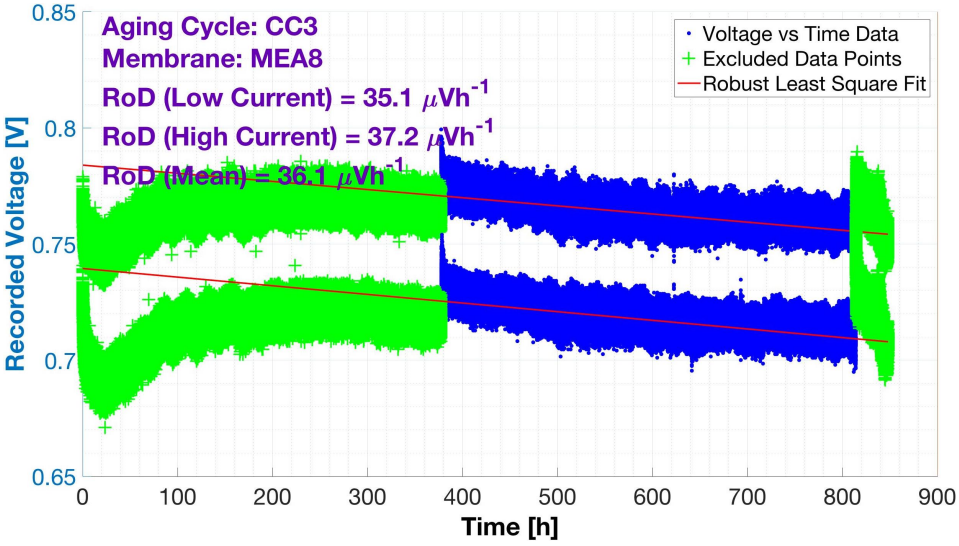

(c) Simulated Vehicle to Grid Experiment 8

Figure 4.8: Computed rate of voltage decay caused by simulated Vehicle to Grid operation under aging cycle CC3 - Cyclic current cycle between 0.03 $\frac{A}{cm^2}$ and 0.01 $\frac{A}{cm^2}$

Table 4.1: Computed rate of voltage decay caused by simulated Vehicle to Grid operation under the various aging cycles

Experiment #/ MEA #	**Type of Aging Cycle**	**Length of Measurement Period** $\left[hours\right]$	**Rate of Degradation** $\left[\mu V h^{-1}\right]$ **all results**	**Standard Deviation all results**	**Rate of Degradation** $\left[\mu V h^{-1}\right]$ **only realistic results**	**Standard Deviation only realistic results**
1	CC1	208.7	40.9	111.67	40.9	6.72
2		189.2	31.4		31.4	
7		162.3	-157.1		-	
3	CC2	187.5	63.9	0.99	63.9	0.99
4		170.0	62.5		62.5	
5	CC3	143.8	-24.3	58.36	-	39.81
6		171.0	92.4		92.4	
8		437	36.1		36.1	

Figures 4.6, 4.7 and 4.8 show the voltage evolution of the test bench FC in simulated Vehicle to Grid operation under the respective equivalent current aging cycles CC1, CC2 and CC3. The blue points are the voltage recorded in measurement period MP1 and the green points are the excluded voltage recordings since they lie outside the measurement period MP1.

The missing data between $45h$ and $85h$ in Figure 4.8 (a) was caused by fuel cell heating issues. The voltage recorded during this period was not analyzed. Due to a short-circuit, the fuel cell heating element was non functional for around $40h$. The issue was resolved by correcting the cause for the short-circuit and such a problem was not faced thereafter. Furthermore, the measurement period for this experiment (Experiment 5) has been adapted accordingly by changing the start of the measurement period from $20h$ to $85h$.

An increasing trend is observed in the voltage evolution of Experiment 7, where measured Rate of Degradation (RoD) is negative. A negative RoD is indicative of performance improvement over use. This is an unrealistic occurrence and this behavior may be caused by incomplete activation of the MEAs, before the start of the experiment. This incomplete activation can be identified by comparing the starting voltage (at time $0s$) of Experiment 7 with Experiment 1 and 2 in Figure 4.6. Similarly, the starting voltage at (at time $0s$) for Experiment 8, which also showed similar increasing voltage trend initially, is also significantly lower as compared to Experiments 5 and 6 in Figure 4.8.

It is likely that over use, the evolution in such a case would reach an inflection point before the appearance of realistic performance decay. If these experiments were continued for longer *i.e* if the measurement period for these experiments were longer, realistic degradation would have been observed. This behavior is seen in Experiment 8 (Figure 4.8 (c)) where the experiment was continued for a longer duration (measurement period is comparatively longer - $437h$). The fuel cell performance in this experiment shows unrealistic improvement between $20h$ and $390h$ of operation, before degradative phenomena begin to hinder performance staring from $390h$.

The increasing trend in the voltage evolution at high current operation of Experiment 5 may be linked to cooling of the cell due to the heater problems faced between $45h$ and $85h$. Incomplete activation might not be the cause for this increasing trend because the starting voltage for Experiment 5 is similar to Experiment 6, which showed realistic performance decay. Cell cooling could have caused water retention within the cell and the increasing voltage trend may be indicative of the retained water being dried. Furthermore, realistic performance decay was also measured at low current operation during this experiment, although it's absolute magnitude was low compared to all other experiments. Therefore, it is likely that such behavior is an outlier.

Finally, the voltage improvement observed in Experiment 8 at $390h$ and $805h$ in Figure 4.8 (c) is not due to implementation of the recovery procedure. The higher voltage recording was caused because of Open Circuit Voltage operation for approximately 5 minutes while refilling the water vessel connected to the humidifier. This behavior was also observed in [22] where temporary voltage recovery phenomena caused by three types of interruptions: polarization curve measurement, maintenance, and temperature excursions; has been reported.

Table 4.1 tabulates all the performance decay rates measured in simulated Vehicle to Grid operation under the respective equivalent current aging cycles CC1, CC2 and CC3. It can be observed that the standard deviation between results of simulated Vehicle to Grid operation under equivalent current aging cycles CC1 and CC3 is high. Since the cause of these unrealistic performance decay results was most likely incomplete activation and an insufficient measurement period, the unrealistic results can be discarded. This highlights the need to repeat the simulated Vehicle to Grid experiments which showed unrealistic performance loss (or performance improvement). Similar to Experiment 8, these experiments should be continued for a longer duration, if such unrealistic performance behavior is observed again.

The realistic results have therefore also been tabulated separately. It is observed that the standard deviation for the results from CC1 and CC3 are now relatively lower. Although, the standard deviation for the results from the CC3 cycles are still high.

The measured realistic performance decay for the MEA in simulated Vehicle to Grid operation under the equivalent constant current (0.03$\frac{A}{cm^2}$) aging cycle CC1 is 40.9 μVh^{-1} and 31.4 μVh^{-1}. For simulated Vehicle to Grid operation under the equivalent constant current (0.01$\frac{A}{cm^2}$) aging cycle CC2, the performance decay measured for the MEAs is 63.9 μVh^{-1} and 62.5 μVh^{-1}. For simulated Vehicle to Grid operation under the equivalent cyclic current (0.03$\frac{A}{cm^2}$ - 0.01$\frac{A}{cm^2}$ - 0.03$\frac{A}{cm^2}$) aging cycle CC3, the mean magnitude of realistic performance loss measured was 92.4 μVh^{-1} and 36.1 μVh^{-1}, showing a large divergence and therefore these experiment needs to be repeated. Nevertheless, the performance decay measured during all experiments are within the range of performance decay for PEMFCs, reported in literature (Table 2 as reported by de Bruijn *et al* in [7]); albeit for a different applications (types of load cycles) and at different experimental conditions.

Furthermore, the realistic performance loss measured for simulated Vehicle to Grid operation under the constant current aging cycles CC1 and CC2 both are lower than 170 μVh^{-1} and 180 μVh^{-1} reported by Pahon *et al* [36] for a constant current cycle of 0.77$\frac{A}{cm^2}$ and 0.45$\frac{A}{cm^2}$, after durations of 147h and 125h respectively. Their study was conducted for a μ-CHP load profile that simulates the behavior of a stationary PEMFC application throughout the year. The active area of the fuel cell used in their study was 44 times the active area of the fuel cell used in this study. Furthermore, both reactant were humidified to 50% RH. The reported rate of degradation is higher as compared to those measured in this study because the measurement period for which performance loss was computed was relatively short (147h and 125h only) and also because the performance degradation was measured including the recoverable performance losses. In the same experiment they also studied the impact of cyclic loads with intermediate operation at OCV and at maximum and 50% of maximum power. They report an overall degradation rate of 75 μVh^{-1} and 76 μVh^{-1} after total test duration of 1000 and 500 hours respectively. They suggest that the constant load degradation is higher than the overall degradation rate because some of the degradation occurring during constant load operation was recovered due to load cycling and OCV operation in the subsequent cyclic load applied on the same fuel cell immediately.

Moving further, from an actual Vehicle to Grid perspective, equivalent current aging cycle CC1 was derived for the Hyundai's Fuel Cell operating at a constant load of 12kW (Table 2.4). The realistic performance degradation measured under constant operation of this aging cycle (CC1) was 40.9 μVh^{-1} and 31.4 μVh^{-1} in Experiments 1 and 2 respectively. Therefore, it could be concluded that for the Hyundai's Fuel Cell in actual Vehicle to Grid operation at constant power of 12kW, the performance degradation undergone would be in the range of 40.9 μVh^{-1} and 31.4 μVh^{-1}. These measured realistic performance degradation rates are very high from a lifetime point of view.

For Experiment 2, the starting voltage observed for the laboratory PEMFC is approximately 0.82V (Figure 4.6 (b)). Assuming an end of life metric of 10% voltage drop from initial voltage [31], this translates to a total lifetime of around 2611h $\left(\frac{10\% \times 0.82}{31.4 \times 10^{-6}}\right)$. These lifetime results are far lower than the lifetimes for fuel cell stacks, which is around 8000h [31]. This could be because of the operating conditions were not optimal and shows that repetition of experiments is required to derive optimal operating conditions for vehicle to grid operation. Furthermore, it could also be caused by the quality of the test bench fuel cell itself, and it could be possible that a fuel cell from a different manufacturer could lead to better results.

Moving further, on comparing results of the constant current aging cycles CC1 (0.03$\frac{A}{cm^2}$) and CC2 (0.01$\frac{A}{cm^2}$), it can be seen that the performance loss is lower for the higher magnitudes of constant current cycle (CC1 - 0.03$\frac{A}{cm^2}$). The lower performance loss at higher constant current may be due to

the improved humidification as a result of higher water production at higher loads; similar to the improving voltage trend observed in the magnified view of the voltage evolution under the cyclic current aging cycle CC3 as seen in Figure 4.3. The product water mass flow for aging cycles CC1 and CC2 were 0.0504 gh^{-1} and 0.0168 gh^{-1} respectively. As a consequence of the constant current density magnitude of CC1 being 3 times that of CC2, the water produced during the CC1 aging cycle was 3 times the quantity of water produced during the CC2 aging cycle. The higher product water mass flow improves humidification characteristics within the cell which could lead to the observed reduction in rate of performance loss.

Moving further, based on the performance decay measured for the constant current aging cycles CC1 (12kW) and CC2 (5kW), it may be concluded that in a future scenario, if a decision is to be made with regards to operating a certain number of FCEVs to service a required Vehicle to Grid load; it would be advisable to operate fewer FCEVs at higher loads instead of operating a larger number of FCEVs at lower loads. That is, from a degradation point of view: to service a given constant Vehicle to Grid load it would be advisable to operate fever FCEVs or FCREEVs at higher load instead of operating larger number of Vehicles at lower loads.

For example, if a constant Vehicle to Grid load of 100kW is to be serviced and there are 20 Fuel Cell Electric Vehicles (FCEVs) available, it would be better to operate only 10 FCEVs constantly delivering 10kW each, instead of operating 20 FCEVs constantly delivering 5kW each; since rate of performance degradation at higher loads is observed to be lower in this study. It should be noted that this scenario is only valid when the power management strategy for these vehicles involves constant Fuel Cell operation, with the High Voltage Battery of the Vehicle not participating in Vehicle to Grid services. Furthermore, operating fewer Vehicles at higher loads would also have a positive impact on the availability of FCEVs for normal operating (driving) purposes.

4.3.2. Impact of simulated Vehicle to Grid operation on Polarization Curves

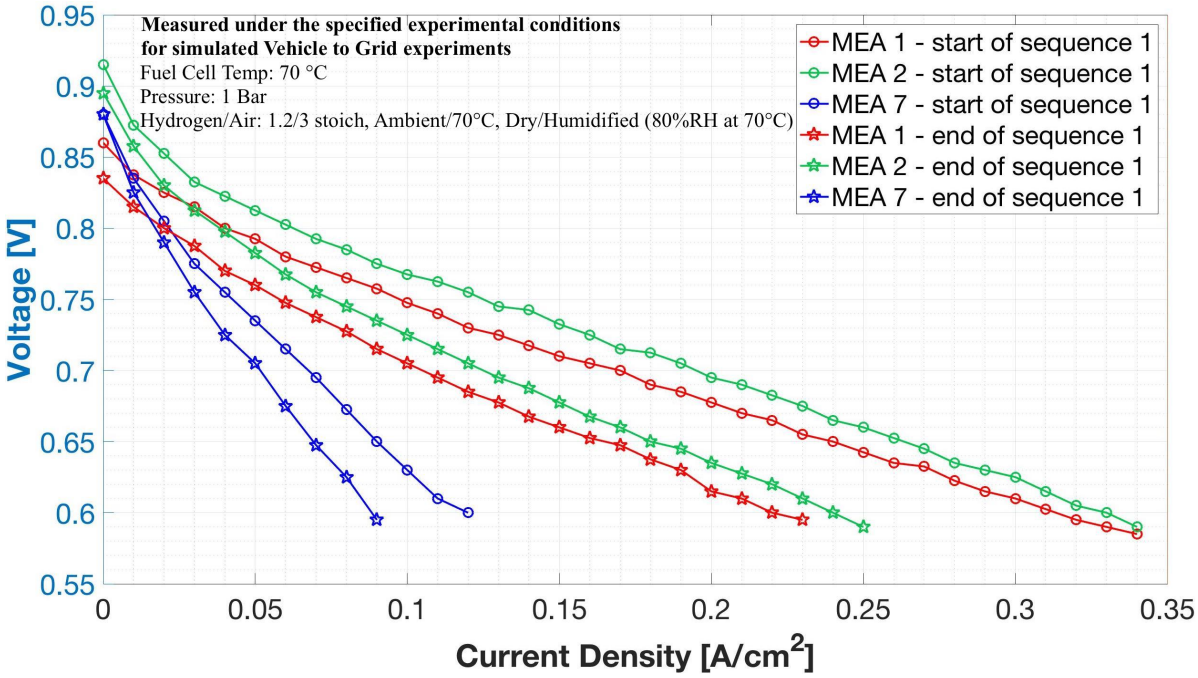

Figure 4.9: Polarization Curves measured at the start and end of Sequence 1 of Vehicle to Grid operation under aging cycle CC1 - Constant current cycle of 0.03 $\frac{A}{cm^2}$

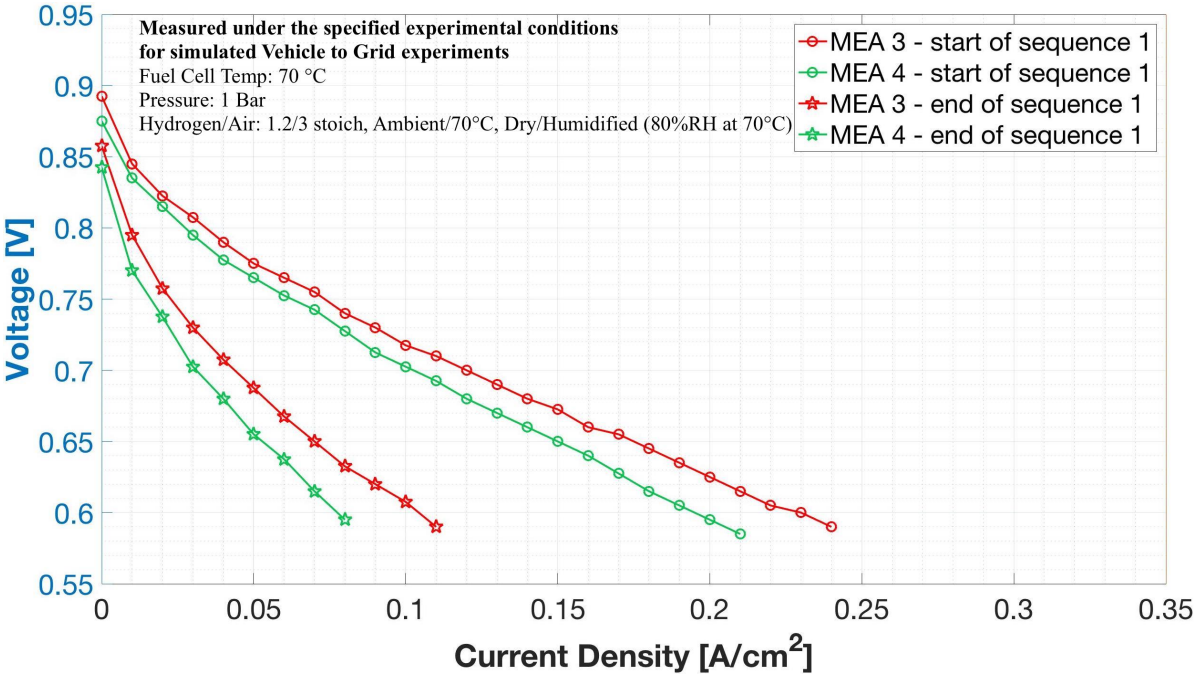

Figure 4.10: Polarization Curves measured at the start and end of Sequence 1 of Vehicle to Grid operation under aging cycle CC2 - Constant current cycle of 0.01 $\frac{A}{cm^2}$

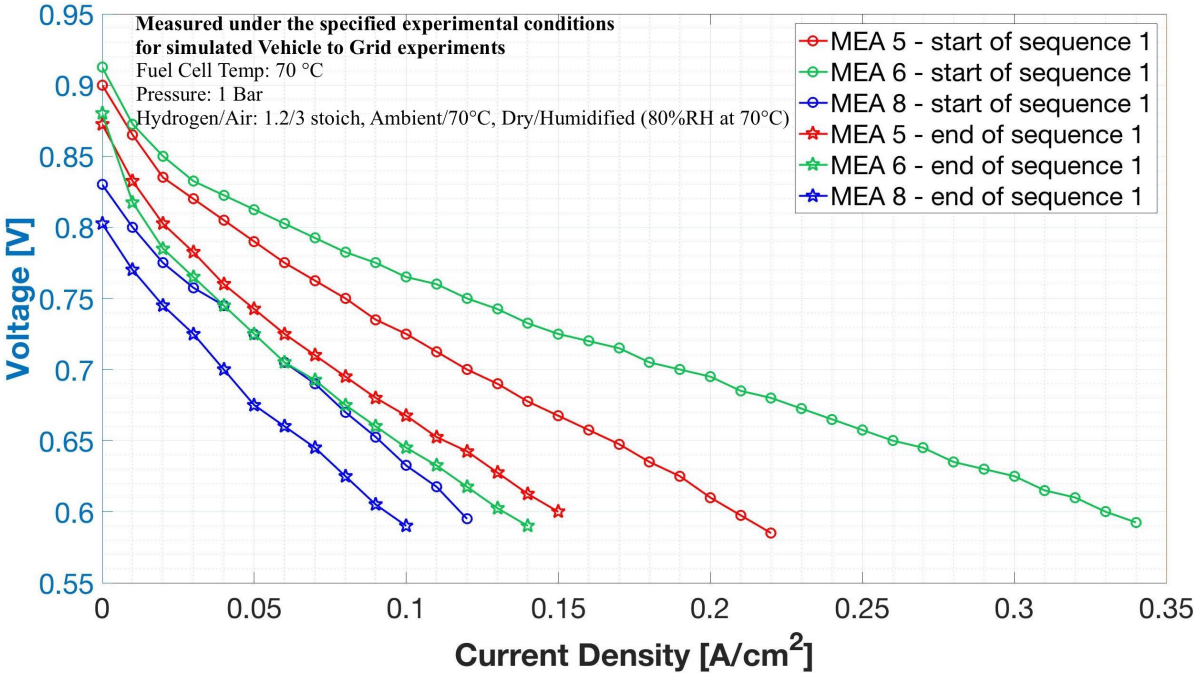

Figure 4.11: Polarization Curves measured at the start and end of Sequence 1 of simulated Vehicle to Grid operation under aging cycle CC3 - Cyclic current cycle between 0.03 $\frac{A}{cm^2}$ and 0.01 $\frac{A}{cm^2}$

Figures 4.9, 4.10 and 4.11 represent the polarization curves before and after Sequence 1 of the respective aging cycles. From the figures it is clear that significant losses occur due to simulated Vehicle to Grid operation under the various aging cycles. It should be noted that the performance losses observed in the polarization curves also include the recoverable performance losses caused due to reversible phenomena. Therefore the magnitude of performance losses computed from the polarization

curve would be higher than the magnitude of irreversible degradation which was computed using the fitting algorithm of the MATLAB Curve Fitting Toolbox™(Table 4.1).

For example, the performance loss measured in Experiment 2 (MEA2) from the polarization curve (Figure 4.9) is 104.8 $\mu V h^{-1}$ at 0.03 $\frac{A}{cm^2}$ after 209.2h, which is the entire length of Sequence 1 and not only Measurement period MP1 (189.2h). Whereas the performance loss measured using the MATLAB Curve Fitting Toolbox™and the data recorded is 31.4 $\mu V h^{-1}$ during the Measurement Period MP1, as seen in Table 4.1. The higher performance loss measured using the polarization curve also contains the recoverable performance losses that occur during the transient period of the first 20h of the test. Thus, it may be concluded that the method used to measure the performance loss in this study, may lead to a more accurate computation of the true measure of irreversible performance losses that occur.

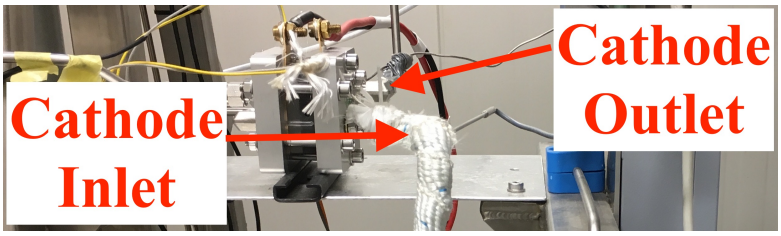

Figure 4.12: Side-view of the PEMFC connected in the test-bench

Furthermore, the significant recoverable losses could have been caused by water retention because of ineffective drying of the fuel cell, thus leading to poor mass transport of reactants to the reaction sites. The ineffective drying could be caused by the piping design of the PEMFC set-up. As seen in Figure 4.12, the inlet for the humidified cathodic reactant was positioned lower than the outlet. The humidified cathodic reactant would therefore have to flow upward through the cell, before exiting at the outlet. Thus the produced steam has to be carried away by the cathodic reactant against the direction of natural flow of water (downward). Furthermore, the outlet of the cathodic side of the cell was not traced, unlike the inlet. Therefore the likelihood of water condensing at the outlet and flowing back into the cell to affect cell performance, is higher in such a type of piping design.

4.4. Summary

All activated Membrane Electrode Assemblies (MEAs) did not perform identically before they were used in the simulated Vehicle to Grid experiments. It was concluded that the difference in performance between new MEAs may be caused by the marginal differences in physical properties, manufacturing difference between the MEAs and by the approximations made while assembling the MEAs into the test-bench PEMFC.

Furthermore, a strong inverse relation between laboratory temperature (day and night) and the voltage measured across the test bench fuel cell was observed. It was concluded that due to its periodic nature, these temperature fluctuations are not expected to impact accuracy of the measured performance loss. Furthermore, since FCEVs are most likely to operate in the outdoors, where periodic environmental temperature fluctuations occur naturally, it was concluded that it could be useful to include the effects of these fluctuations while conducting studies related to Fuel Cell Electric Vehicle to Grid operation.

Moving further, some of the performance losses measured in the simulated Vehicle to Grid experiments showed unrealistic voltage evolution characteristics where the voltage delivered by the PEMFC improved under the aging cycle imposed. It was concluded that insufficient testing duration and insufficient MEA activation was the reason for this; and realistic performance losses would have been observed if these simulated experiments were continued for longer durations. This was verified by continuing one experiment for a longer duration ($\approx$850h) as compared to the other experiments (all less than 300h). The fuel cell performance in this experiment shows unrealistic improvement until 390h of continuous operation, after which realistic performance degradation was observed and measured.

The measured realistic performance decay for simulated Vehicle to Grid operation under the equivalent constant current (0.03$\frac{A}{cm^2}$) aging cycle CC1 was found to be 40.9 μVh^{-1} and 31.4 μVh^{-1}. For simulated Vehicle to Grid operation under the equivalent constant current (0.01$\frac{A}{cm^2}$) aging cycle CC2, the performance decay measured was 63.9 μVh^{-1} and 62.5 μVh^{-1}. For simulated Vehicle to Grid operation under the equivalent cyclic current (0.03$\frac{A}{cm^2}$ - 0.01$\frac{A}{cm^2}$ - 0.03$\frac{A}{cm^2}$) aging cycle CC3, the mean magnitude of realistic performance loss measured was 92.4 μVh^{-1} and 36.1 μVh^{-1}. Due to the high divergence of the performance loss results obtained for CC3, it was concluded that there is a need to repeat these experiment. Nevertheless, the performance decay measured during all experiments were within the range of performance decay for PEMFCs, reported in literature (Table 2 as reported by de Bruijn *et al* in [7]).

Furthermore, since the performance decay measured for simulated Vehicle to Grid operation under constant current (0.03 $\frac{A}{cm^2}$) aging cycle CC1 was lower than that measured at constant current (0.01 $\frac{A}{cm^2}$) aging cycle CC2, it was concluded that from a degradation point of view: to service a given constant Vehicle to Grid load it would be advisable to operate fever FCEVs or FCREEVs at higher load instead of operating larger number of Vehicles at lower loads.

Finally, it was also concluded that the performance losses measured using the polarization curves should not be interpreted as a true measure of irreversible performance loss. This is because the performance loss also contains the performance loss caused due to recoverable phenomena. Thus, it was concluded that the method used to measure the performance loss in this study, may lead to a more accurate computation of the true measure of irreversible performance losses that occur.

5

Conclusions

The objective of this study was to measure the impact of Vehicle to Grid operation on the Fuel Cell of Fuel Cell and Fuel Cell Range Extender Electric Vehicles - FCEVs and FCREEVs.

Through this study it was first concluded that there is a need for conducting simulated Vehicle to Grid experiments on a laboratory PEMFC test-bench; because of the inability to conduct long-term dedicated Vehicle to Grid experiments using the TU Delft Hyundai Fuel Cell Electric Vehicle and actual Vehicle to Grid set-up. Furthermore, it was described how limited control over the power management strategy programmed into the Hyundai Fuel Cell Electric Vehicle leads to the need for conducting simulated Vehicle to Grid experiments on a laboratory test-bench.

A small-scale experiment was then designed to simulate Vehicle to Gird operation of the $100kW$ Fuel Cell stack in the TU Delft Hyundai Fuel Cell Electric Vehicle (FCEV), on a laboratory PEMFC test-bench of $5cm^2$ active area. The Hyundai's Vehicle to Grid mode Fuel Cell load cycle that was simulated on the laboratory PEMFC during this study was developed based on a literature survey and considering Vehicle to Grid scenarios in which the Vehicle is likely to operate. Three load cycles for the Hyundai's Fuel Cell were selected to be simulated: 1. LC1 - Fuel Cell operation at constant load of $12kW$ 2. LC2 - Fuel Cell operation at constant load of $5kW$ and 3. LC3 - Cyclic load fuel cell operation between $12kW$ and $5kW$ in 15 minute blocks. Following this, a method was proposed to translate the selected load cycles (LC1, LC2 and LC3) specific to the Hyundai FCEV's Fuel Cell to equivalent current cycles specific to the PEMFC set-up on which Vehicle to Grid operation was simulated. This resulted in three equivalent current cycles (CCs) that were then imposed on the test-bench PEMFC. The three equivalent current cycles were: 1. CC1 - PEMFC operation at constant current of $0.03\frac{A}{cm^2}$ 2. CC2 - PEMFC operation at constant current of $0.01\frac{A}{cm^2}$ and 3. CC3 - Cyclic current PEMFC operation between $0.03\frac{A}{cm^2}$ and $0.01\frac{A}{cm^2}$ in 15 minute blocks.

Furthermore, the operating conditions that occur in the Hyundai FCEV's Fuel Cell was also derived from data recorded in the Vehicle during actual Vehicle to Grid operation. These conditions have a strong impact the performance loss of the Fuel Cell, and therefore needed to be simulated on the test bench PEMFC on which the equivalent current cycles were imposed. This ensured that the results obtained at the laboratory PEMFC was applicable to the actual Fuel Cell with greater accuracy.

Following this, the simulated Vehicle to Grid experiments were conducted on the $5cm^2$ active area PEMFC for the three equivalent current cycles (CCs) for durations ranging from $180h$ to $850h$, under the derived experimental conditions for simulated Vehicle to Grid experiments. Some of the performance losses measured in the simulated Vehicle to Grid experiments showed unrealistic voltage evolution characteristics where the voltage delivered by the PEMFC improved under the aging cycle imposed. It was concluded that insufficient testing duration and insufficient MEA activation was the reason for this; and realistic performance losses would have been observed if these simulated experiments were continued for longer durations. This was also verified in one of the simulated Vehicle to

Grid experiments.

The measured realistic performance decay for simulated Vehicle to Grid operation under the equivalent constant current (0.03$\frac{A}{cm^2}$) aging cycle CC1 was 40.9 μVh^{-1} and 31.4 μVh^{-1}. For simulated Vehicle to Grid operation under the equivalent constant current (0.01$\frac{A}{cm^2}$) aging cycle CC2, the performance decay measured was 63.9 μVh^{-1} and 62.5 μVh^{-1}. For simulated Vehicle to Grid operation under the equivalent cyclic current (0.03$\frac{A}{cm^2}$ - 0.01$\frac{A}{cm^2}$ - 0.03$\frac{A}{cm^2}$) aging cycle CC3, the mean magnitude of realistic performance loss measured was 92.4 μVh^{-1} and 36.1 μVh^{-1}. Due to the high divergence of the performance loss results obtained for CC3, it was concluded that there is a need to repeat these experiment. Nevertheless, the performance decay measured during all experiments were within the range of performance decay for PEMFCs, reported in literature (Table 2 as reported by de Bruijn *et al* in [7]).

The key takeaways of this research are:

- Long term simulated Vehicle to Grid experiments need to be conducted on a laboratory test-bench to accurately quantify the impact of Vehicle to Grid operation on the fuel cells of Fuel Cell Electric Vehicles and Fuel Cell Range Extender Electric Vehicles - FCEVs and FCREEVs.
- The experiment designed to simulate Vehicle to Grid operation on a laboratory test bench is useful and provide reasonable insight into the Fuel Cell performance decay that could occur in actual Vehicle to Grid operation.
- Performance losses measured using the polarization curves should not be misinterpreted as a true measure of irreversible performance loss because this measure also contains the performance loss caused due to recoverable phenomena.
- From a degradation point of view: to service a given constant Vehicle to Grid load it would be advisable to operate fever FCEVs or FCREEVs at higher load instead of operating larger number of Vehicles at lower loads.

6

Recommendations

This study provides a framework to estimate impact of Vehicle to Grid (V2G) operation on automotive fuel cells. However, there are a few changes that would contribute greatly to improving this work.

- The set-up can also be adapted to simulate more accurate driving conditions by dynamically controlling the mass flow of the reactants and the humidification to suit the dynamic load that defines a driving load cycle. Adaptation would require replacing the Mass Flow Controllers and changing the piping design to bring all the set-up components closer to the fuel cell to avoid lag between application of the dynamic load and response of the controller set-points. The current humidification unit (CEM) used, should be sufficient to follow the dynamic load.

- Experiments which show unrealistic degradation initially should be continued for a longer duration.

- The piping design may be improved to ensure that the cathodic outlet is below the inlet. If the current piping design has indeed led to water retention in the fuel cell, changing the design would negate this.

- Finally, a precision instrument could be used to ensure that the tightening torque applied while assembling the MEA into the test-bench single cell PEMFC, is constant.

A

Graph depicting experimental measurement period for computing voltage degradation

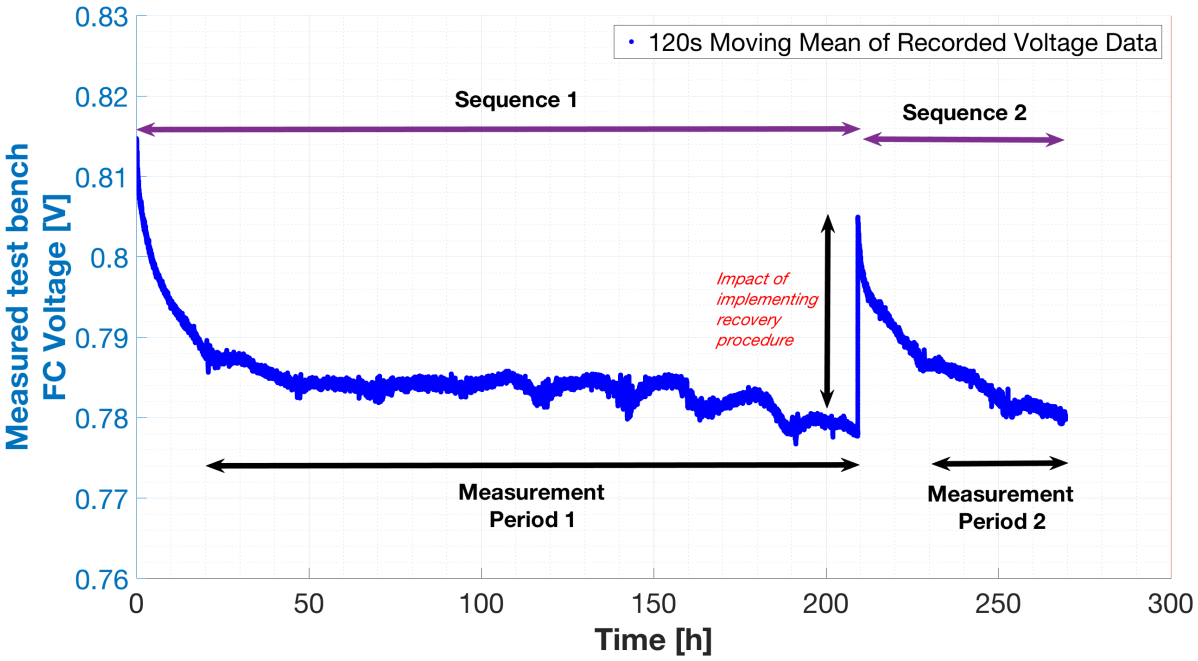

Figure A.1: Voltage evolution curve for Experiment 3 depicting the sequences and the performance measurement periods

B

General Theory regarding degradation in PEMFCs

B.1. Fuel Cell theory

A fuel cell is an electrochemical device (a galvanic cell) that converts chemical energy into electrical energy producing heat and water/steam as byproducts of the reaction (for hydrogen and air as reactants). In some cases, if the reactants are different, additional byproduct include carbon dioxide and lower forms of hydrocarbons. The absence of combustion means that there are no NO_x emissions. Furthermore, since Sulphur is considered to be detrimental to the fuel cell, the reactants are always Sulphur-free, therefore the risk of SO_x emissions is also mitigated.

A fuel cell is constructed from the following generic components: electrodes (anode and cathode), electrolyte, catalyst, gas diffusion layers, mono (or bi) polar flow plates, gaskets to provide sealing, current collectors and end plates. Fuel cells may be stand-alone, known as single cells, or may be a set of single cells connected in series or parallel (usually series) to form stacks. The common fuel cell types include Proton Exchange Membrane fuel cells (PEMFC), Direct Methanol Fuel Cells (DMFC), Alkaline Fuel Cells (Cells), Phosphoric Acid Fuel Cells (PAFC), Molten Carbonate Fuel Cells (MCFC) and Solid Oxide Fuel Cells (SOFC). They differ from each other mainly because of the material of construction of the electrolyte and the electrodes, and also because of the operating temperature range.

For Hydrogen/Oxygen (air) fuel cells such as PEMFC, the fuel cell studied in this research, oxidation of the fuel (hydrogen) occurs at the anode and reduction of the oxidant (oxygen/air) occurs at the cathode; the proton migrates across the electrolyte (membrane) from the anode to the cathode and the electron migrates from the anode to the cathode through the external circuit. The product, water or steam, is released at the cathode in this type of fuel cell. The overall redox reaction is:

For Anode:

$$2H_2 \longrightarrow 4H^+ + 4e^- \tag{B.1}$$

For Cathode:

$$O_2 + 4e^- + 4H^+ \longrightarrow 2H_2O \tag{B.2}$$

For Cathode:

$$2H_2 + O_2 \longrightarrow 2H_2O + \delta G \tag{B.3}$$

Where $\delta G = -237 \frac{kJ}{mol}$ is the change in Gibbs free energy of formation. The electrical work done in a system is represented by the energy available to do external work - the Gibbs free energy. In fuel

cells the external work involves moving electrons from one electrode to the other, through the external circuit. An electrochemical reaction is always accompanied by a change in Gibbs energy of formation due to energy release. The energy released is computed by subtracting the free energy of the products from that of the reactants.

The theoretical electric potential of a fuel cell is thermodynamically given by the Nernst equation:

$$E = E^0 + \frac{RT}{2F} \times \left(\frac{P_{H_2} \times P_{O_2}^{0.5}}{P_{H_2O}} \right) \tag{B.4}$$

Where P represents the operating partial pressure of the appropriate reactants (subscript); T is the temperature in $Kelvin$; R is the universal gas constant in $\frac{J}{kgK}$; F is the Fraday's constant in $\frac{C}{g\ mole}$; and E^0 is the theoretical or ideal electric potential in V.

The theoretical/ideal potential for a Hydrogen/Oxygen fuel cell is 1.23V at 25 ºCand 1atm pressure. From the equation it can be concluded that an increase in partial pressure of reactants and/or system pressure would lead to an increase in theoretical operating voltage . Conversely, the theoretical operating voltage would reduce with increase in operating temperature and increase in fuel utilization (which reduces reactant partial pressure).

The actual useful voltage of a fuel cell is less than the thermodynamic theoretical voltage. This is due to the losses caused by the design, operation and the fuel cell materials used. These losses are categorized as: ohmic $[ir]$, activation $[A\ ln\frac{i}{i_0}]$, fuel crossover and internal current leakage $[A\ ln\frac{i_n}{i_0}]$, and mass transport or concentration losses $[me^{ni}]$, and are expressed by the following relation:

$$V = E - ir - Aln\left(\frac{i + i_n}{i_0} \right) + me^{ni} \tag{B.5}$$

Where i is the current density in $\frac{A}{cm^2}$; r is the electric resistance per unit area in $\frac{\Omega}{cm^2}$; A is the coefficient of the natural logarithm form of the Tafel equation in V; i_n is the fuel crossover current density in $\frac{\Omega}{cm^2}$; i_0 is the exchange current density at the electrode-electrolyte interface in $\frac{\Omega}{cm^2}$; and where m and n are constants in V and $\frac{cm^2}{A}$ respectively.

A typical polarization curve for a PEMFC, with the different losses, is shown in the Figure B.1.

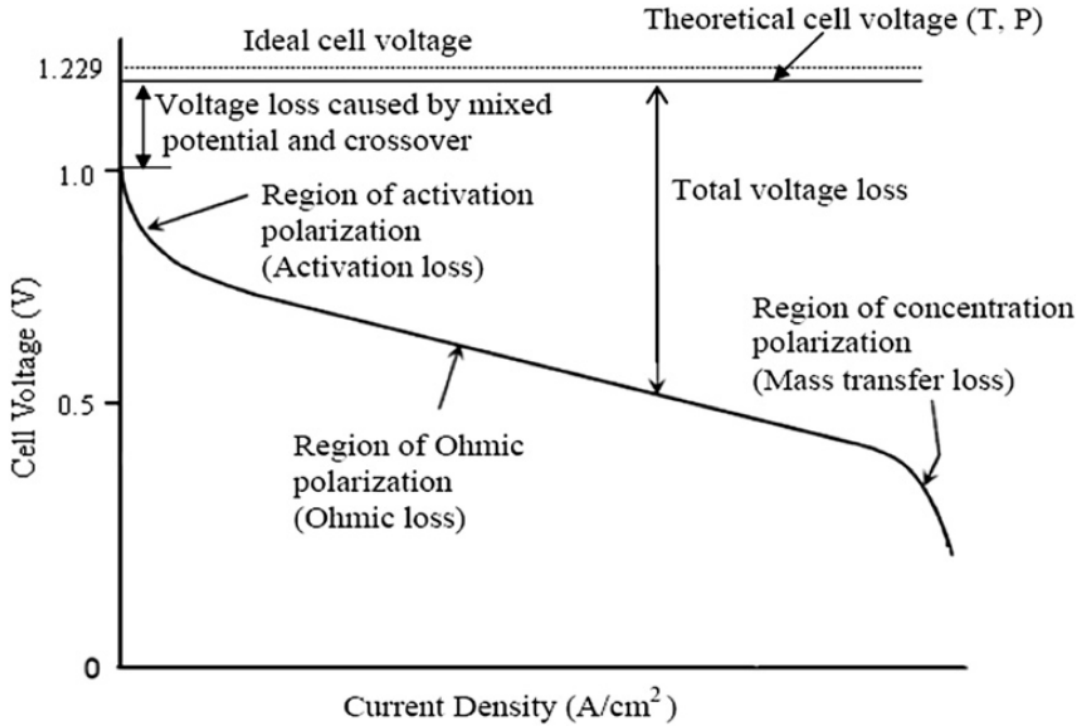

Figure B.1: Typical polarization curve for a PEMFC [57]

Another important criterion for defining fuel cell performance is power density. The power density is the product of the generated voltage at a particular current density. It is expressed in $Watts$ or $\frac{Watts}{cm^2}$, and is defined by the following expression

$$P_{cell} = I_{cell} \times V_{cell} \tag{B.6}$$

A typical power density curve, along with the corresponding polarization curve is shown in the Figure B.2 below. The peak is called the maximum power density point and is often used to evaluate the performance of a fuel cell. It should be noted that maximum power density is not always attained at maximum current density. Furthermore, it can be see that the same power density can be obtained at two different current densities; but in order to deliver a particular power density, it is advisable to operate the fuel cell at a current density which lies to the left of the peak power. This is because fuel consumption increases with increasing current density, thereby decreasing fuel cell efficiency for the same power delivery. Therefore, the optimum operating point always lies to the left of the peak power point. For the MEAs tested during this study, since the minimum voltage was restricted to 0.6V, the maximum power point was never obtained during fuel cell characterization (making the polarization and corresponding power density curves). As a consequence, the fuel cell was always functioning at its optimum operating point.

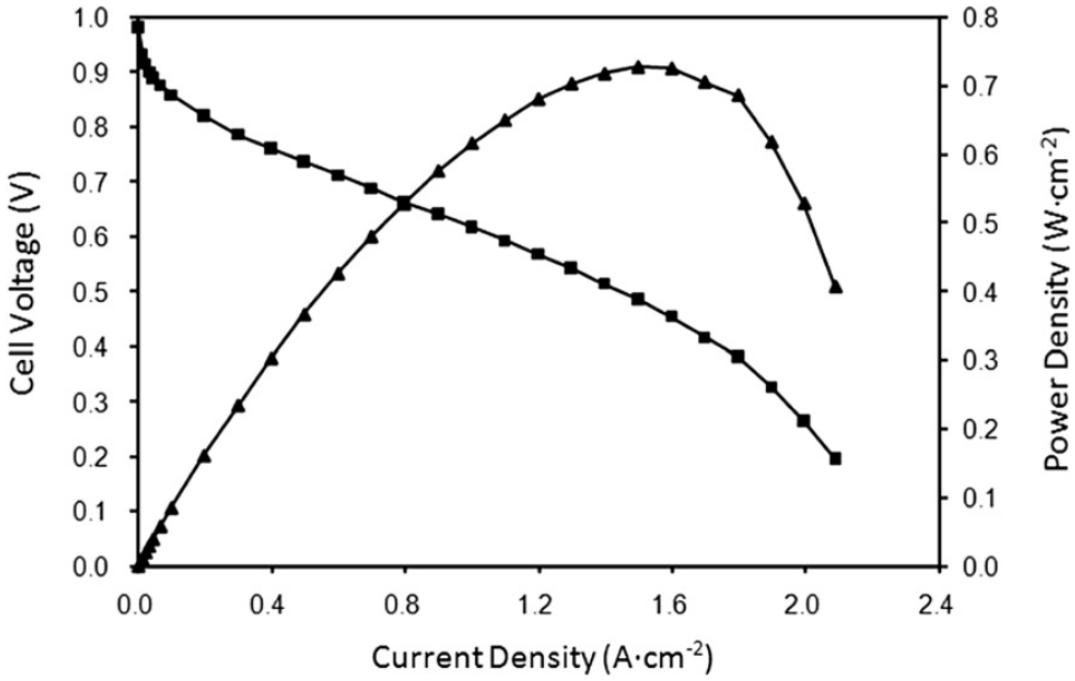

Figure B.2: Typical power curve for a PEMFC [57]

The efficiency of a fuel cell is another important parameter used to describe a fuel cell. The efficiency of a fuel cell strongly depends on the fuel cell type, the fuel utilization and the fuel type. The overall fuel cell efficiency for a stack is given by:

$$\epsilon_{FC} = \epsilon_r^{cell} \epsilon_V \epsilon_F \mu_F \epsilon_H \times 100\% \tag{B.7}$$

where,

ϵ_r^{cell} is the thermodynamic fuel cell efficiency – defined as the ratio of electric energy produced to the enthalpy change during the electrochemical reaction (or energy released due to burning the fuel)
ϵV is the electrochemical efficiency – defined as the actual voltage to the theoretical maximum voltage E
ϵE is the Faradaic efficiency – defined as the experimental (actual) current [I_{exp}] to the maximum possible current [I_{max}]
μ_F is the fuel utilization coefficient – defined as the actual fuel reacted to the fuel supplied to the fuel cell on a mass basis
ϵ_H is the hydrocarbon efficiency – defined as the ration of heating value of all fuel components that are converted electrochemically to the heating value of the fuel supplied. This term is not valid for PEMFCs since pure Hydrogen is supplied, but becomes valid in case of MCFCs where natural gas is supplied as the fuel but Hydrogen is converted electrochemically

For automotive fuel cells operating in vehicle-to-grid mode, another efficiency term called Tank-to-Grid efficiency, is important. It gives the efficiency with which the chemical energy stored in the fuel tank of the FCEV is converted to AC electrical energy delivered to the grid, and is expressed by the relation

$$\epsilon_{TTG} = \frac{m_{fuel} \times HHV_{fuel}}{3600 \times E_{grid}} \times 100\% \tag{B.8}$$

where,

m_{fuel} the quantity of Hydrogen consumed during the testing period in kg
HHV_{fuel} is the Higher Heating Value of Hydrogen in $\frac{kJ}{kg}$ $\left(141.8 \times 10^3 \frac{kJ}{kg}\right)$
E_{grid} is the total DC electrical energy delivered to the grid in kWh

This term includes the efficiency of all intermediate components of the fuel cell and Balance of Plant (BoP) components the FCEV, and also include the efficiency of the DC to AC converter, in the discharger unit, that connects the fuel cell of the FCEV with the national grid.

For fuel cell stacks, such as the ones used for automotive applications, volume-, mass- and cost-specific power densities are more common performance parameters. The mass-specific power density is the ratio of the power delivered by the stack (in $Watts$) to the total mass of the stack (in kg). The volume-specific power density is the ratio of the power delivered by the stack (in $Watts$) to the total volume of the stack (in $Liter$, m^3 or cm^3). The cost-specific power density is the ratio of the power delivered by the stack (in $Watts$) to the total cost of the stack (in \$, €etc.). These three parameters highlight the need to simplify stack design and develop light weigh, low density and inexpensive materials for stack manufacturing.

B.2. Construction of PEM fuel cells

Figure B.3 identifies the different components of a single PEM fuel cell. The key components include the membrane electrode assembly (MEA) the flow field plate, the current collectors and sealing materials. The MEA is composed of the anode, electrolyte (membrane), cathode, catalyst layer and the gas diffusion layer. Multiple single cells connected in series form a fuel cell stack. Single cells may be connected in series to form PEM fuel cell stacks. Stacks are useful because they compound fuel cell power delivery thereby improving power density. Fuel cell stacks are used for automotive and other high power applications. Single cell usage is usually restricted to experimental studies in laboratory settings.

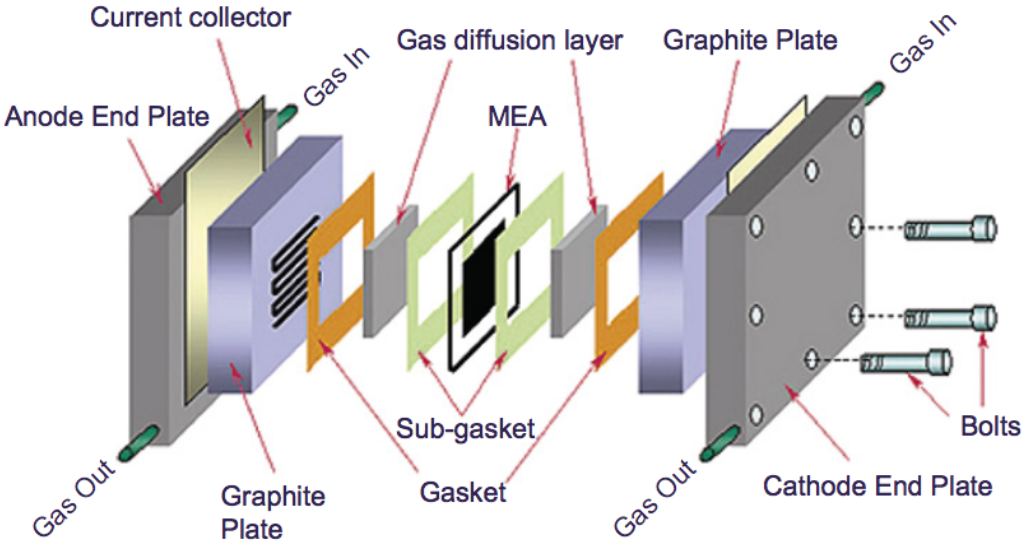

Figure B.3: Generic construction of a single-cell PEMFC [57]

In the following paragraphs, some components of a PEM fuel cell will be discussed separately.

1. **Membrane (solid electrolyte) electrode assembly**

   The function of the membrane is to not only serve as a conducting medium for the protons but also to separate (electrically insulted) the anode form the cathode). The commonly used membranes are perfluorosulfonic acid (PFSA) membranes such as Nafion®and Flemion®. Out of these, Nafion®is more commonly used. In the late 1960s, DuPont was responsible for developing this polytetrafluoroethylene(PTFE)-based polymer, consisting of polymeric materials base of carbo and fluorine atoms with sulphonic side chains. Nafion®membrane is a non-reinforced film based Nafion®ionomers in acidic (H^+) form. Nafion®is preferred because of its high proton conductivity, non-electronic conductivity, ability to withstand chemical attacks, thermal and mechanical stability and its unique structure. The PTFE base is hydrophobic which helps in driving out the produced water, while the sulphonic side chains are hydrophilic than maintain sufficient hydration to improve protonic conductivity. Relative humidity and temperature are known to have a significant impact on proton conductivity [56].

   The catalyst layer is another important component of the MEA. These form the sites for the hydrogen-oxidation and oxygen-reduction reactions. They are thin layers which are composed of catalyst powders, proton conducting ionomer (like Nafion®) and PTFE. They possess the ability to transport protons and reactant gasses while also removing produced water. The most commonly used catalyst in modern day PEM fuel cells is highly dispersed Platinum (Pt), although they pose challenges with regards to cost, sensitivity to impurities and insufficient stability/durability under fuel cell operating conditions [57].). Due to the sluggish nature of the reaction kinetics of the oxygen reduction reaction at the cathode, more electrocatalyst are required on this side to overcome the large overpotential [57].There is also a possibility that due to this the catalyst on the cathodic side may be consumed faster. Therefore, in recent years significant efforts have been made to develop Pt-based catalysts for the cathode side. For the anodic side, modern day Pt catalyst perform satisfactorily.

   The carbon-based electrodes (anode and cathode) are coated along with the catalyst layers on to the membrane, thereby providing the sites for electrochemical reactions. Furthermore, the gas diffusion layers (GDLs) are located on either side of the electrodes. Usually the GDL comprises of two layers: the backing layer or the macroporous substrate layer (MSL) and the microporous layer (MPL). The GDL is expected to be hydrophobic (to remove water) and hydrophilic (to improve humidity distribution). To achieve this, the GDL is usually treated. For instance, carbon powders and solvent, which are hydrophilic in nature, are impregnated with PTFE to increase hydrophobicity, thus forming a slurry. This slurry is then coated on the carbon matrix based MSL to form a thin MPL layer. The inner side of the GDL provide support for the catalyst layer whereas the outer side is responsible for distributing the reactants evenly and removing the produced water. It also provides electronic contact with the flow plates.

2. **Flow Plates**

   The flow filed plates are another component that impact fuel cell performance. They are electronically conducting mediums constructed from metals or non-metals. In single cells, the flow channels occur on only one side of the plates. These plates are known as mono-polar plates, and provide electronic connection between the MEA and the current collectors. In stack with multiple single cells in series, the channels occur on both sides, therefore these plates are termed as bipolar plates. These provide electronic connection between two adjacent MEAs, whereas the last two flow plates are essentially mono-polar plates connecting the outermost MEA with the current collectors. The flow plates are responsible for reactant distribution, water removal and for providing structural support to the MEA.

   The requirements for flow plate materials are high electronic conductivity, good chemical and mechanical stability, impermeability to reactant gases, low cost, light weight, and easy fabrication [57]. Most commonly used flow plate materials for PEM fuel cells are graphite plates and

metal plates coated with Nickel or Silver. Although they are electronically highly conductive and chemically stable, the disadvantage of graphite plates as compared to very thin metal plates is with regards to weight and therefore cost. The weight is a significant parameter when considering flow plate materials for automotive applications. The weight is less important for stationary fuel cells, albeit the cost accompanying weight is of considerable importance.

The configuration of the flow field the dimensions of the flow channels also have a significant impact on fuel cell performance. They impact reactant distribution and water removal capabilities of the flow plates [57]. The configuration of the flow patterns and their dimensions have an impact on pressure drop as the reactants flow through - thereby causing irregular reactant distribution and inefficient water removal. Various flow field configurations have been employed in order to improve fuel cell performance, these include: pin-type, straight-parallel, interdigitated, single-serpentine and multi-serpentine flow fields [57]. Of these, the most typical flow patterns used in today's PEM fuel cells are straight-parallel and single-serpentine flow patterns.

3. **Current collectors**

   As the name suggests, the current collectors are responsible for collecting the current generated by the fuel cell reactions. They are in direct contact with the flow plates and the external load. The electrons flow from the anodic current collector to the cathodic current collector, through the external circuit, thereby doing electronic work. The material used for the current collectors should be electrochemically and mechanically stable, electronically conductive, cheap and light. Typical material that are used today to manufacture current collectors include copper, stainless steel, titanium and aluminum. To improve electronic conductivity, coated materials such as gold coated copper or gold coated aluminum may also be used for current collector manufacturing.

4. **Other components**

   Sealing materials are usually inserted between the MEA and the flow plates to restrict gas or coolant leakage. Placing these has a significant impact of membrane performance as well as safety. Sealing materials are required to be thermally, electrochemically, chemically and mechanically stable. They should also be compressible, have very low gas permeability, and should be cheap and easy to fabricate. Common materials used for manufacturing PEM fuel cell sealing include PTFE films and silicon elastomers [57].

   The end plate is another important component of a PEM fuel cell. They are placed on outside of the current collectors and do not participate in the electrochemical reactions. They are electronically insulated using an insulating polymeric plate placed between itself and the current collectors. They contain holes through with the tightening bolts are passed through and also contain apertures for the reactant entry and exit piping. To reduce overall weight, robust materials such as aluminum and other polymers are used for end plate manufacturing.

B.3. Automotive Fuel Cell Systems

The fuel cell stack is an integral component of the fuel cell power systems in FCEVs. Along with batteries, polymer electrolyte membrane fuel cells (PEMFCs) are one of the promising energy converters for electric automotive applications. As a result of the absence of combustion processes, and therefore independence from Carnot cycle limitations, the fuel cells have high conversion efficiencies as compared to Internal combustion engines. Both fuel cells and batteries directly convert chemical to electrical energy. Unlike batteries, the fuel is not stored in the electrodes of the fuel cell, but is rather supplied from a separate sub-system. Therefore, as long as fuel and oxidant are fed to the fuel cell, electrical energy can be delivered, not considering durability and efficiency criterions.

Some of the challenges that fuel cell developers face, particularly developers of non-stationary PEM fuel cells with highly dynamic power cycles, deals with evenly supplying reactants to all single cells of the stack and removing the produced water efficiently [9]. Therefore, the limited durability of automotive PEM fuel cells under a wide range of operating conditions is a technical barrier that needs to be overcome to encourage commercialization of FCEVs.

The automotive fuel cell system, beside the PEM fuel cell stack, also consists of auxiliary components such as the fuel tank, air compressor, fuel pump, humidifiers, temperature controllers, electronic system for DC to AC conversion etc. For the Hyundai ix35 FCEV, the Hydrogen is delivered by the Hydrogen blower. To improve conversion efficiency, there also exists an Anode recycle blower that returns the unused hydrogen at the outlet of the stack, to the inlet. For the cathode side, multiple components are used to pre-condition and deliver the air; some of these include a compressor/blower, air filter and humidifier. The auxiliary components are usually powered by the stack itself, and this is known as Balance of Plant (BoP) requirement of the stack.

Finally, the power electronic components are responsible for delivering the torque. These components are not important while considering V2G operation, but are nevertheless an important part of an FCEV. The schematic below represents the control system components and electricity flow within the Hyundai FCEV.

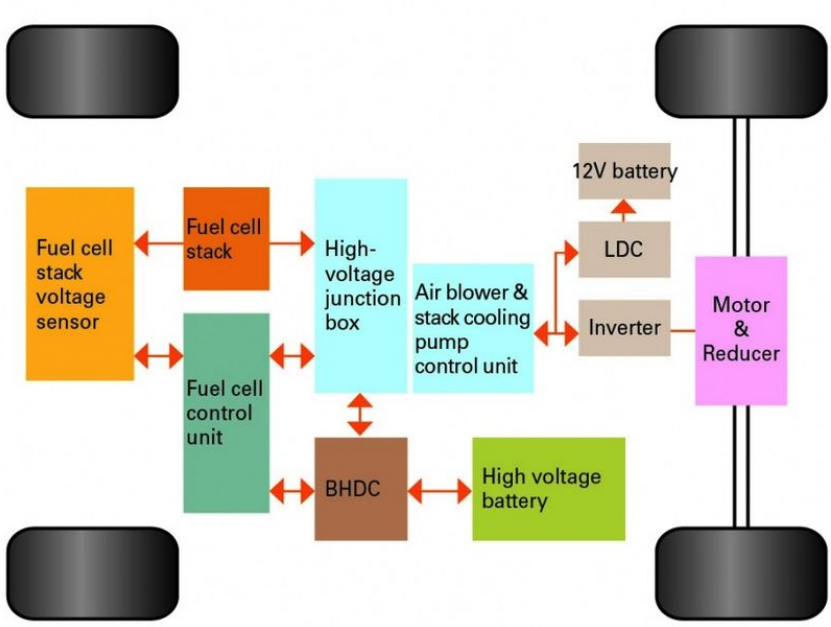

Figure B.4: Control system components and electricity flow within the Hyundai FCEV [3]

B.4. Degradation mechanisms that occur in PEM fuel cells

Internal as well as external factors have a significant impact on the durability of fuel cells. These factors include design and assembly, operating conditions (e.g. cell voltage, temperature, humidity *etc.*), operating modes (e.g. startup-shutdown, potential or load cycling *etc.*), presence of impurities and/or contaminants in the reactants and environmental conditions (*e.g.* subzero temperatures and cold starts).

Improper design of the flow fields and improper assembly such as uneven tightening pressure, may lead to occurrence of degradative phenomena such as inefficiency water removal and reactant distribution. Inefficient water removal causes flooding which in turn leads to localized fuel starvation. Fuel starvation is known to cause corrosion of the anodic carbon support by local oxidation, which leads

to loss of anodic electrochemically active area. Furthermore, dynamic operations, similar to the ones experienced by automotive fuel cells, may lead to highly dynamic relative humidity and temperature changes, which in turn may lead to durability losses.

Startup and shutdown are also known to cause fuel cell degradation. The anodic flow channels may be filled with air that diffuses from the cathodic side, during periods of prolonged shutdown. On startup, when the fuel enters these anodic flow channels, transient air/fuel boundaries are generated. These air/fuel boundaries cause cathodic potentials as high as 1.2-1.5 V [9]. These high potential excursions cause carbon corrosion of the catalyst support material. Carbon corrosion leads to free floating catalyst (Pt) particles, which coalesce. As a consequence of this coalescence, net electrochemically active catalytic area reduces. Furthermore, water electrolysis may also occur through "reverse current" mechanisms on the cathodic side, freeing up protons locally (not the ones transported across the membrane) for the reduction reaction at the cathode, which also leads to performance losses by carbon corrosion cause by the free radicals.

Impurities such as reactant contaminants (CO, H_2S during reforming to produce Hydrogen and NO_x and SO_x from the air intake) as well as metallic system-derived ones (metallic ions and silicon from corrosion of catalyst, mono/bi-polar plates, membranes and sealing materials); cause performance losses through multiple mechanisms such as: kinetic effects – as a result of poisoning of anodic and cathodic catalyst sites, and mass transfer effects – as a result of structural changes, loss of hydrophobicity and failure of catalyst layers and/or GDLs.

For PEM powered FCEVs, startup in subzero temperatures also pose considerable barriers that limits market penetration. When fuel cells are exposed to subzero temperatures freezing of water causes porosity changes in the catalytic layers (CL), GDL and membrane itself. Furthermore, it gives rise to uneven planar mechanical stresses across the membrane CL boundary. These phenomena lead to delamination on the CL from the membrane as well as loss of electrochemically active surface area (ESCA) in the electrodes.

PEM degradation may be broadly categorized under membrane, catalyst/catalyst support, GDL and sealing gasket degradation. The failure modes that occur in the membrane can be classified as electrochemical, mechanical and thermal failure modes. The catalyst and the catalyst layer degradation causes loss of reactant sites, conductivity losses, decrease in reactant mass transport and water management ability. Each of these terms have been elaborated on in the following subsections.

1. **Membrane Degradation**

   Mechanical failure of the membrane occurs on the formation of cracks, tears or pinholes in the membrane. The causes for the occurrence of these failure modes may be inherent mechanical defects in the membrane structure or improper MEA fabrication processes. The area of the membrane along the edges of the flow field, inlet channels of the reactants or around the sealing area are also prone to perforations and cracks, due to excessive non-uniform mechanical stresses. During dynamic operation, the overall dimension changes caused by low or non-humidification [57] and relative humidity cycling [57] can also be detrimental to the mechanical integrity of the membrane. The membrane experiences in-plane tension under low RH conditions, while it experiences in-place compression when it swells under high RH or wet conditions [57].

   As the name suggests, thermal degradation occurs in PEM fuel cells occurs when the fuel cell operates at temperatures outside of the operating temperature range of 60℃to 80℃. At high temperatures, the PFSA polymers in the membrane experiences serious break down around their glass transition temperatures. This has encouraged development of special materials for high-temperature (more than 100℃) PEM fuel cells. Since these fuel cells are not employed for automotive applications, elaboration on these has been omitted here.

   Chemical/electrochemical degradation of the membrane material occurs because of chemical

reactions at the anodic and cathodic catalytic (Pt) sites that lead to peroxide (HO•) and hydroperoxide (HOO•) radical formation. These radicals are known to attack the catalyst material itself as well as the membrane material by attacking the polymer backbone of the PFSA membrane. Studies have suggested that the production of these radicals is accelerated during OCV operation and low humidity conditions [7].

2. **Catalyst and Catalyst Support Degradation**

   Platinum (Pt) and alloys of Pt are the most commonly used catalyst for fuel cells. Carbon, because of its good mass transport and conductive properties and because of its stability under nominal operating conditions, it the proffered support structure for the catalyst in PEM fuel cells. Both Pt and carbon are also able to adhere to the performance and cost criteria for PEM fuel cell manufacturing. However, from a durability stand point, the Pt catalyst is still not able to meet the requirements for operating in harsh and dynamic conditions.

   Pure Pt catalyst may be contaminated by impurities that may have been delivered externally through the reactants, or locally through corrosion of fuel cell components. Furthermore, the ECSA reduces because of sintering of the catalyst particles that have detached from the carbon support, and have migrated across the support itself, or into the electrolyte.

   Corrosion of the carbon support structure is also a problem that has received considerable attention. Due to its inherently slow kinetics, carbon corrosion is negligible in PEM fuel cells. However, the presence of catalyst such as PT/C or PtRu/C accelerate the corrosive reactions. Carbon support structural corrosion are considered to be induced through two modes: (1) through air/fuel fronts that are generated during startup and shut down cycles (2) fuel starvation (hydrogen exhaustion) at the anode under steady-state operating conditions – which leads to high negative anodic potential which has to be neutralized locally by water and carbon oxidation [9]. Carbon corrosion leads to reduction in the number of sites available for catalyst anchorage and in extreme cases leads to electrode failure.

3. **Catalyst and Catalyst Support Degradation**

   As described earlier the GDL is composed of carbon black powder and hydrophobic agent such as PTFE. These composites are prone to chemical attacks by radicals (HO•) and to electrochemical (voltage) oxidation during fuel cell operation. Reduction in availability of PTFE and carbon particles leads to structural changes of the GDL. They also cause reduction in conductivity and hydrophobicity of the GDL material. This impacts cell performance by causing electron conduction and water removal problems. Furthermore, mechanical stresses due to local drying or improper assembly may also weaken GDL structures. In literature, several GDL degradation mechanisms have been proposed [57]. Finally, it should be pointed that the carbon structure within the GDL are more stable as compared to those present in the CL. This is because of the absence of the Pt particle in the GDL structure, unlike the CL and the electrodes.

4. **Catalyst and Catalyst Support Degradation**

   The seal material is primarily exposed to mechanical stresses owing to the variable temperature environments. Temperature or thermal cycling causes alternating compression and relaxation stresses, which has degradative effects on fuel cell performance due to formation and propagation of cracks and other mechanical failure modes. These may lead to leakage of reactants and coolant as well as pressure perturbations in pressurized operation.

Since vehicle-to-grid operation is similar to stationary PEM fuel cell operation, most of the degradative mechanism mentioned above are pertinent. However, it must be noted that some of the mentioned

phenomena might not have occurred during continuous steady-state operating conditions of some of the experiments during this study *i.e* constant operating conditions and constant non-cyclic power delivery, with the absence multiple startup and shutdown sequences. Finally, it should be highlighted that the focus of this study was not to identify the degradative phenomena that might occur during V2G operation, but was rather to quantify the performance loss in V2G operation. Therefore, the information provided in the preceding paragraphs only serve the purpose of briefly informing the interested reader about the degradative phenomena that occur during PEM fuel cell operation.

C

Piping and Instrumentation Diagram for experimental set-up

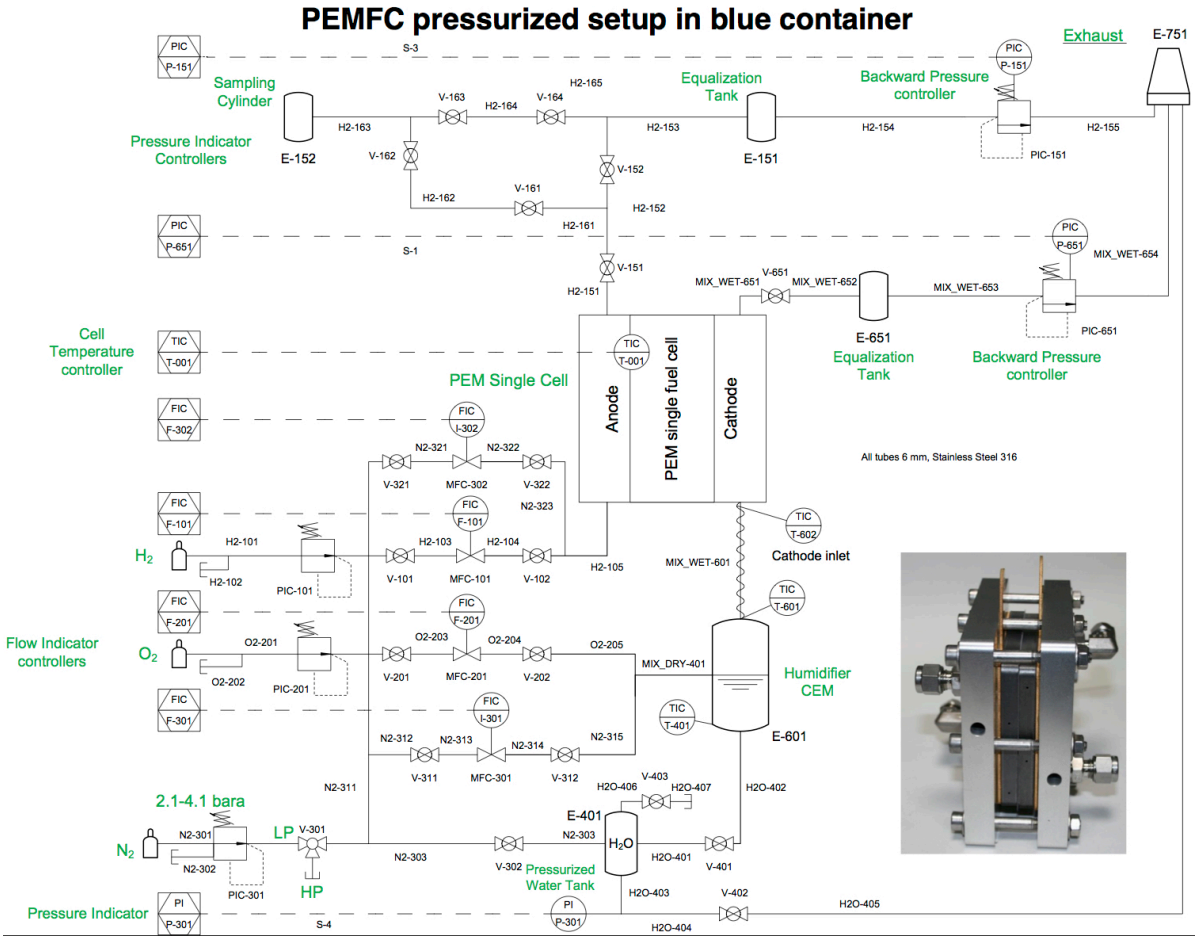

Figure C.1: P&ID

Instrument List									
Tag	**Service**	**Line Size**	**Material**	**Operating Pressure**	**Design Pressure**	**Operating Temperature**	**Design Temperature**	**Capacity**	**Brand, Type**
F-101	Hydrogen (gas)	6 mm		1.0 - 3.0 bara Calibrated: In: 2.1 bara Out: 1 .0 bara	8 bara	calibrated: 20ºC operating: 0-30 ºC	-10…+70ºC	500 mL/min	Bronckhorst, EL-FLOW, F-201CV Mass flow Controller F-201C-FA-33-V
F-201	Oxygen (gas)	6 mm		1.0 - 3.0 bara Calibrated: In: **2.5** bara Out: 1 .0 bara	8 bara	calibrated: 20ºC operating: 0-30 ºC	-10…+70ºC	100 mL/min	Bronckhorst, EL-FLOW, F-201CV Mass flow Controller F-201C-FA-33-V
F-301	Nitrogen (gas)	6 mm		1.0 - 3.0 bara Calibrated: In: **2.5** bara Out: 1 .0 bara	8 bara	calibrated: 20ºC operating: 0-30 ºC	-10…+70ºC	500 mL/min	Bronckhorst, EL-FLOW, F-201CV Mass flow Controller F-201C-FA-33-V
F-302	Nitrogen (gas)	6 mm		1.0 - 3.0 bara Calibrated: In: 2.1 bara Out: 1 .0 bara	8 bara	calibrated: 20ºC operating: 0-30 ºC	-10…+70ºC	500 mL/min	Bronckhorst, EL-FLOW, F-201CV Mass flow Controller F-201C-FA-33-V
P-151	Hydrogen (gas)	6 mm		1.0 - 3.0 bara	60 barg	0-65ºC	-10…+70ºC	1 ln/min	Bronkhorst, EL-PRESS P-702CV back pressure controller P-702CV-21KR-RAD-33-V
P-301	Nitrogen (gas)	6 mm		1.0 - 3.0 bara	41.0 bara	0-65ºC			Wika
P-651	Nitrogen, Oxygen, Water (gas)	6 mm		1.0 - 3.0 bara	60 barg	0-65ºC	-10…+70ºC	1 ln/min	Bronkhorst, EL-PRESS P-702CV back pressure controller P-702CV-21KR-RAD-33-V
T-001	N.A.	N.A.		N.A.	N.A.	control range: 0-80ºC	control range: 0…800ºC Ambient range: 0…65ºC	N.A.	RKC instrument,SB1 1-channel type temperature controller, SB1K04-T-4*NN1N with Thermocouple
T-401	Part of E-601								
T-601	Part of E-601								
T-602	N.A.	N.A.		N.A.	N.A.	0-80ºC	control range: 0…800ºC Ambient range: 0…65ºC	N.A.	RKC instrument,SB1 1-channel type temperature controller, SB1K04-T-4*NN1N with Thermocouple
E-601	Nitrogen, Oxygen, Water (gas)	6 mm	SS-316	0.0 - 2.0 barg	25 barg	0- 30 ºC	200 ºC	5 g/h H2O 4 ln/min gas	CEM BRONKHORST, W-102A-333-K

Figure C.2: Instrument List of the setup

Pipeline List								
Tag	Service	Line Size	Material	Operating Pressure	Design Pressure	Operating Temperature	Design Temperature	Quantity
H2-101	Hydrogen (gas)	6 mm	SS-316	0.0 - 2.0 barg	330.8 barg	0- 30 °C	517 °C	1
H2-102	Hydrogen (gas)	6 mm	SS-316	0.0 - 2.0 barg	330.8 barg	0- 30 °C	517 °C	1
H2-103	Hydrogen or Nitrogen (gas)	6 mm	SS-316	0.0 - 2.0 barg	330.8 barg	0- 30 °C	517 °C	1
H2-104	Hydrogen (gas)	6 mm	SS-316	0.0 - 2.0 barg	330.8 barg	0- 30 °C	517 °C	1
H2-105	Hydrogen or Nitrogen (gas)	6 mm	SS-316	0.0 - 2.0 barg	330.8 barg	0- 30 °C	517 °C	1
H2-151	Hydrogen or Nitrogen (gas)	6 mm	SS-316	0.0 - 2.0 barg	330.8 barg	0- 80 °C	517 °C	1
H2-152	Hydrogen or Nitrogen (gas)	6 mm	SS-316	0.0 - 2.0 barg	330.8 barg	0- 65 °C	517 °C	1
H2-153	Hydrogen or Nitrogen (gas)	6 mm	SS-316	0.0 - 2.0 barg	330.8 barg	0- 65 °C	517 °C	1
H2-154	Hydrogen or Nitrogen (gas)	6 mm	SS-316	0.0 - 2.0 barg	330.8 barg	0- 65 °C	517 °C	1
H2-155	Hydrogen or Nitrogen (gas)	6 mm	SS-316	0.0 barg	330.8 barg	0- 65 °C	517 °C	1
H2-158	Hydrogen or Nitrogen (gas)	6 mm	SS-316	0.0 - 2.0 barg	330.8 barg	0- 65 °C	517 °C	1
H2-159	Hydrogen or Nitrogen (gas)	6 mm	SS-316	0.0 - 2.0 barg	330.8 barg	0- 65 °C	517 °C	2
H2-161	Hydrogen or Nitrogen (gas)	6 mm	SS-316	0.0 - 2.0 barg	330.8 barg	0- 65 °C	517 °C	1
H2-162	Hydrogen or Nitrogen (gas)	6 mm	SS-316	0.0 - 2.0 barg	330.8 barg	0- 65 °C	517 °C	1
H2-163	Hydrogen or Nitrogen (gas)	6 mm	SS-316	0.0 - 2.0 barg	330.8 barg	0- 65 °C	517 °C	1
H2-164	Hydrogen or Nitrogen (gas)	6 mm	SS-316	0.0 - 2.0 barg	330.8 barg	0- 65 °C	517 °C	1
H2-165	Hydrogen or Nitrogen (gas)	6 mm	SS-316	0.0 - 2.0 barg	330.8 barg	0- 65 °C	517 °C	1
H2O-401	Water (liquid)	6 mm	SS-316	0.0 - 2.0 barg	330.8 barg	0- 30 °C	517 °C	1
H2O-402	Water (liquid)	6 mm	SS-316	0.0 - 2.0 barg	330.8 barg	0- 30 °C	517 °C	1
H2O-403	Water (liquid)	6 mm	SS-316	0.0 - 2.0 barg	330.8 barg	0- 30 °C	517 °C	1
H2O-404	Water (liquid)	6 mm	SS-316	0.0 - 2.0 barg	330.8 barg	0- 30 °C	517 °C	1
H2O-405	Water (liquid)	6 mm	SS-316	0.0 - 2.0 barg	330.8 barg	0- 30 °C	517 °C	1
H2O-406	Water (liquid)	6 mm	SS-316	0.0 - 2.0 barg	330.8 barg	0- 30 °C	517 °C	1
H2O-407	Water (liquid)	6 mm	SS-316	0.0 - 2.0 barg	330.8 barg	0- 30 °C	517 °C	1
MIX_DRY-401	Nitrogen & Oxgen (gas)	6 mm	SS-316	0.0 - 2.0 barg	330.8 barg	0- 30 °C	517 °C	1
MIX_WET-601	Nitrogen, Oxygen, Water (gas)	6 mm	SS-316	0.0 - 2.0 barg	330.8 barg	0- 80 °C	517 °C	1
MIX_WET-651	Nitrogen, Oxygen, Water (gas)	6 mm	SS-316	0.0 - 2.0 barg	330.8 barg	0- 80 °C	517 °C	1
MIX_WET-652	Nitrogen, Oxygen, Water (gas)	6 mm	SS-316	0.0 - 2.0 barg	330.8 barg	0- 80 °C	517 °C	1
MIX_WET-653	Nitrogen, Oxygen, Water (gas)	6 mm	SS-316	0.0 - 2.0 barg	330.8 barg	0- 70 °C	517 °C	1
MIX_WET-654	Nitrogen, Oxygen, Water (gas)	6 mm	SS-316	0.0 barg	330.8 barg	0- 70 °C	517 °C	1
N2-301	Nitrogen (gas)	6 mm	SS-316	0.0 - 2.0 barg	330.8 barg	0- 30 °C	517 °C	1
N2-302	Nitrogen (gas)	6 mm	SS-316	0.0 - 2.0 barg	330.8 barg	0- 30 °C	517 °C	1
N2-303	Nitrogen (gas)	6 mm	SS-316	0.0 - 2.0 barg	330.8 barg	0- 30 °C	517 °C	2
N2-306	Nitrogen (gas)	6 mm	SS-316	0.0 - 2.0 barg	330.8 barg	0- 30 °C	517 °C	2
N2-311	Nitrogen (gas)	6 mm	SS-316	0.0 - 2.0 barg	330.8 barg	0- 30 °C	517 °C	1
N2-312	Nitrogen (gas)	6 mm	SS-316	0.0 - 2.0 barg	330.8 barg	0- 30 °C	517 °C	1
N2-313	Nitrogen (gas)	6 mm	SS-316	0.0 - 2.0 barg	330.8 barg	0- 30 °C	517 °C	1
N2-314	Nitrogen (gas)	6 mm	SS-316	0.0 - 2.0 barg	330.8 barg	0- 30 °C	517 °C	1
N2-315	Nitrogen (gas)	6 mm	SS-316	0.0 - 2.0 barg	330.8 barg	0- 30 °C	517 °C	1
N2-321	Nitrogen (gas)	6 mm	SS-316	0.0 - 2.0 barg	330.8 barg	0- 30 °C	517 °C	1
N2-322	Nitrogen (gas)	6 mm	SS-316	0.0 - 2.0 barg	330.8 barg	0- 30 °C	517 °C	1
N2-323	Nitrogen (gas)	6 mm	SS-316	0.0 - 2.0 barg	330.8 barg	0- 30 °C	517 °C	1
O2-201	Oxygen (gas)	6 mm	SS-316	0.0 - 2.0 barg	330.8 barg	0- 30 °C	517 °C	1
O2-202	Oxygen (gas)	6 mm	SS-316	0.0 - 2.0 barg	330.8 barg	0- 30 °C	517 °C	1
O2-203	Oxygen (gas)	6 mm	SS-316	0.0 - 2.0 barg	330.8 barg	0- 30 °C	517 °C	1
O2-204	Oxygen (gas)	6 mm	SS-316	0.0 - 2.0 barg	330.8 barg	0- 30 °C	517 °C	1
O2-205	Oxygen (gas)	6 mm	SS-316	0.0 - 2.0 barg	330.8 barg	0- 30 °C	517 °C	1

Figure C.3: Pipeline List of the setup

Equipment List

Tag	Service	Line Size	Material	Operating Pressure	Design Pressure	Operating Temperature	Design Temperature	Capacity	Brand, Type
E-151	Hydrogen or Nitrogen (gas)	6 mm	SS-316	0.0 - 2.0 barg		0- 65 ºC			
E-152	Hydrogen or Nitrogen (gas)	6 mm	SS-316	0.0 - 2.0 barg		0- 65 ºC			
E-401	Water (liquid)	6 mm	SS-316	0.0 - 2.0 barg		0- 30 ºC			
E-651	Nitrogen, Oxygen, Water (gas)	6 mm	SS-316	0.0 - 2.0 barg		0- 65 ºC			

Valve List

Tag	Service	Line Size	Material	Operating Pressure	Design Pressure	Operating Temperature	Design Temperature	Capacity	Brand, Type
MFC-101	Hydrogen (gas)	6 mm		1.0 - 3.0 bara Calibrated: In: 2.1 bara Out: 1 .0 bara	8 bara	calibrated: 20ºC operating: 0-30 ºC	-10…+70ºC	500 mL/min	Bronckhorst, EL-FLOW, F-201CV Mass flow Controller F-201C-FA-33-V
MFC-201	Oxygen (gas)	6 mm		1.0 - 3.0 bara Calibrated: In: **2.5** bara Out: 1 .0 bara	8 bara	calibrated: 20ºC operating: 0-30 ºC	-10…+70ºC	100 mL/min	Bronckhorst, EL-FLOW, F-201CV Mass flow Controller F-201C-FA-33-V
MFC-301	Nitrogen (gas)	6 mm		1.0 - 3.0 bara Calibrated: In: **2.5** bara Out: 1 .0 bara	8 bara	calibrated: 20ºC operating: 0-30 ºC	-10…+70ºC	500 mL/min	Bronckhorst, EL-FLOW, F-201CV Mass flow Controller F-201C-FA-33-V
MFC-302	Nitrogen (gas)	6 mm		1.0 - 3.0 bara Calibrated: In: 2.1 bara Out: 1 .0 bara	8 bara	calibrated: 20ºC operating: 0-30 ºC	-10…+70ºC	500 mL/min	Bronckhorst, EL-FLOW, F-201CV Mass flow Controller F-201C-FA-33-V
V-101	Hydrogen (gas)	6 mm	SS-316	1.0 - 3.0 bara	204	0-30 ºC	-23 …+ 204ºC		NUPRO, SS-6P4T-MM
V-102	Hydrogen (gas)	6 mm	SS-316	1.0 - 3.0 bara	204	0-30 ºC	-23 …+ 204ºC		NUPRO, SS-6P4T-MM
V-151	Hydrogen or Nitrogen (gas)	6 mm	SS-316	1.0 - 3.0 bara	204	0-80 ºC	-23 …+ 204ºC		NUPRO, SS-6P4T-MM
V-152	Hydrogen or Nitrogen (gas)	6 mm	SS-316	1.0 - 3.0 bara	204	0-65 ºC	-23 …+ 204ºC		NUPRO, SS-6P4T-MM
V-161	Hydrogen or Nitrogen (gas)	6 mm	SS-316	1.0 - 3.0 bara	204	0-65 ºC	-23 …+ 204ºC		NUPRO, SS-6P4T-MM
V-162	Hydrogen or Nitrogen (gas)	6 mm	SS-316	1.0 - 3.0 bara	204	0-65 ºC	-23 …+ 204ºC		NUPRO, SS-6P4T-MM
V-163	Hydrogen or Nitrogen (gas)	6 mm	SS-316	1.0 - 3.0 bara	204	0-65 ºC	-23 …+ 204ºC		NUPRO, SS-6P4T-MM
V-164	Hydrogen or Nitrogen (gas)	6 mm	SS-316	1.0 - 3.0 bara	204	0-65 ºC	-23 …+ 204ºC		NUPRO, SS-6P4T-MM
V-201	Oxygen (gas)	6 mm	SS-316	1.0 - 3.0 bara	204	0-30 ºC	-23 …+ 204ºC		NUPRO, SS-6P4T-MM
V-202	Oxygen (gas)	6 mm	SS-316	1.0 - 3.0 bara	204	0-30 ºC	-23 …+ 204ºC		NUPRO, SS-6P4T-MM
V-301	Nitrogen (gas)	6 mm	SS-316	1.0 - 3.0 bara	173 bara	0-30 ºC	148ºC		Swagelok, SS-43GXS6MM
V-302	Nitrogen (gas)	6 mm	SS-316	1.0 - 3.0 bara	173 bara	0-30 ºC	148ºC		Swagelok, SS-43GS6MM
V-311	Nitrogen (gas)	6 mm	SS-316	1.0 - 3.0 bara	204	0-30 ºC	-23 …+ 204ºC		NUPRO, SS-6P4T-MM
V-312	Nitrogen (gas)	6 mm	SS-316	1.0 - 3.0 bara	204	0-30 ºC	-23 …+ 204ºC		NUPRO, SS-6P4T-MM
V-321	Nitrogen (gas)	6 mm	SS-316	1.0 - 3.0 bara	204	0-30 ºC	-23 …+ 204ºC		NUPRO, SS-6P4T-MM
V-322	Nitrogen (gas)	6 mm	SS-316	1.0 - 3.0 bara	204	0-30 ºC	-23 …+ 204ºC		NUPRO, SS-6P4T-MM
V-401	Water (liquid)	6 mm	SS-316	1.0 - 3.0 bara	173 bara	0-30 ºC	148ºC		Swagelok, SS-43GS6MM
V-402	Water (liquid)	6 mm	SS-316	1.0 - 3.0 bara	204	0-30 ºC	-23 …+ 204ºC		NUPRO, SS-6P4T-MM
V-403	Water (liquid)	1/4"	SS-316	1.0 - 3.0 bara	60 barg	0-30 ºC	-30 … +50 ºC		Eriks RX fig. 3186
V-651	Nitrogen, Oxygen, Water (gas)	6 mm	SS-316	1.0 - 3.0 bara	173 bara	0-65 ºC	+10 … +65ºC		Swagelok, SS-426SMM

Figure C.4: Equipment and Valve List of the setup

D

Steps followed while conducting the experiments

The steps performed before, during and after conducting the experiments, have been presented here in the exact order in which they were performed.

1. **Pre-experiment preparation**
   - (i) Check reactant pressures in bottles vessel and take necessary actions if required
   - (ii) Check water content and pressure in water vessel and take actions if deemed necessary
   - (iii) Empty equalization tank on both cathode and anode sides
2. **Activation procedure**
   - (i) Assemble cell
   - (ii) Begin heating the cell and the tracing element
   - (iii) Start reactant flows
   - (iv) Start humidification unit
   - (v) Begin Pressurizing System to 2 $Bar(g)$
   - (vi) Activate at CV of 0.6V for 2-3 hours
   - (vii) Make Polarization Curve at 2 $Bar(g)$
   - (viii) De-pressurize gradually to 0.5 $Bar(g)$
   - (ix) Make Polarization Curve at 0.5 $Bar(g)$

   After implementing the activation procedure, the following steps were performed to start the experiment. It must be noted that there was always a time duration of 5-10 minutes between completion of the activation procedure and starting the experiment.
3. **Experiment start procedure**
   - (i) De-pressurize gradually to 1 $Bar(a)$ and set experimental conditions
   - (ii) Wait for 10-15 mins for the cell to achieve steady state
   - (iii) Make Polarization Curve at experimental conditions and find CC value
   - (iv) Perform EIS measurements at experimental conditions
   - (v) Open cathode outlet
   - (vi) Start experiment by applying load
   - (vii) Begin logging required parameters

4. **Experiment stop procedure**

   (i) Stop logging all parameters and save the required data
   (ii) Turn off the load to operate the fuel cell in OCV mode
   (iii) Make the Polarization Curve
   (iv) Perform EIS measurements at experimental conditions
   (v) Perform recovery procedure if required. If not, then perform steps (vi)-(viii)
   (vi) Shut down humidification
   (vii) Reduce flows gradually
   (viii) Turn off all heating devices

Details of the Recovery Procedure applied

The following steps were developed based on the recovery procedure steps suggested in [13]; but some of the steps had to be adapted to suit the test bench in use.

(i) Switching off load to bring cell to OCV

(ii) Make Polarization Curve at experimental conditions

(iii) Perform EIS measurements at experimental conditions

(iv) Stop humidification

(v) Purge with dry air and hydrogen

(vi) Open anode and cathode outlet to allow atmospheric air to enter the cell through diffusion

(vii) Purge with nitrogen on both sides sides

(viii) Turn off all heating - cool down

(ix) Turn off gas flows

(x) Leave cell overnight

(xi) Purge anode pipe with pure Hydrogen to remove any trapped Nitrogen, then reconnect anode outlet to downstream pipes

(xii) Start heating and set experiment conditions

(xiii) Make Polarization Curve at experimental conditions

(xiv) Perform EIS measurements at experimental conditions

(xv) Restart CC experiment

Details of the Membrane Activation Procedure applied

The Membrane Electrode Assembly (MEA) strongly determines the performance of a PEM fuel cell. The MEA is composed of the anode where fuel oxidation occurs, a cathode where oxygen reduction takes place and a membrane which is responsible for protonic transportation. To improve the kinetics of the reduction and oxidation reaction, noble metal catalyst such as platinum are mixed in the carbon support structure of the two electrodes. Thus, the loading of the catalyst has a strong influence on the performance of the fuel cell.

To improve the catalyst utilization, the MEA is first exposed to high pressure, temperature and humidity conditions. This helps break-into the catalyst reaction sites thereby improving membrane performance at relatively milder conditions. The process of exposing the MEA to harsh conditions for a short period of time (approximately 2-3 hours) in order to facilitate reaction site break in is known as membrane activation procedure.

During the course of this research, a new MEA was used for each experiment. This eliminated the probability of degradative effects of previous tests contaminating the results of the current test. Therefore, before testing each load profile, a membrane had to be activated before electrochemical characterization followed by conducting the long-term experiment. The membrane activation procedure was provided by the supplier of the MEA and constituted the following steps:

(i) After assembling a new MEA into the test cell, the inlet and outlet pipes for reactant flow were connected

(ii) The fuel cell was then heated to 70

(iii) Following this the pressure on both sides of the membrane was gradually increased until a system pressure of 3 $Bar(a)$ was reached. The Hydrogen flow was set to 100 $\frac{mln}{min}$ and the Air flow was set at 150 $\frac{mln}{min}$ during the pressurization phase. Since the pressure on the air (cathode) side increases faster due to its higher density and flow rate as compared to Hydrogen, the pressure on the air side was increased in steps, always ensuring that the pressure difference across the membrane did not exceed 0.1 $Bar(g)$. This was done to avoid inducing unwanted mechanical stresses due to higher pressure difference, which could damage the membrane.

(iv) During the pressurization phase, the air was constantly humidified to 50% relative humidity at 70. Since relative humidity is dependent on pressure, this was done by changing the liquid mass flow rate of the CEM at every increment of air side intermediate pressure by 0.1$Bar(g)$

(v) On reaching 3 $Bar(a)$, the Hydrogen flow was changed to 50 $\frac{mln}{min}$ and the Air flow was set at 150 $\frac{mln}{min}$. These correspond to stoichiometry of 2.79 and 2.12 for Hydrogen and Air respectively, and were specified for the activation process, by the fuel cell supplier. The said values for gas stoichiometric factors were chosen to ensure that there was enough reactant gases for the red-ox reactions to occur, even at low current densities, without the drying out the membrane too quickly

(vi) Humidification of the air was unchanged

(vii) It was then ensured that the open circuit voltage was between 0.85V and 1.0V. Lower OCV would signify either leakages around the fuel cell or gas-crossover across the MEA

(viii) Once the set conditions were had been reached and the OCV was acceptable, the load unit connected to the fuel cell was put into constant voltage (CV) mode. A voltage of 0.6 V was applied and the current was measured for 2-3 hours; or until the current stabilized instead of constantly increasing. The increasing trend of the current, at constant voltage, represents the “break-in” process

(ix) Following activation, two sets of performance polarization curves were measured, one at 3$Bar(a)$ and the other at 0.5$Bar(a)$. This was done to compare the performance of the activated MEA with that claimed by the MEA supplier. Following this the system was gradually de-pressurizing to the experimental condition of 1$Bar(a)$, constantly ensuring that the pressure difference on either side of the MEA did not exceed 0.1$Bar(g)$

Steps followed while making polarization curve

The Polarization Curve (IV) was measured by operating the electronic load in constant current (CC) mode and sweeping the set current from 0A to a current density at which the voltage delivered was 0.6V or slightly lower, no lower than 0.58V. The current was changed in steps of 0.05A. At each step the cell was allowed to operate at the set current density for 10 seconds before the voltage was recorded. This was done so that the cell could achieve a steady state of operation, thus ensuring that each step may be considered as a quasi-steady state. A total of four current sweeps were performed - two from 0A to maximum current density and two in the reverse direction. An average of the four voltage values recorded during each current sweep, was considered to be the voltage delivered at that current step. Furthermore, it must be specified that the conditions when measuring the polarization curve the experimental conditions.

For comparison and analysis purposes, the polarization curve was also measured at the end of each experiment of sequence.

E

Relation between Hyundai's Vehicle speed and Fuel Cell power

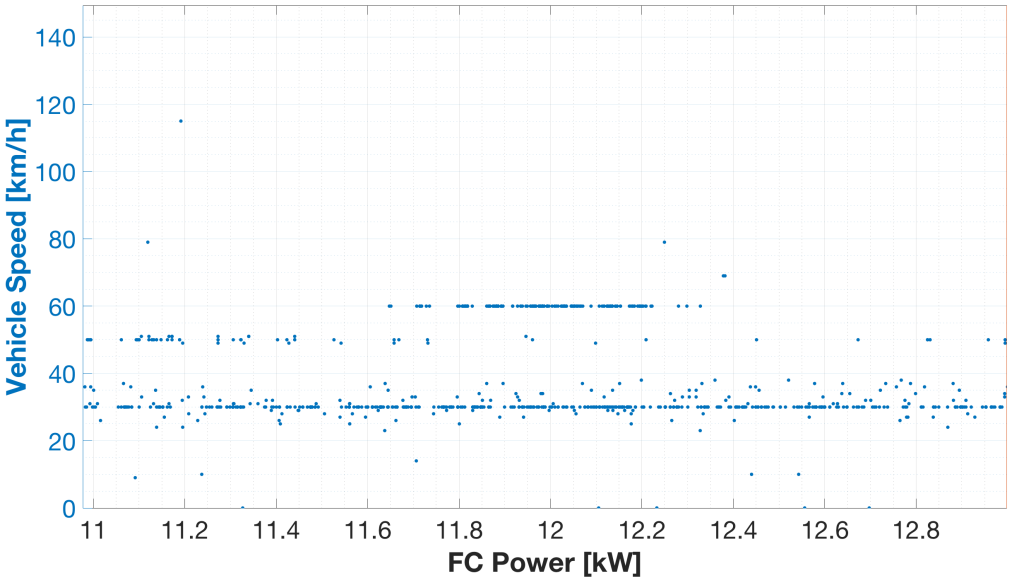

Figure E.1: Vehicle speed and Fuel Cell Power relation for Hyundai ix35 Fuel Cell Electric Vehicle

Bibliography

[1] Least-Squares Fitting - MATLAB & Simulink - MathWorks Benelux. URL https://nl.mathworks.com/help/curvefit/least-squares-fitting.html.

[2] British standards institute (13306: 2001) : Maintenance terminology, April 2001. URL http://www2.arnes.si/~sspvjeme/SIST_EN_13306.pdf.

[3] July 2013. URL http://www.greencarcongress.com/2013/07/ix35-20130721.html.

[4] Rod Borup, Jeremy Meyers, Bryan Pivovar, Yu Seung Kim, Rangachary Mukundan, Nancy Garland, Deborah Myers, Mahlon Wilson, Fernando Garzon, David Wood, et al. Scientific aspects of polymer electrolyte fuel cell durability and degradation. *Chemical reviews*, 107(10):3904–3951, 2007.

[5] Huicui Chen, Pucheng Pei, and Mancun Song. Lifetime prediction and the economic lifetime of proton exchange membrane fuel cells. *Applied Energy*, 142:154–163, 2015.

[6] McKinsey & Company. A portfolio of power-trains for europe: a fact-based analysis on the role of battery electric vehicles, plug-in hybrids and fuel cell electric vehicles. Technical report, 2010. URL http://www.eesi.org/files/europe_vehicles.pdf.

[7] FA De Bruijn, VAT Dam, and GJM Janssen. Durability and degradation issues of pem fuel cell components. *Fuel cells*, 8(1):3–22, 2008.

[8] Matthieu Dubarry, Arnaud Devie, and Katherine McKenzie. Durability and reliability of electric vehicle batteries under electric utility grid operations: Bidirectional charging impact analysis. *Journal of Power Sources*, 358:39–49, 2017.

[9] Ulrich Eberle, Bernd Müller, and Rittmar Von Helmolt. Fuel cell electric vehicles and hydrogen infrastructure: status 2012. *Energy & Environmental Science*, 5(10):8780–8798, 2012.

[10] Mehrdad Ehsani, Milad Falahi, and Saeed Lotfifard. Vehicle to grid services: Potential and applications. *Energies*, 5(10):4076–4090, 2012.

[11] U.S. Energy Information Administration (EIA). International energy outlook 2016. Technical report, Office of Energy Analysis, Washington, DC, 2016. URL https://www.eia.gov/outlooks/ieo/pdf/0484(2016).pdf.

[12] Michael W Fowler, Ronald F Mann, John C Amphlett, Brant A Peppley, and Pierre R Roberge. Incorporation of voltage degradation into a generalised steady state electrochemical model for a pem fuel cell. *Journal of power sources*, 106(1):274–283, 2002.

[13] Pawel Gazdzick, Jens Mitzel, Daniel Garcia Sanchez, Mathias Schulze, and K Andreas Friedrich. Evaluation of reversible and irreversible degradation rates of polymer electrolyte membrane fuel cells tested in automotive conditions. *Journal of Power Sources*, 327:86–95, 2016.

[14] Hyundai. Hyundai ix35 fcev emergency response guide, 2012.

[15] International Energy Agency (IEA). Technology Roadmap Hydrogen and Fuel Cells. Technical report, 2015. URL http://www.iea.org/publications/freepublications/publication/TechnologyRoadmapHydrogenandFuelCells.pdf.

[16] International Energy Agency (IEA). Global EV Outlook 2017 Together Secure Sustainable Global EV outlook 2017. Technical report, 2017. URL www.iea.org/t{&}c/.

[17] Bernhard Jansen, Carl Binding, Olle Sundstrom, and Dieter Gantenbein. Architecture and communication of an electric vehicle virtual power plant. In *Smart Grid Communications (SmartGridComm), 2010 First IEEE International Conference on*, pages 149–154. IEEE, 2010.

[18] John Juriga. Hyundai Motor Group's Development of the Fuel Cell Electric Vehicle. 2012. URL `https://www.hydrogen.energy.gov/pdfs/htac{_}may2012{_}hyundai.pdf`.

[19] Alexander Kabza. Fuel cell formulary, 2015.

[20] Willett Kempton and Steven E Letendre. Electric vehicles as a new power source for electric utilities. *Transportation Research Part D: Transport and Environment*, 2(3):157–175, 1997.

[21] Shyam S Kocha. Electrochemical degradation: electrocatalyst and support durability. *Polymer Electrolyte Fuel Cell Degradation*, page 89, 2011.

[22] Sumit Kundu, Michael Fowler, Leonardo C Simon, and Rami Abouatallah. Reversible and irreversible degradation in fuel cells during open circuit voltage durability testing. *Journal of Power sources*, 182(1):254–258, 2008.

[23] Jianqiu Li, Zunyan Hu, Liangfei Xu, Minggao Ouyang, Chuan Fang, Junming Hu, Siliang Cheng, Hong Po, Wenbin Zhang, and Hongliang Jiang. Fuel cell system degradation analysis of a chinese plug-in hybrid fuel cell city bus. *International Journal of Hydrogen Energy*, 41(34):15295–15310, 2016.

[24] R Lin, B Li, YP Hou, and JM Ma. Investigation of dynamic driving cycle effect on performance degradation and micro-structure change of pem fuel cell. *International Journal of Hydrogen Energy*, 34(5):2369–2376, 2009.

[25] Mingyang Liu, Cheng Wang, Jianbo Zhang, Jianlong Wang, Zhongjun Hou, and Zongqiang Mao. Diagnosis of membrane electrode assembly degradation with drive cycle test technique. *International Journal of Hydrogen Energy*, 39(26):14370–14375, 2014.

[26] Francis Mwasilu, Jackson John Justo, Eun-Kyung Kim, Ton Duc Do, and Jin-Woo Jung. Electric vehicles and smart grid interaction: A review on vehicle to grid and renewable energy sources integration. *Renewable and Sustainable Energy Reviews*, 34:501–516, 2014.

[27] F Nandjou, J-P Poirot-Crouvezier, M Chandesris, J-F Blachot, C Bonnaud, and Y Bultel. Impact of heat and water management on proton exchange membrane fuel cells degradation in automotive application. *Journal of Power Sources*, 326:182–192, 2016.

[28] National Grid. Understanding Electric Demand, 2016. URL `https://www9.nationalgridus.com/niagaramohawk/non_html/eff_elec-demand.pdf`.

[29] Michael Nikowitz. *Advanced Hybrid and Electric Vehicles: System Optimization and Vehicle Integration*. Springer, 2016.

[30] Peter Odetola, Patricia Popoola, Olawale Popoola, and David Delport. Electrodeposition of functional coatings on bipolar plates for fuel cell applications–a review. In *Electrodeposition of Composite Materials*. InTech, 2016.

[31] Fuel Cell Technology Office. Fuel cell technologies office multi-year research, development, and demonstration plan. Technical Report 3.4 Fuel Cells, Annual Progress Report, U.S. Department of Energy, 2016 - section 3.4 updated on May 2017.

[32] V Oldenbroek, S Alva, B Pyman, L B Buning, P A Veenhuizen, and A J M Van Wijk. Hyundai ix35 fuel cell electric vehicles : degradation analysis for driving and vehicle-to-grid usage. In *EVS30 International Battery, Hybrid and Fuel Cell Electric Vehicle Symposium*, pages 1–11, Stuttgart, 2017.

[33] V Oldenbroek, S Alva, B Pyman, L B Buning, P A Veenhuizen, and A J M Van Wijk. Hyundai ix35 fuel cell electric vehicles : degradation analysis for driving and vehicle-to-grid usage. In *EVS30 International Battery, Hybrid and Fuel Cell Electric Vehicle Symposium*, pages 1–11, Stuttgart, 2017.

[34] Vincent Oldenbroek, Victor Hamoen, Samrudh Alva, Carla Robledo, Leendert Verhoef, and Ad Van Wijk. Fuel Cell Electric Vehicle-to-Grid : Experimental feasibility and operational performance. In *6th European PEFC and Electrolyser Forum*, number July, pages 1–21, Lucerne, 2017.

[35] Vincent Oldenbroek, Leendert A Verhoef, and Ad JM van Wijk. Fuel cell electric vehicle as a power plant: Fully renewable integrated transport and energy system design and analysis for smart city areas. *International Journal of Hydrogen Energy*, 42(12):8166–8196, 2017.

[36] E Pahon, S Morando, R Petrone, M-C Péra, D Hissel, N Yousfi-Steiner, S Jemei, R Gouriveau, D Chamagne, P Moçotéguy, et al. Long-term tests duration reduction for pemfc μ-chp application. *International Journal of Hydrogen Energy*, 42(2):1527–1533, 2017.

[37] Pucheng Pei and Huicui Chen. Main factors affecting the lifetime of proton exchange membrane fuel cells in vehicle applications: A review. *Applied Energy*, 125:60–75, 2014.

[38] Pucheng Pei, Qianfei Chang, and Tian Tang. A quick evaluating method for automotive fuel cell lifetime. *International Journal of Hydrogen Energy*, 33(14):3829–3836, 2008.

[39] Raffaele Petrone, Daniel Hissel, MC Péra, Didier Chamagne, and Rafael Gouriveau. Accelerated stress test procedures for pem fuel cells under actual load constraints: State-of-art and proposals. *International Journal of Hydrogen Energy*, 40(36):12489–12505, 2015.

[40] Hajo Ribberink, Ken Darcovich, and Fleurine Pincet. Battery life impact of vehicle-to-grid application of electric vehicles. In *the proc. of the International Electric Vehicle Symposium and Exhibition*, 2015.

[41] Marianne P Rodgers, Leonard J Bonville, H Russell Kunz, Darlene K Slattery, and James M Fenton. Fuel cell perfluorinated sulfonic acid membrane degradation correlating accelerated stress testing and lifetime. *Chemical reviews*, 112(11):6075–6103, 2012.

[42] Patrick Salman, Eva Wallnöfer-Ogris, Markus Sartory, Alexander Trattner, Manfred Klell, Helfried Müller, Axel-Oscar Bernt, Michael Martin, Knut Schiefer, Manfred Limbrunner, et al. Hydrogen-powered fuel cell range extender vehicle–long driving range with zero-emissions. Technical report, SAE Technical Paper, 2017.

[43] Wolfgang Schmittinger and Ardalan Vahidi. A review of the main parameters influencing long-term performance and durability of pem fuel cells. *Journal of power sources*, 180(1):1–14, 2008.

[44] Bruno Scrosati, Jürgen Garche, and Werner Tillmetz. *Advances in battery technologies for electric vehicles*. Woodhead Publishing, 2015.

[45] Jing Shan, Rui Lin, Shixiang Xia, Dengcheng Liu, and Qian Zhang. Local resolved investigation of pemfc performance degradation mechanism during dynamic driving cycle. *International journal of hydrogen energy*, 41(7):4239–4250, 2016.

[46] Shell. ENERGY OF THE FUTURE? Sustainable Mobility through Fuel Cells and H 2, 2017. URL `http://www.shell.de/medien/shell-publikationen/shell-hydrogen-study/_jcr_content/par/toptasks_e705.stream/1496312627865/46fec8302a3871b190fed35fa8c09e449f57bf73bdc35e0c8a34c8c5c53c5986/shell-h2-study-new.pdf`.

[47] Detlef Stolten, Remzi C Samsun, and Nancy Garland. *Fuel cells: data, facts, and figures*. John Wiley & Sons, 2016.

[48] Georgios Tsotridis, Alberto Pilenga, Giancarlo De Marco, and Thomas Malkow. EU HARMONISED TEST PROTOCOLS FOR PEMFC MEA TESTING IN SINGLE CELL CONFIGURATION FOR AUTOMOTIVE APPLICATIONS - European Commission. Technical report, 2015. URL `https://ec.europa.eu/jrc/en/publication/eur-scientific-and-technical-research-reports/eu-harmonised-test-protocols-pemfc-mea-testing-single-cell-configuration-automotive`.

[49] Vaisala Oyj. HUMIDITY CONVERSION FORMULAS - Calculation formulas for humidity. Technical report, 2013. URL http://www.vaisala.com/VaisalaDocuments/Applicationnotes/Humidity_Conversion_Formulas_B210973EN-F.pdf.

[50] AJM Van Wijk and Leendert Verhoef. *Our car as power plant*. Ios Press, 2014.

[51] Norbert Wagner and Andreas Kaspar Friedrich. Dynamic operational conditions. *Encyclopedia of Electrochemical Power Sources (ECPS), Elsevier*, pages 912–930, 2009.

[52] Dai Wang, Jonathan Coignard, Teng Zeng, Cong Zhang, and Samveg Saxena. Quantifying electric vehicle battery degradation from driving vs. vehicle-to-grid services. *Journal of Power Sources*, 332:193–203, 2016.

[53] Luting Wang and Bo Chen. Model-based analysis of v2g impact on battery degradation. Technical report, SAE Technical Paper, 2017.

[54] Bingbing Wu, Ming Zhao, Weiyu Shi, Wenming Liu, Jianguo Liu, Danmin Xing, Yingfang Yao, Zhongjun Hou, Pingwen Ming, Jun Gu, et al. The degradation study of nafion/ptfe composite membrane in pem fuel cell under accelerated stress tests. *International journal of hydrogen energy*, 39(26):14381–14390, 2014.

[55] Jingrong Yu, Toyoaki Matsuura, Yusuke Yoshikawa, Md Nazrul Islam, and Michio Hori. In situ analysis of performance degradation of a pemfc under nonsaturated humidification. *Electrochemical and solid-state letters*, 8(3):A156–A158, 2005.

[56] Jianlu Zhang, Yanghua Tang, Chaojie Song, Zetao Xia, Hui Li, Haijiang Wang, and Jiujun Zhang. Pem fuel cell relative humidity (rh) and its effect on performance at high temperatures. *Electrochimica Acta*, 53(16):5315–5321, 2008.

[57] Jiujun Zhang, Jifeng Wu, and Huamin Zhang. *PEM fuel cell testing and diagnosis*. Newnes, 2013.

[58] Shengsheng Zhang, Xiaozi Yuan, Haijiang Wang, Walter Mérida, Hong Zhu, Jun Shen, Shaohong Wu, and Jiujun Zhang. A review of accelerated stress tests of mea durability in pem fuel cells. *International journal of hydrogen energy*, 34(1):388–404, 2009.

[59] Da Zhu, Dominic Pasquale Patella, Roland Steinmetz, and Pajnapa Peamsilpakulchorn. *The Bhutan Electric Vehicle Initiative: Scenarios, Implications, and Economic Impact*. World Bank Publications, 2016.